

GPO PRICE \$ _____

CFSTI PRICE(S) \$ _____

Hard copy (HC) 2.00

Microfiche (MF) - 65

ff 653 July 65

N 68-23843
(ACCESSION NUMBER)

170
(PAGES)

(THRU)

1

NASA CR 66627
(NASA CR OR TMX OR AD NUMBER)

(CODE)

33

(CATEGORY)

FACILITY FORM 602

Progress Report

On

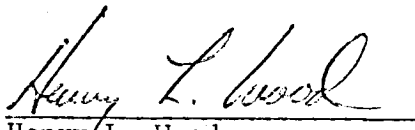
NASA Research Grant

NGR 47-004-024

A STUDY OF THE APPLICATION OF MICROWAVE TECHNIQUES TO THE
MEASUREMENT OF SOLID PROPELLANT BURNING RATES

Submitted to
The
National Aeronautics and Space Administration

By



Henry L. Wood
Professor of Mechanical Engineering



Walter F. O'Brien, Jr.
Assistant Professor of
Mechanical Engineering

Period Covered: September 1, 1966 - August 31, 1967

Virginia Polytechnic Institute
Blacksburg, Virginia
April, 1968



II. TABLE OF CONTENTS

	<u>Page</u>
I. TITLE	1
II. TABLE OF CONTENTS	2
III. LIST OF FIGURES	5
IV. LIST OF TABLES	7
V. LIST OF SYMBOLS	8
VI. INTRODUCTION	10
VII. REVIEW OF LITERATURE	12
Introduction	12
Burning Rate Measurement Techniques	
Non-Microwave	12
Microwave Burning Rate Measurement Techniques	21
Related Microwave Techniques	27
Discussion	34
VIII. THE INVESTIGATION	40
Objective	40
Microwave Burning Rate Measurement	40
Microwave Source	43
Microwave Reflections	45
Waveform of the Detected Signal	51
Microwave Attenuation	56
Summary	62
Experimental Apparatus	63
Instrumentation	64

	<u>Page</u>
Simulator	73
Test Rocket Motor	76
List of Equipment	83
Test Procedure	86
Simulated Tests	87
Atmospheric Tests	89
Test Rocket Motor Firings	90
Data Reduction Techniques	94
Pressure Data	96
Thermocouple Data	96
Microwave Data	97
Data and Results	102
Simulated Tests	102
Atmospheric Tests	104
Test Rocket Motor Firings	104
IX. DISCUSSION OF RESULTS	115
Simulated Tests	115
Atmospheric Tests	118
Test Rocket Motor Firings	119
X. SUMMARY AND CONCLUSIONS	131
XI. RECOMMENDATIONS	134
XII. ACKNOWLEDGMENTS	136
XIII. BIBLIOGRAPHY	137

	<u>Page</u>
XIV. APPENDICES	143
Appendix A. Electromagnetic Nomenclature and Symbolism	143
Appendix B. Design of 30 GHz Microwave Lens-Corrected Horn Collimator	147

III. LIST OF FIGURES

	<u>Page</u>
Figure 1. - Continuous burning rate measurement technique	15
Figure 2. - Schematic of ultrasonic burning rate apparatus	18
Figure 3. - Microwave apparatus for measuring burning rate of propellant strands	22
Figure 4. - Arrangement of microwave components for high pressure strand burner burning rate measurement	25
Figure 5. - Typical microwave test system	28
Figure 6. - Effect of aluminum concentration on the measured attenuation produced by single and double slabs of dummy propellant formulation	29
Figure 7. - Microwave burning rate measurement technique ..	41
Figure 8. - Models for attenuation analysis	60
Figure 9. - Block diagram of microwave burning rate measurement system	65
Figure 10. - Photograph of microwave burning rate system equipment arrangement	66
Figure 11. - Test rocket motor assembly	68
Figure 12. - High pass filter and variable gain device	70
Figure 13. - Data acquisition system arrangement	72
Figure 14. - Photograph of end burning rocket motor simulator used for simulated tests	75
Figure 15. - Photograph of test rocket motor	77
Figure 16. - Photograph of shield, cooling tank and rocket motor in test cell	80

	<u>Page</u>
Figure 17. - Propellant charge and insulators	82
Figure 18. - Atmospheric pressure combustion test in progress	91
Figure 19. - Typical data from test rocket motor firing	95
Figure 20. - Reduction method for microwave data	101
Figure 21. - Area of burning surface influencing return signal through 3 inches of AeReCo 2 aluminized propellant	116
Figure 22. - Comparison of microwave measured burning rates with ultrasonic measured burning rates for propellant TPH-8009	122
Figure 23. - Comparison of microwave measured burning rates with strand burning rates for propellant TPH-8009	123
Figure 24. - Typical propellant burning surface regression history measured by microwave method	124
Figure 25. - Typical propellant burning rates at intervals of 0.038 inches measured by microwave method	126

IV. LIST OF TABLES

	<u>Page</u>
Table 1. - Test Propellant Formulations	81
Table 2. - Effect of Different Metal Reflectors on Return Signal Transmitted through Three Inches of AeReCo 2 Propellant	103
Table 3. - Results of Atmospheric Combustion Pressure Tests - Penetrability of Propellant Charges by Microwaves	105
Table 4. - Test Conditions and Data - Rocket Motor Firings	106
Table 5. - Test Data - Rocket Motor Firings	107
Table 6. - Average Test Results - Rocket Motor Firings	108
Table 7. - Individual Microwave One-Half Cycle Times	109
Table 8. - Test Results - Individual One-Half Cycle Microwave Burning Rates and Cumulative Values	110-111
Table 9. - Electromagnetic Property Data and Results - Propellant TPH-8009	114
Table 10. - Comparison of Electromagnetic Property Data	129

V. LIST OF SYMBOLS

E	complex electric intensity
H	complex magnetic intensity
T	transmission coefficient
V	voltage
K	10^3
M	10^6
G	10^9
Hz	cycles per second
c	constant
f	frequency
j	imaginary coordinate
k	wave number
p	pressure
r	burning rate
t	time, seconds
v	velocity
x	coordinate axis
y	coordinate axis
z	coordinate axis
Γ	reflection coefficient
γ	propagation constant

ϵ permittivity
 ϵ' a-c capacitvity
 ϵ'' dielectric loss factor
 η wave impedance
 λ wavelength
 μ permeability, also 10^{-6}
 φ phase angle
 ω circular frequency

VI. INTRODUCTION

A knowledge of the burning rate of the propellant in a solid propellant rocket motor is of basic importance in rocket technology. The design of an operational solid propellant rocket motor is dependent upon accurate knowledge of the burning rate of the propellant as a function of the variables which control it.

Burning rate information for propellants is normally generated experimentally, since the current state of combustion theory does not allow the prediction of burning rates of new formulations. Further, the burning rate of solid propellants has been found to depend upon the propellant environment, and variations in burning rate due to design factors must be evaluated experimentally. With the current need for more precise prediction and control of solid propellant rocket performance, there has been considerable interest in improved methods for burning rate measurement. Emphasis has been placed upon methods which do not require location of devices within the solid propellant grain, undesirable because of obvious manufacturing difficulties and potential effects upon the measured variable. There is also a need for burning rate measurement methods which are capable of measuring burning rates in operational rocket motors, as well as under laboratory conditions.

The microwave burning rate measurement method of the subject investigation appeared, at the outset, to satisfy the above criteria.

Feasibility of the technique had previously been demonstrated by other investigators. The subject investigation shows that the microwave technique studied is capable of accurately measuring solid propellant burning rates under actual rocket motor operating conditions.

The method involves the transmission of microwaves through the unburned solid propellant, directed toward the burning surface of the solid propellant. A reflection of the microwaves occurs at the burning surface, and as the propellant burns, the phase of the reflected signal changes. The reflected signal is then compared with a portion of the transmitted signal to obtain burning rate information. The unburned solid propellant is a dielectric material, and as such allows transmission of the microwave signal. A microwave window must be provided for transmission of the microwaves through a metallic rocket motor case.

The following material describes the results of an experimental investigation of the microwave burning rate measurement technique, with a review of pertinent literature and supporting analyses.

VII. REVIEW OF LITERATURE

Introduction

The measurement of the burning rate of solid propellants has been the subject of considerable research and development in recent years. Closed bomb and small test motor burning rate measurement techniques have been the accepted and conventional methods in propellant research for some time. They continue to be in wide use. Recently the need for more accurate burning rate measurements under special conditions has spawned work in the field. Examples of the various techniques in use and under research are covered in the following material. Sections include: (1) burning rate measurement techniques, non-microwave; (2) microwave burning rate measurement techniques; (3) related microwave techniques, and, (4) discussion.

Burning Rate Measurement Techniques

Non-Microwave

The burning rate-pressure relation for solid rocket propellants has almost classically been determined employing the strand burner, or Crawford bomb¹. This closed bomb device is normally pressurized with a neutral atmosphere such as nitrogen. A long thin strand of propellant

¹Superscript Arabic numerals refer to references contained in the bibliography.

inhibited laterally burns like a cigarette and as it burns, successively cuts several wires embedded in the strand. Measurement of the time elapsed between cutting of the strands permits determination of the average burning rate of the propellant between the wires. Many modifications of the basic technique have been used. Stewart and Moon² of the Naval Ordnance Test Station provided sharp variations in the cross section of the propellant strand. Passage of the flame front was indicated by the disturbance of the pressure record. Optical methods have also been employed to photograph the burning strand. Requirements for conducting the test are that the strand must be small and that the pressure in the bomb must remain nearly constant. The Crawford bomb and related techniques have found their major applications for the measurement of burning rates during propellant research, and for comparing burning rates of different propellants.

For reasonably accurate measurement and prediction of rocket motor burning rates, small test motors have been employed prior to design of operational motors.³ Such motors can use different nozzles for each combustion pressure or non-neutral grain burning geometry in order to generate the required burning rate-pressure data. Rates are determined from pressure-time-charge size data, taking into account any non-neutral burning geometry of the grain. Charges used in these test motors are usually small, of the order of 10 to 20 pounds of propellant. Many designs for small test motors have been developed to meet special requirements.

Osborn, Burick, Ho and others of the Jet Propulsion Center of Purdue University conducted extensive investigations of continuous measurement of solid propellant burning rates.⁴ A technique for the direct and continuous measurement of the burning rate of solid rocket propellants under simulated motor conditions was developed. The technique involved a closed loop servomechanism which positioned a solid propellant sample within a two-dimensional combustion chamber. In order to provide a feedback signal to the servomechanism, three different transducer systems were investigated; a microwave technique, ultrasonic techniques, and a radioactive isotope system.

As can be seen from Figure 1, the microwave measurement technique involved the passing of waves through the propellant burning zone to determine the position of the burning surface. Ho⁵ conducted a feasibility study for the use of both ultrasonic and microwave techniques. Based on analysis of expected microwave attenuation as the waves passed through the combustion gases, it was concluded that the microwave system was not readily adaptable as a feedback transducer for the servomechanism technique. Strong dependence of the microwave attenuation upon the combustion conditions (ionization of the combustion gases) was cited as the main difficulty. It was noted that combustion gas ionization could be expected to vary with the molecular species present in the gases as well as the temperature. Consequently, a separate microwave transducer calibration system would be required for adapting the transducer to the servomechanism measurement system

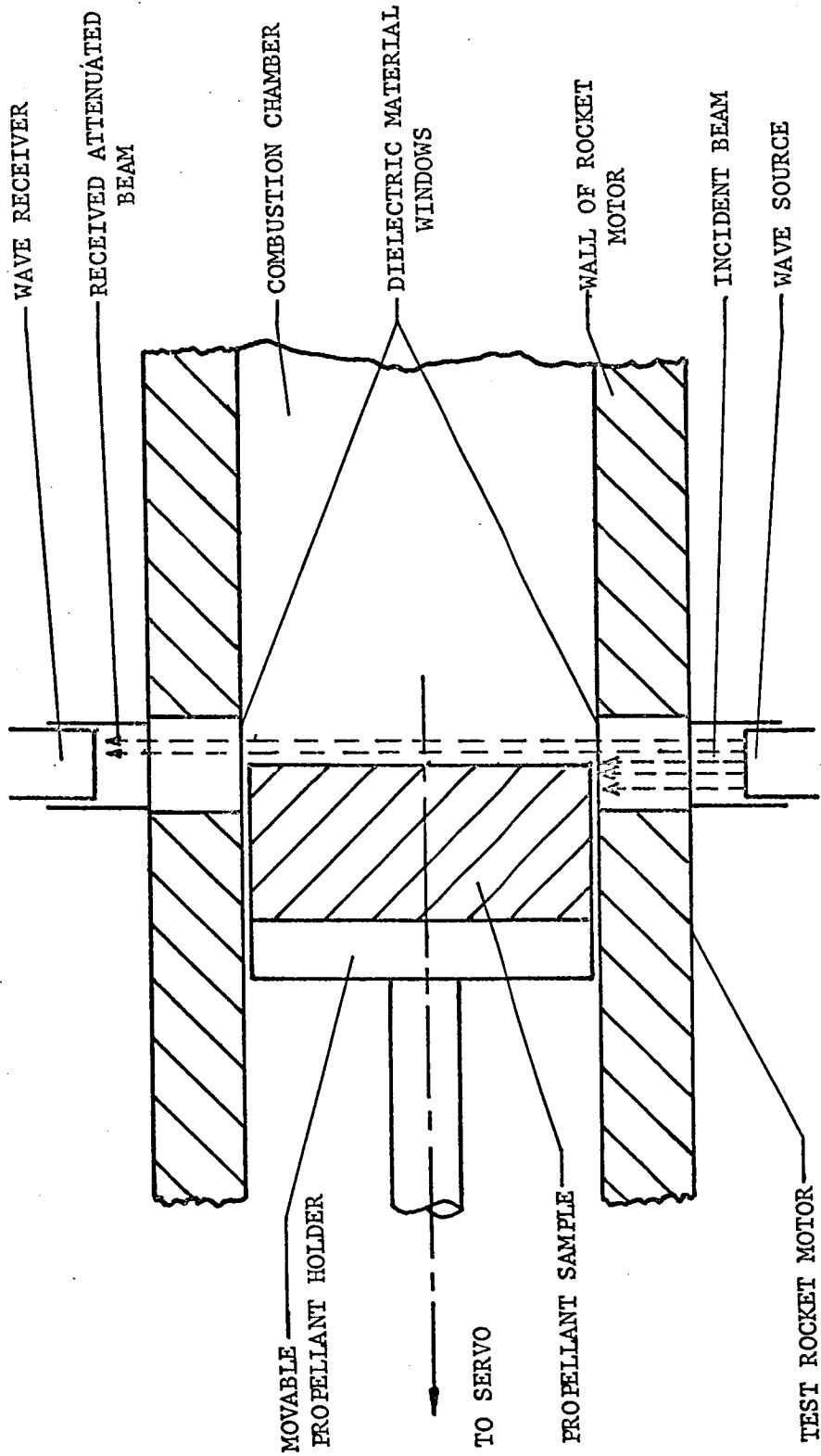


Figure 1. - Continuous burning rate measurement technique

for each different propellant and combustion pressure. (The method studied by Ho is not the same in principle as that used in the subject investigation.) In the same work, Ho analyzed ultrasonic attenuation, resonance, and pulse-reflection techniques for direct burning rate measurement. The technique involved measurement of the time required for a sonic pulse to travel from the transducer to the burning surface and then back (the echo) to the transducer. It was concluded that the pulse-reflection technique using ultrasonic frequencies of 400 KHz or somewhat lower was the most promising of the three ultrasonic methods considered. However, it was noted that, since the Young's Modulus of solid propellant is usually quite low, the ultrasonic wave would be greatly attenuated. In order to receive a sufficiently large reflection, it was suggested that the propellant temperature be kept around -20 to -40 °F. Thus, the practicality of the ultrasonic technique seemed questionable.

Since the results of the feasibility study outlined above showed doubtful promise for the microwave and ultrasonic techniques, a gamma-ray or radiographic technique was investigated.⁶ Figure 1 again shows the essential features of the method, except that gamma rays were employed rather than microwaves. It was shown that the attenuation of the gamma rays was chiefly a function of material density. Therefore, the attenuation of the gamma rays by the combustion products could be neglected. The emitted beam intensity was a function only of the position of the propellant sample because a

motion of the propellant would provide a variable attenuation of the emitted energy. The transducer signal was found by experiment to produce a linear signal for approximately 0.040 inches of linear movement of the propellant sample. The gamma ray transducer was judged the most suitable for application as a burning rate sensor. A servomechanism system was designed to position the propellant in the test rocket motor, using output of the gamma ray transducer as the feedback signal. It was reported that linear burning rate data was successfully obtained for several different propellant formulations. Burning rate data was presented for a propellant code named "B", showing burning rates from approximately 0.15 to 0.35 inches per second at 100 to 400 psia combustion pressures, and for another propellant "C", which produced burning rates from approximately 0.25 to 0.33 inches per second at 200 to 500 psia combustion pressure.

Hale⁷ has conducted research on an ultrasonic pulse-echo technique for burning rate measurement. The ultrasonic pulse-echo technique was employed in an end burning rocket motor. Figure 2 shows the experimental arrangement. Ultrasonic energy was transmitted at a frequency of 1 MHz, in pulses at a rate of 600 times per second. Propellant samples were 1 and 1.5 inches thick. Results of 23 firings of the PBAA - 16 per cent aluminized propellant (TPH-8009) showed that ultrasonically measured burning rates compared favorably with data obtained by standard methods. The pressure range covered approximately 500 to

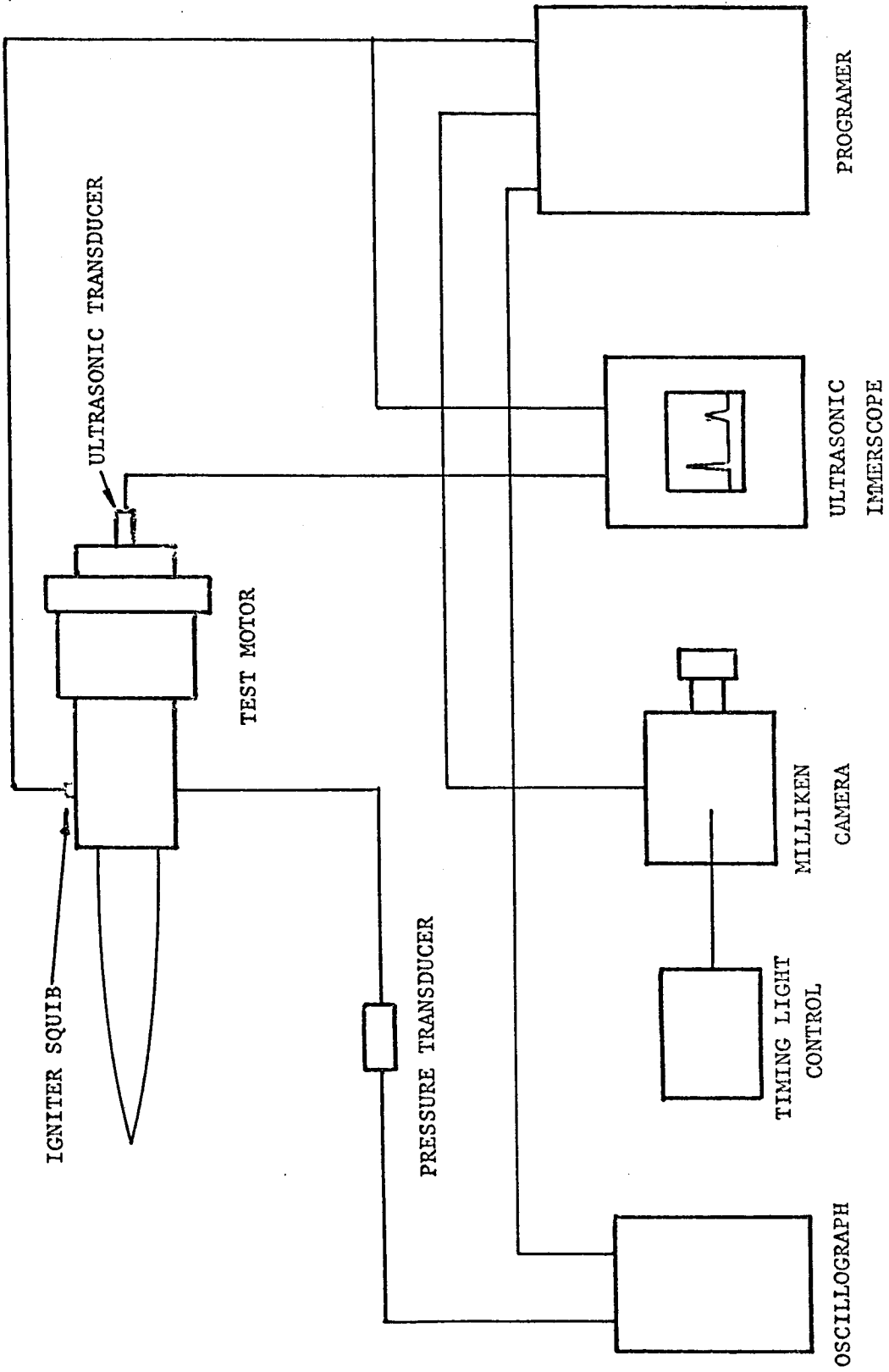


Figure 2. - Schematic of ultrasonic burning rate apparatus.

1000 psia. There was no observed effect of the measurement system on burning rates of the propellant. Continuing research is currently being conducted to improve the performance of the system.

Continuous measurement of burning rates using a capacitance variation technique was the subject of research by Hermance.⁸ A strand of propellant of square cross section was bonded on two sides to 0.012 mm tin foil strips. Since the propellant (a polysulphide-ammonium perchlorate formulation) was a material of high dielectric constant, a capacitor was formed. The measured capacitance was related to the amount of propellant between the foil strips. The variation of capacitance as burning progressed was measured by placing the propellant capacitor in a resonant L-C circuit. The circuit was excited at 10.7 MHz. Burning rate data at pressures of 1, 10, 20, and 60 atmospheres were obtained and compared with data obtained from the use of fuse wires. Additional work is currently underway to determine the accuracy and general applicability of the method.

Radiography as a technique for viewing the burning of propellant grains in operating motors has been demonstrated by Seamons^{9,10}. A five-inch rocket motor with a tubular grain was used in the reported work. A 300 kv x-ray machine was used to irradiate a section of the motor. The shadow image of the propellant grain formed on a phosphor screen was intensified and presented as an image on a 0.63-inch-diameter phosphor screen for photography. A movie camera recorded the images at eight frames per second. It was noted that more sophisticated

equipment would allow a camera speed of up to 100 frames per second. Burning rate of the propellant could be measured with the aid of a film reader.

The use of probes of various types to sense the arrival of the combustion zone has been reported by several investigators. Dickenson¹¹ and others employed a dual conductor probe in an erosive burning study. This probe system indicated exposure to combustion gases by a change in conductivity between the two conductors in the probe. The associated detection system permitted up to 50 probes to be used. Probes were installed in their appropriate positions prior to casting the propellant in the combustion chamber. Average burning-rate measurements over periods of approximately 0.5 second were obtained.

An embedded wire technique for burning rate measurement was developed by Osborn and Bethel.¹² Several 0.0045-inch-diameter wires were embedded in a small piece of propellant, which was later bonded to the grain of a test rocket motor. The wires were so located that they were sequentially exposed to the combustion zone. The wires were connected internally in the surrounding propellant so that the monitoring of total network resistance indicated the breaking of each wire. Lead-antimony wires were used, since experiments indicated that such wires would not transmit a significant amount of heat into the unburned propellant, and therefore would not cause a cone-burning condition around the wire.

A variation of the embedded probe technique involves the use of radioactive needles. A feasibility demonstration of such a device is being conducted by several workers at TRW Systems.¹³ "Needles" containing trace quantities of radiochemicals are designed to be placed so as to dynamically measure the ablation and erosion of rocket nozzle liner materials. The continuous method of measurement involves the observation of a reduced count rate as the "needle" is eroded. Analyses of several pertinent problems have been reported, and the work is continuing. In the referenced report the technique is proposed to measure nozzle erosion, but is obviously adaptable to the measurement of propellant burning rates.

Microwave Burning Rate Measurement

Techniques

Johnson¹⁴ first showed the feasibility of a microwave technique for burning rate measurement. He noted the difficulties in calculating the actual burning rate behavior of a grain, and reviewed several currently employed techniques for measuring burning rates. A microwave technique involving the reflection and combination of incident and reflected microwaves was suggested, basically the same method employed in the subject study. The use of a "magic tee" for greater measurement sensitivity was discussed. An experiment designed to prove the feasibility of the technique was conducted. Figure 3

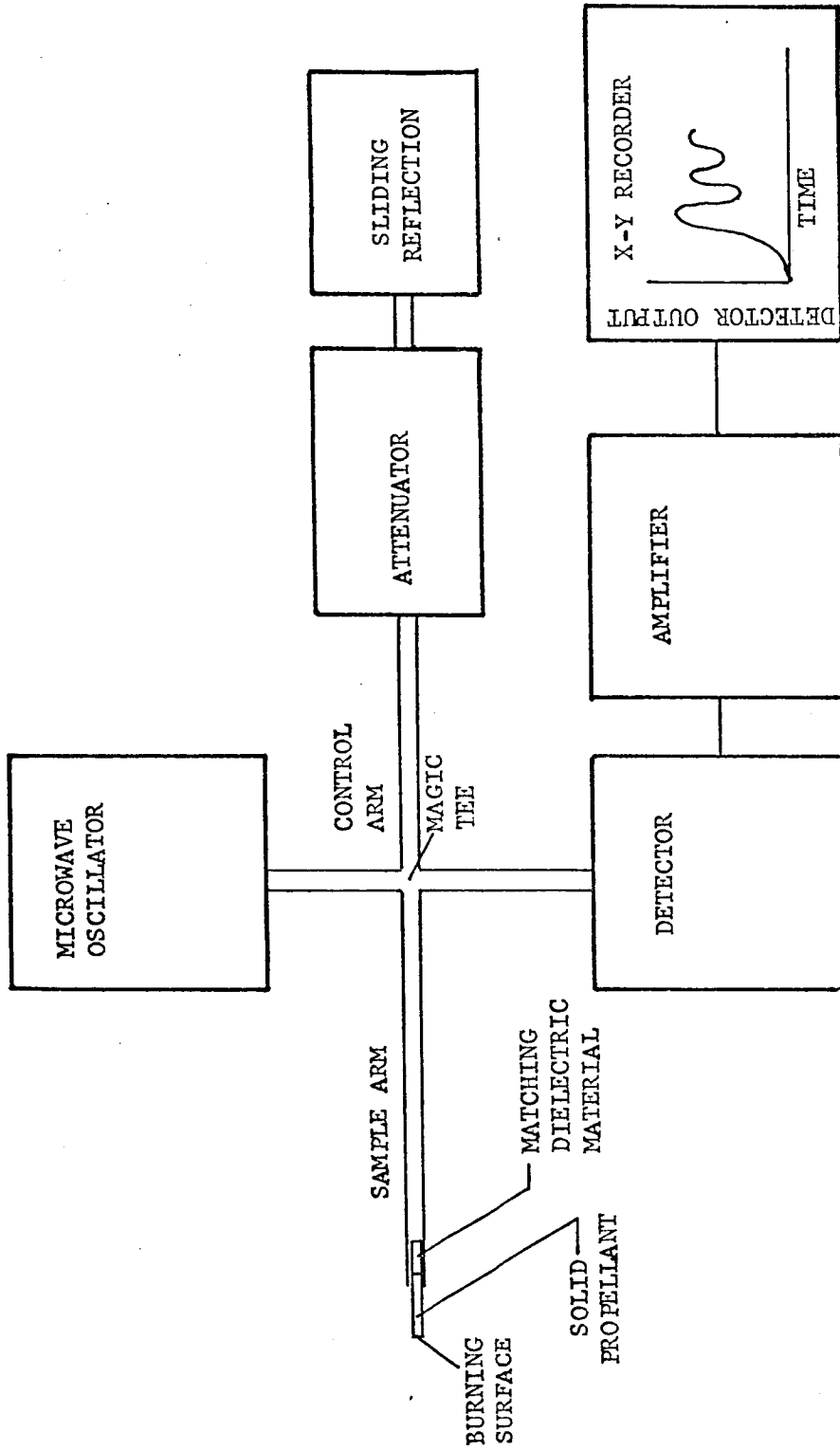


Figure 3. - Microwave apparatus for measuring burning rate of propellant strands

shows the experimental arrangement which was employed. Solid propellant was burned in an open waveguide at zero pressure, and rate data were obtained. The test was not conducted under normal rocket propellant burning conditions, but feasibility was demonstrated. For data reduction, the wavelength of the radiation in the propellant filled waveguide was determined by sliding a small probe along a slot in the waveguide. Since a standing wave existed in the waveguide, distances measured between successive minima were taken as one-half wavelength. A wavelength of 0.268 inches (0.680 cm) was measured. The frequency of the microwave radiation was unspecified, as was the propellant composition. Burning rates of approximately 0.05 to 0.02 in/sec were measured. A technique for measuring burning rate at two points of a propellant grain was proposed. Cauley¹⁵ has proved the feasibility of a similar method, employing simulated burning surfaces, in work paralleling the subject investigation. Two points having differing burning rates were simulated by reflecting 30 GHz microwaves from rotating helices. Differences in the rate of approach of the helices (i.e. their rates of rotation) were successfully sensed and measured by the system. The microwave methods employed were essentially those of the subject investigation.

Research using microwave techniques for burning rate measurement was conducted by Cole.¹⁶ A self-pressurizing closed-bomb system was employed to observe deflagration characteristics of solid propellants at pressures as high as 200,000 psi. Purposes of the research were to

bridge the gap between the usual solid propellant deflagration and detonation regimes, and to provide knowledge of propellant burning rates in the 2,000 to 20,000 psi "intermediate" pressure range for feasibility studies of rockets operating at such combustion pressures. A schematic diagram of the apparatus employed is shown in Figure 4. The microwave system operated at 24 GHz, with a maximum power of 250 milliwatts. Microwaves entering the wave guide were reflected from the burning propellant surface, as well as from other material interfaces and discontinuities. An E-H plane tuner was used to partially "match" the microwave load formed by the bomb and its associated waveguide to the microwave source. This helped overcome experimental problems associated with a large reflected signal level change due to less attenuation as the propellant burned. The principle employed to detect the motion of the burning surface involved mixing reflected waves from a stationary surface and the moving (propellant burning) surface. A discussion and analysis of the process was presented. The method produced r-p (burning rate-pressure) data in reasonably good agreement with independent r-p measurements from 2" diameter rocket motor firings and a small number of 1/8" diameter strand burning experiments. Five firings of the bomb were made with microwave burning rate instrumentation, producing burning rates from 0.2 to 20 inches per second at 200 to 30,000 psia. Firings numbers four and five yielded somewhat higher burning rates than the reference data, while firing number two produced data at considerable variance

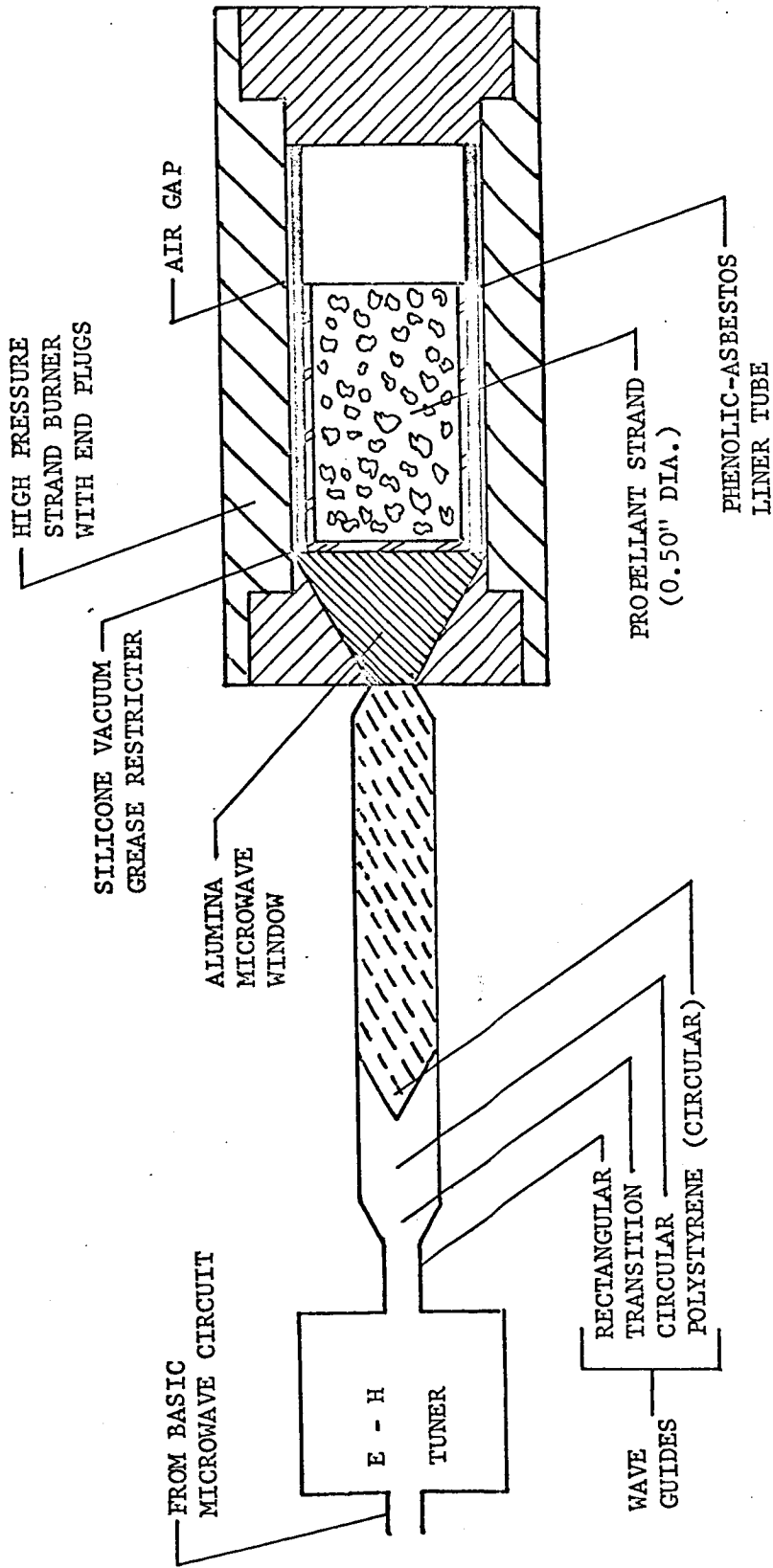


Figure 4. - Arrangement of microwave components for high pressure strand burner burning rate measurement

with reference data. Firing number one produced data only to 2100 psia, when the microwave signal became unusable. Data was also analyzed and burning rates determined employing a pressure rate-of-rise technique. Microwave wavelengths in the propellant were determined at atmospheric pressure from known charge lengths and microwave data. Wavelengths were found to be of the order of 0.250 inches at 24 GHz. For all firings, the propellant was a PBAA-75 per cent 15 μ ammonium perchlorate formulation.

It was concluded from the above experiments that microwave interferometry held singularly good promise as an instrumentation technique for high pressure burning rate determinations using closed bombs. However, further development was deemed necessary. The major source of error appeared to be in the determination of effective microwave wavelengths in the sample configuration used. This was compounded by the dimensions of the strand burner, which were small relative to the wavelengths used. The burner thus appeared as a dielectric filled cylindrical waveguide to the microwaves. The major limitation cited was the microwave absorption characteristics of some propellant formulations.

Jenks and Devault¹⁷ of Allegany Ballistics Laboratory reported use of a microwave burning rate measurement device in a classified report. Austin¹⁸ of the Naval Ordnance Station has also reported use of the microwave burning rate technique in combustion research, also in the classified literature.

Related Microwave Techniques

Brandon¹⁹ of Rohm and Haas studied the use of microwaves for detecting fissures in solid propellant grains, and for determining the degree of polymerization during curing of solid propellants. Included in the reported work were studies of microwave attenuation in the X-band (8.1 to 12.4 GHz) and the K-band (22.0 to 26.0 GHz). Solid propellant formulations containing both powdered aluminum and aluminum staple (wire-like pieces of aluminum 1/8" to 5/16" long) were tested. Two grades of powdered aluminum were used, Reynolds 400 (6.4 μ) and Alcoa 1230 (13.0 μ), and percent-by-weight of aluminum powder was varied from 0 to 50 per cent. The experimental arrangement for attenuation measurements is shown in Figure 5. Attenuation tests for powdered aluminum were made at a fixed frequency of 10.3 GHz. Multiple slabs of propellant were used to vary the total sample thickness. Reflected signal levels were observed to decay in an oscillatory manner as thickness of propellant was increased, as the various thicknesses passed through multiples of the wavelength of electromagnetic propagation in the samples. Correlation of data for various aluminum concentrations produced the graph shown in Figure 6. As shown, attenuation of 10.3 GHz microwaves increased by about 0.144 decibels per centimeter of propellant thickness per weight percent of aluminum. The spread of attenuation data in Figure 6 was attributed to standing

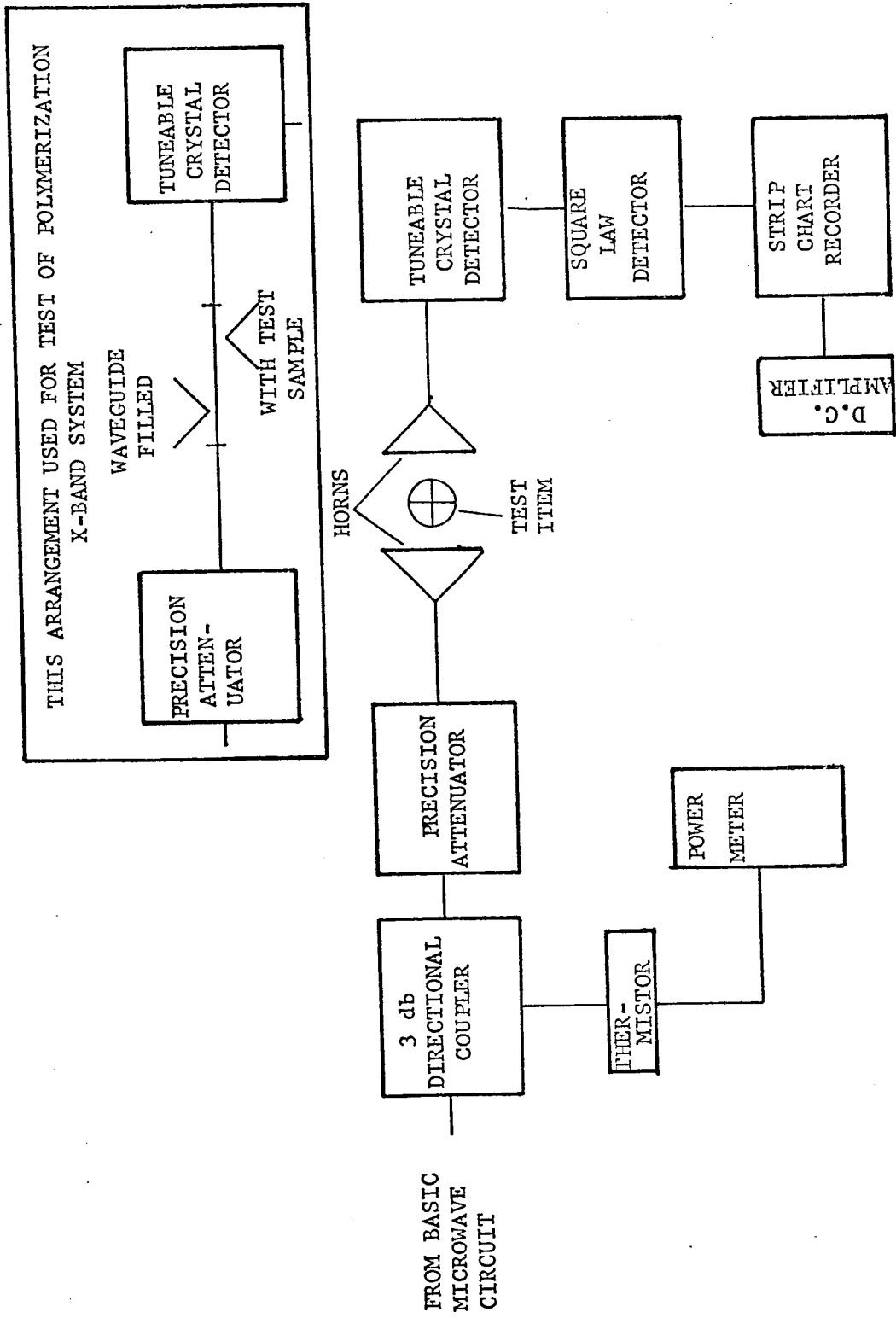


Figure 5. - Typical microwave test system.

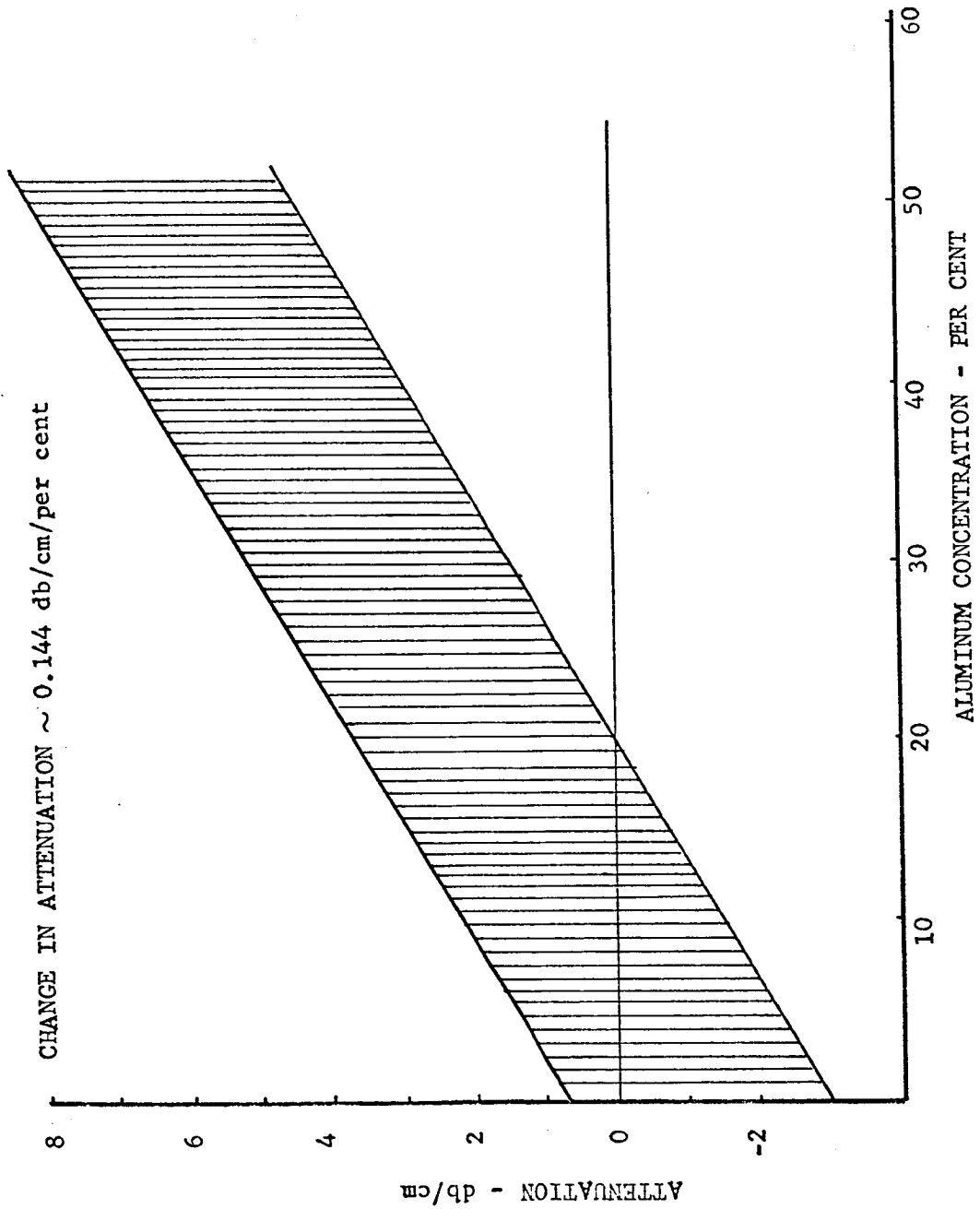


Figure 6. - Effect of aluminum concentration on the measured attenuation produced by single and double slabs of dummy propellant formulation.

wave effects. Separate experiments established that the inclusion of a propellant/propellant interface in the signal path (test specimen constructed of two layers of propellant) also increased attenuation.

Another series of experiments conducted by Brandon and covered in the same report involved measurement of microwave attenuation by slabs of dummy propellant oriented at angles to the incident waves. Theory of electromagnetic waves incident on dielectric boundaries²⁰ predicts an angle for total transmission and zero reflection of the waves (the Brewster Angle) for polarizations such that the electric field is parallel with the plane of incidence. For the case of the electric field perpendicular to the plane of incidence, a continuous increase in reflected power with increase of the angle of incidence is predicted. The experiments described above showed a decrease in attenuation (an increase in transmitted power) near the apparent Brewster angle for parallel electric fields and the expected decrease in transmitted power with incidence angle for perpendicular fields.

Experiments with dummy propellant charges (cast in the shape of a solid propellant rocket grain with an internal star perforation) were described in the above report. Of interest to the present investigation was the attenuation observed at 10 GHz when microwaves were passed through the grain in the axial direction. (The grains were cast in bakelite tubes 10 inches long by 3-1/2 inches in diameter, having the above mentioned star perforation). For grains having no internal imperfections, less than 1/2 db attenuation was noted.

Microwave measurement techniques have found considerable application in the study of shock and detonation wave velocities. For this application, microwave techniques are clearly indicated because of the difficulty of employing any other method without disturbing the progress of the shock wave. The highly ionized region immediately following a strong shock provides an excellent microwave reflector, and the shock tube normally employed can be easily selected for dominant mode (TE_{11}) cylindrical waveguide propagation. Shock wave velocities are high, and when reflected and incident waves are mixed, a "beat" or Doppler frequency of several KHz is produced, which is easily handled electronically. Further, for shock tube applications, there is little difficulty involved in calculating the guide wavelength since the filling material is air or a light gas, having near free space electromagnetic properties.

The literature contains many references to the use of microwave techniques for shock and detonation wave measurements. In 1957, Hey, Pinson and Smith²¹ described an arrangement for measuring shock velocity in argon. A signal at 5.0 GHz was injected at the extreme downstream end of the tube. The tube had a cross sectional area of 5.4 cm^2 , producing a guide wavelength of 8.08 cm, while allowing only single mode microwave propagation. A shock was produced in argon by the use of hydrogen at 30 atmospheres. A shock Mach number of approximately 10, corresponding to a velocity of about 3.2 km/sec. was measured by combining the incident signal from the oscillator with the reflected signal from the shock in a crystal mixer. The Doppler effect produced

by the oncoming shock was thus measured. Shaping circuits converted the crystal output to a series of sharp pulses, the interval between each representing travel of the shock wave through a distance of 4.04 cm ($1/2$ guide wavelength). For convenience of measurement, the number of pulses was reduced by a factor of four, and resolution was thus limited to averaging the velocity over 16.16 cm intervals.

Cawsey²² and others employed the above mentioned microwave method for measurement of detonation velocities in solid explosives. The work included a discussion of microwave theory applicable to the prediction of the shape of the "interference fringes" (to use optical terminology) produced by the mixing of the incident and reflected waves. It was noted that more symmetric fringes produced better resolution, and in theory infinite resolution of the shock velocity would be allowed as a limit for the case of perfect symmetry. Their apparatus employed a hybrid or "magic" tee arrangement for mixing the sent and reflected waves. The frequency (34.5 GHz) was chosen for single mode propagation in the circular guide containing the solid explosive, and for good resolution. Extreme care was taken to minimize reflections other than those from the detonation wave, and very symmetric fringes were produced, allowing $1/4$ wave (approximately 2mm) resolution. The dielectric properties of a number of explosives, including tetryl, TNT, PETN and RDX in a paraffin binder were measured at 34.5 GHz. All were found to be relatively low loss dielectrics, the highest loss tangent being 0.0037

for crystalline PETN. A detailed description of detonation wave velocity measurement in tetryl was given. It was estimated that mean velocity of the detonation wave was measured correct to approximately two per cent. Principal error possibilities that were recognized included the degree of coincidence of the detonation front and the microwave reflection plane, the accuracy of parameter estimation (for example, density of the sample under test) and the accuracy of the photographic recording process employed.

Recently, other investigators have refined the above techniques for special studies. Johnson²³ employed 10 to 33 GHz microwaves to study transient growth to detonation in ammonium perchlorate and Composition C-4. Velocity-distance curves were derived from the data. The microwave wavelength was determined in the test charges by observing the number of wavelengths traversed by a detonation front as it moved through a charge of known length. Attention was given to the launching of a pure mode in the test samples. A pure mode could not be launched in a 1-inch diameter by 6-inch long charge at 24 GHz, but was obtained in samples under four inches long with four square-inch cross sections. A small diameter polystyrene rod waveguide was placed against the base of the sample, which was then treated as an infinite dielectric medium. Dunn and Blum²⁴ employed electronic signal conditioning for better data presentation. Using a 2.7 GHz signal, measurement of shock velocity in a 3-inch diameter, 30-foot shock tube was facilitated by clipping of the 20-40 KHz Doppler signal to produce a square wave output. A

similar signal generated by a 1.42 GHz signal in a 6-inch diameter, 112-foot shock tube was fed to a discriminator, so that changes in Doppler frequency due to shock wave speed variations appeared at the discriminator output as a d.c. level change. A resonance technique was employed by Aro and Walsh²⁵ to determine the frequency for best transmission in their shock tube. A brass slug was moved in the tube to simulate a shock front, and TM_{01} guide wavelengths were determined experimentally in this way. Results were compared with measurements by electronic counter, triggered by wires along the tube.

Discussion

Burning rate measurement in solid propellant devices has been identified as an item of major concern in the design and testing of such devices. The review of literature has shown that there has been much interest in the subject, and that a variety of techniques has been investigated. Each of the techniques reviewed has a range of applicability dependent upon the fundamental operating principles. The material which follows is intended to discuss the strengths, weaknesses and applicability of the various burning rate measurement methods.

Techniques involving fuze wires or altered propellant geometry for detection of flame front passage are limited to closed bomb devices or special test motors. The requirements for placement of the flame front detection devices dictate a special design for their use, or may eliminate an application altogether. Further, devices such as fuze

wires may affect the burning of the propellant near them, especially in small scale devices. Such devices must also be incremental in nature; that is, the burning rate must be sampled at intervals limited by the practical requirements of placing the flame front indicators.

Probe and embedded wire techniques have been the object of considerable interest, and reliably sense burning rate when properly designed. Probes of the resistance wire, thermocouple and radioactive type have been investigated. If embedded in unburned propellant, a probe must have heat transfer properties so as to prevent coning, presenting difficult and special design problems for each application. It is obviously undesirable to require special casting or loading techniques to accommodate the probes. Such techniques are usually incremental, the interval of sensing of the burning rate being dependent upon the spacing of the sensing elements. (The continuous measurement radioactive probe technique is an interesting exception.) The simple reliability of probe techniques is unsurpassed, however, and a thermocouple probe technique is employed in the subject investigation to verify the measurements made.

A fundamental advantage is gained when employing any of the techniques involving externally generated fields or waves for burning rate measurement, whether electric or sonic. The unburned propellant and the combustion zone are not subjected to the influence of foreign mechanical devices. Further, no special fabrication techniques are required to locate probes, wires, etc. Unless excessively high power

PAGE 36 MISSING
FROM ORIGINAL
DOCUMENT

associated with x-rays of high intensity, and the present high cost of the technique.

The capacitance technique as studied by Hermance is at present limited to use as a laboratory technique, essentially as a strand burner. The system produces a continuous burning rate measurement, but does not seem capable of local burning rate measurement.

Ultrasonic pulse-echo systems employ externally generated sound wave pulses passing through the unburned propellant. No special preparation of the propellant is required, and the technique would seem to be readily adaptable to a variety of test conditions. Although the pulse-echo technique is incremental in nature, pulse rates can easily be increased to the point that distance measurements are made at intervals corresponding to the roughness of the propellant burning surface. Obviously, no further resolution is possible. The system can thus be called a continuous burning rate measurement device. It would seem that the technique is adaptable to local burning rate measurements by "focusing" of the ultrasonic beam, but this has not yet been determined. Experimental work has shown that the technique is extremely sensitive to inclination of the burning surface. Burning rate measurement has been possible only for normal incidence of the ultrasonic waves at the burning surface. With presently available equipment, 1.5 inches of propellant is the maximum thickness that has been penetrated.

Doppler microwave burning rate measurement systems appear to have considerable potential for continuous burning rate measurement. Investigations covered in this review have proven the feasibility of the method.

Microwave energy is readily generated over a wide range of frequencies and power levels. Although not yet investigated, the microwave Doppler signal contains instantaneous burning rate information, and thus qualifies as a continuous technique. The electromagnetic character of microwaves permits optical-type focusing, and local measurement of burning rates is thus possible, probably to a greater extent than with any other system. Miniaturized flight-weight microwave systems are well known, and the same technology would enable the design of an on-board burning rate measurement system for flight tested solid propellant rockets. The principal difficulty would appear to be with the microwave energy losses in propellants, which have been found to be high. Based on the review of literature just presented, further investigation of the microwave Doppler technique is deemed necessary and desirable. The use of near millimeter wavelengths for better resolution in measurement of burning rates under actual rocket motor combustion conditions has yet to be investigated. Study of collimating devices for focusing of the microwave energy is also indicated, both for measurement of local burning rates and for higher gain or utilization of the available microwave energy. More efficient data reduction techniques must be found to make use of the continuous burning rate information contained in the microwave Doppler signal, and to make the process easier and faster. It is felt that investigation in these areas is required to advance the microwave burning rate measurement technique. This need and the established

potential of the method as one of the best burning rate measurement techniques led to the subject investigation.

VIII. THE INVESTIGATION

Objective

The objective of the subject investigation was to apply Doppler microwave techniques to the continuous local measurement of solid rocket propellant burning rates under actual rocket motor combustion conditions.

Microwave Burning Rate Measurement

This technique of measurement of the regression rate of burning solid propellants bears a close relation to Doppler radar techniques. Fundamentally, the process involves the observance of the rate of phase change of microwaves reflected from the burning interface of a solid propellant. The rate of phase change is measured with respect to a convenient phase datum, normally a portion of the transmitted microwave signal. Mixing of the transmitted and received waves gives rise to a periodic time varying difference signal whose frequency is commonly referred to as the Doppler frequency. One cycle of the Doppler frequency signal is generated as the received microwave signal completes 360 degrees of phase change with respect to the datum, the transmitted microwave signal. The relation of rate of phase change to generated difference frequency is given by the differential equation

$$\frac{d(\varphi_T - \varphi_R)}{dt} = \frac{d\varphi_r}{dt} = 2\pi f_D \quad . \quad (8.1)$$

Continuous measurement of the frequency f_D provides continuous knowledge of the value of the microwave phase angle time derivative. This derivative is related to the time derivative of the position of the burning surface, the burning rate, in a manner to be discussed in a following section. In terms of integrated forms, noting that

$$2\pi f_D = \frac{d\varphi_D}{dt} \quad (8.2)$$

then

$$\varphi_r = \varphi_D + c \quad . \quad (8.3)$$

Equation (8.3) states that one degree of phase change of the difference signal corresponds to one degree of phase change of the received microwaves with respect to the transmitted microwaves. An alternative picture of the microwave burning rate measurement technique is thus presented. If the relation of phase change of the microwave signals to the movement of the burning surface is known, then the measurement of phase change of the difference signal will provide this information.

The fundamental aspects of the technique may be visualized with the aid of Figure 7. A microwave source of appropriate power and frequency is employed to generate the microwave energy. This energy is divided and propagates along guided paths A and B. That which travels along path A proceeds to the rocket motor under test. Quantities of the microwave energy traveling into the rocket motor are reflected

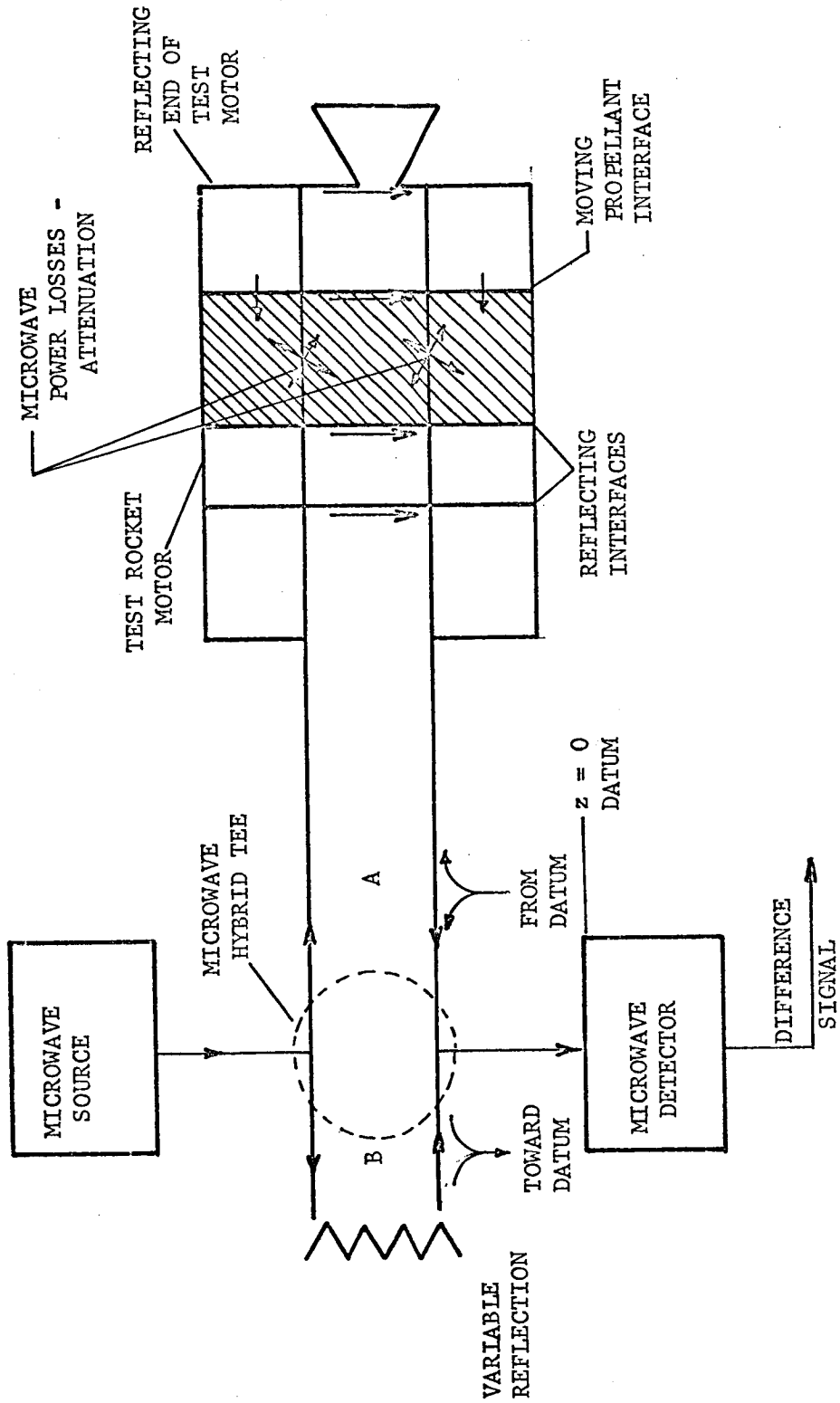


Figure 7. - Microwave burning rate measurement technique.

from each stationary interface. A reflecting interface exists at every discontinuity of dielectric constant within the test rocket motor. A quantity of microwave energy is also reflected from the moving interface formed by the transition from solid propellant to gaseous propellant; that is, the burning surface. Some microwave energy continues to the end of the test motor and is reflected. Microwave power losses occur all along the propagation paths and are especially large in the solid propellant itself. A composite reflected microwave signal propagates in the return direction along path A and is directed to the microwave detector. The reflection generated at the moving propellant interface is of varying phase, as has been mentioned. This varying phase microwave energy is combined with that reflected from the stationary interfaces, which is of constant phase. Microwave energy from the variable reflection propagates along path B and is also directed into the microwave detector. The process of directing the reflected microwave energy A and B to the detector produces a vector subtraction of the two signals, causing a difference signal to be produced by the detector. While the above discussion describes the basic features of the technique, it is necessary to discuss each of the aspects in more detail.

Microwave Source

The possible choices of a microwave source for the present investigation were quite broad. The frequency of the microwaves could quite practically range down to the regions of the microwave spectrum where

free-space wavelengths are several centimeters, and up to the frequencies representing the limits of present day technology. There is a fundamental advantage to be gained by the use of higher frequencies. The wavelength of a wave, defined as the distance in which the phase of the wave increases by 2π at any instant, is given by

$$\lambda = \frac{v_p}{f} \quad (8.4)$$

where v_p is the phase velocity.

Calculation of the free space wavelength for frequencies of 300 MHz, 3 GHz and 30 GHz gives values of approximately 1 meter, 10 centimeters and 1 centimeter respectively. It has been mentioned that the difference signal produced by the microwave detector changes in phase an amount equal to the change of phase of the microwave energy reflected from the burning surface with respect to the transmitted microwave energy. The movement of the burning surface results in a phase change of 2π radians for translation through a distance of one-half wavelength.

If the wavelength of 30 GHz radiation in solid propellant were 1 centimeter, then 1/2 centimeter of burning would produce a 2π phase change. Errors in phase measurement would therefore produce errors in burning rate measurement of small percentages of 1/2 centimeter, rather than of 5 or 50 centimeters in the 3 GHz or 300 MHz case.

Another advantage of higher frequencies is that all components, including collimating devices, can be smaller, improving the ability of the system to sense local burning rates. Higher attenuation losses and more difficulty in generating high frequency microwaves is a disadvantage. As frequencies increase, losses in solid propellants become

greater, as do transmission losses in waveguide. The conclusion from the above observations is that the choice of microwave frequency is a trade-off, involving several factors. In the subject investigation, 30 GHz microwaves were employed.

Modulation of the microwave energy is an important consideration. A microwave source which allows audio frequency square wave modulation of the transmitted energy is desirable. The use of audio frequency AC amplifiers for the detected signal is permitted, with the associated gain and stability advantages. Square wave modulation at 1000 Hz was used in the subject investigation.

Microwave Reflections

The microwave reflection problem of interest to the subject investigation is that of a uniform plane wave normally incident on a plane dielectric interface. The reflection of principal interest is that from the burning surface - combustion zone interface. Of secondary interest are the reflections occurring from other interfaces in the microwave path, since energy which would have reached the burning surface reflection interface is diverted and effectively lost. The following analysis explains the reflection phenomenon and allows an estimate of the magnitude of the various reflections.

Consider the boundary between two regions of different dielectric materials. Plane and reflected waves traveling in dielectric region 1 in the z direction may be represented by the complex quantities

$$E_x^{(1)} = E_o \left[\exp(-jk_1 z) + \Gamma \exp(jk_1 z) \right]^* \quad (8.5)$$

$$H_y^{(1)} = \frac{E_o}{\eta_1} \left[\exp(-jk_1 z) - \Gamma \exp(jk_1 z) \right]$$

where Γ , the reflection coefficient is defined by equation (8.5).

The transmitted wave in region 2 may be expressed in terms of E_o by introducing a transmission coefficient T . Thus,

$$\begin{aligned} E_x^{(2)} &= E_o T \exp(-j k_2 z) \\ H_y^{(2)} &= \frac{E_o}{\eta_2} T \exp(-j k_2 z) \end{aligned} \quad (8.6)$$

The wave impedance, η , in a region is defined by the ratio of the electric and magnetic fields. This definition has been used to form equations (8.5) and (8.6). It is a fundamental principle that wave impedances normal to a material boundary must be continuous. Thus,

$$\eta_1 = \frac{E_x^{(1)}}{H_y^{(1)}} = \frac{E_x^{(2)}}{H_y^{(2)}} = \eta_2 \quad (8.7)$$

Substituting equations (8.5) and (8.6) in (8.7) and solving for Γ at $z = 0$,

$$\Gamma = \frac{\eta_2 - \eta_1}{\eta_2 + \eta_1} \quad (8.8)$$

Noting that E_x must be continuous at the boundary $z = 0$,

* Notation used for the description of electromagnetic fields is outlined in Appendix A.

$$T = 1 + \Gamma = \frac{2\eta_2}{\eta_2 + \eta_1} \quad (8.9)$$

For the purposes of the subject investigation, it is desirable to compute the values of Γ and T for the various interfaces. For a perfect dielectric,

$$\eta = \sqrt{\frac{\mu}{\epsilon}} \quad (8.10)$$

For real dielectrics, η is complex and is given by

$$\eta = \sqrt{\frac{\mu}{\epsilon'}} + j \frac{\epsilon''}{2\epsilon'} \sqrt{\frac{\mu}{\epsilon'}} \quad (8.11)$$

While the dielectrics of interest here are not perfect, ϵ'' is, in general, much less than ϵ' and a satisfactory estimate of reflection parameters may be made under the perfect dielectric assumption. Thus, under the conventional dielectric assumption that $\mu_1 = \mu_2 = \mu_0$,

$$\Gamma = \frac{\sqrt{\epsilon_1'} - \sqrt{\epsilon_2'}}{\sqrt{\epsilon_1'} + \sqrt{\epsilon_2'}} \quad \text{and} \quad T = 1 + \Gamma = \frac{2\sqrt{\epsilon_1'}}{\sqrt{\epsilon_1'} + \sqrt{\epsilon_2'}} \quad (8.12)$$

The effect of reflections with respect to the complex electric intensity is of particular interest, since the electric intensity is the measured quantity in the burning rate measurement system. Referring to equation (8.5), the reflection coefficient is seen as the ratio of the amplitude of the reflected electric intensity vector to the incident. Thus, for good transmission properties at an interface, ideally $\epsilon_1' = \epsilon_2'$, or no interface of a-c capacitvity exists. For a

strong reflection such as is desired at the burning surface, maximum inequality in ϵ_1' and ϵ_2' is desirable.

Information concerning the relative phase of the incident and reflected waves may also be obtained employing equation (8.5). Note that the wavelength of the radiation in region 1 is

$$\lambda_1 = \frac{2\pi}{k_1} \quad (8.13)$$

Substituting equation (8.13) into equation (8.5) for the electric vector,

$$E_x^{(1)} = E_o \left[\exp \left(-j \frac{2\pi}{\lambda_1} z \right) + \Gamma \exp \left(j \frac{2\pi}{\lambda_1} z \right) \right] \quad (8.14)$$

The distance z is taken with reference to the boundary between region 1 and 2. Equation (8.14) shows that between every point $z = N \frac{\lambda_1}{2}$, where N is an integer, a phase change of 2π occurs between the incident and reflected waves. Similarly, a movement of $\frac{\lambda_1}{2}$ of the boundary between regions 1 and 2 will cause a phase change of 2π between the incident and reflected waves. Such an interface movement is the effect of burning surface movement as propellant is consumed. Thus, the burning of a distance of one wavelength in the propellant gives rise to a 2π phase shift between incident and reflected waves, as was stated at the beginning of the discussion of microwave techniques. This relative phase shift is preserved throughout the microwave burning rate measurement system and appears at the detector, which senses electric intensity.

It is obviously necessary to know the wavelength of the microwave radiation in the propellant. Measurement of the phase shift or rate of phase shift as the propellant burns is of no value unless the relation to burning surface movement is known. There are many acceptable methods for determining the wavelength of the radiation in the propellant. One of the best techniques is to record the number of complete cycles (2π phase shifts) that the reflected signal completes with reference to the incident signal during the burning of a known length of propellant. Since it has been established that a 2π phase shift indicates that $1/2$ wavelength of propellant has been burned, equation (8.15) may be employed to calculate the wavelength.

$$\lambda_{\text{propellant}} = \frac{2L_p}{N} \quad (8.15)$$

where L_p is the length of the propellant burned.

N is the number of 2π phase shifts observed (not necessarily an integer).

This method is particularly adaptable to experimental arrangements such as in the subject investigation where the length of the propellant charge can be easily and accurately measured. There is a clear advantage in that the wavelength is determined under the actual experimental conditions. It is quite possible to calculate the wavelength from other data, however. The wavelength of radiation in a dielectric medium may be expressed in terms of the a-c capacitivity, ϵ' , as

$$\lambda = \frac{2\pi}{k'} = \frac{2\pi}{\omega \sqrt{\mu\epsilon'}} \quad (8.16)$$

It has already been mentioned that the permeability, μ , of a non-magnetic dielectric material is assumed equal to that of free space with good accuracy. Hence, a knowledge of ϵ' allows the calculation of λ for any frequency ω . There are a variety of methods for the measurement of properties of dielectric materials. These include free-space methods, measurements in waveguides and resonance techniques. Summary discussions and reference to the various methods are given in Chapter 6 of Reference 20. It should be noted that extreme care must be exercised in computing wavelengths from one experiment for application to another. If this is to be done, a detailed analysis of the modes of propagation of the microwaves in both experiments is absolutely necessary. If possible, wavelength determination under the actual experimental conditions as described initially is desirable.

While relative phase relations between incident and reflected waves are maintained throughout the microwave burning rate system, wavelengths vary according to the propagational conditions. One wavelength exists in the waveguide connecting the experimental apparatus, another in the plexiglass used in various positions and yet another in the propellant. It is possible to observe the movement of a standing wave in the waveguide connecting the microwave source and the test rocket motor (path A in Figure 1). A standing wave is formed in this waveguide by addition of incident and reflected waves according to

equation (8.5) modified for waveguide propagation. As the burning surface moves, the changing phase of the reflection will cause the position of a particular phase point on the standing wave to move. If this point were tracked, it would be found that for each propellant wavelength burned, the phase point would move two waveguide wavelengths, according to principles already discussed. Since the waveguide wavelength is considerably longer than the wavelength in the propellant, a tracking device would travel at a faster rate than the propellant surface. This rate could be related to the propellant burning rate through knowledge of the relative wavelengths, but it is not, in raw form, the propellant burning rate.

Waveform of the Detected Signal

As shown in Figure 7, the microwave signals reach the detector by way of paths A and B. The initial power splitting and the directing of the return signals is accomplished by means of a hybrid junction in the microwave burning rate measurement system. The properties of this junction are such as to cause the vector difference of waves traveling from directions A and B to appear in the detector arm. The following analysis results in an equation for the detected output signal. This equation is necessary for following analyses and for data reduction.

Assume that the complex electric intensity of the incident wave in a waveguide is represented by equation (8.17)

$$E_i = |E_i| \sin \frac{n\pi}{b} y \exp (j \gamma z) \quad (8.17)$$

The form of equation (1) is adjusted for TE modes in rectangular waveguide. Detailed discussion of the origin of the various terms may be found in Reference 26. For the purposes of the present analysis, the term $\sin \frac{n\pi}{b} y$ is not required since the detector is at the center of the waveguide and the field variation in the y direction is of no concern. The propagation constant γ is related to the free space wave number k , but this relation is not needed in this analysis. For TE propagation in rectangular waveguides only an E_x is present. The analysis can therefore proceed with notation of the form as in equation (8.18).

$$E_{x_i} = |E_{x_i}| \exp (j \gamma z) \quad (8.18)$$

For the present purposes, the "incident" direction is understood to be away from the waveguide hybrid tee of Figure 7, in either the A or B direction. Reflected waves are assumed to be traveling toward the detector of Figure 7, from either the A or B direction. A reflected wave occurring because of some discontinuity in the wavepath may be represented as

$$E_{xr_1} = |E_{xr_1}| \exp \left[-j (\gamma z + \varphi_1) \right] \quad (8.19)$$

where φ_1 is a constant phase shift indicating arbitrary location of the reflecting surface (1). In general,

$$|E_{xr_1}| < |E_{x_1}| \quad (8.20)$$

A second reflected wave due to a second discontinuity is

$$E_{xr_2} = |E_{xr_2}| \exp[-j(\gamma z + \varphi_2)] \quad (8.21)$$

The composite reflected wave from n reflections may then be represented as

$$E_{xr_c} = E_{xr_1} + E_{xr_2} + \dots + E_{xr_n} \quad (8.22)$$

It is easily shown that like-traveling waves may be summed as in equation (8.22) to a single expression of the form

$$E_{xr} = |E_{xr}| \exp[-j(\gamma z + \varphi)] \quad (8.23)$$

Composite reflected waves as represented by equation (8.23) reach the crystal detector from paths A and B, through the hybrid tee. It is a property of the hybrid that the vector difference of waves traveling from the A and B direction is formed in the detector arm. Thus, the signal as seen by the detector is

$$E_D = E_{xr_A} - E_{xr_B} \quad (8.24)$$

Again referring to Figure 7, the composite signal E_{xr_A} contains signals originating from many reflections as well as the reflection from the burning surface E_{xr}' . It is convenient to lump all constant reflections, whether from the A or B direction, into a composite static

reflection term E_{xr_c} . The moving reflection due to the burning surface is thus separated. Equations (8.25) outline the steps.

$$\begin{aligned}
 E_D &= E_{xr_A} - E_{xr_B} \\
 E_D &= E_{xr_A}' - (E_{xr_B} + E_{xr}') \quad (8.25) \\
 E_D &= E_{xr_C} - E_{xr}'
 \end{aligned}$$

In expanded form, the above result may be expressed as in equation (8.26).

$$E_D = |E_{xr_C}| \exp(-j \gamma z) - |E_{xr}'| \exp[-j(\gamma z + \varphi)] \quad (8.26)$$

where φ is the variable phase angle of the reflection from the burning surface,

$$\varphi = \frac{2\pi z_P}{\frac{\lambda_P}{2}}$$

The crystal detector is an amplitude sensitive device having square law response. It is not sensitive to the phase of the detected wave, but only to amplitude changes which occur because of changing phase relations among the reflected waves. The crystal response may be represented by equation (8.27).

$$V_{\text{crystal}} = c |E_D|^2 \quad (8.27)$$

Calculation of the absolute value of equation (8.26) and substitution in equation (8.27) results in the following expression.

$$V_{\text{crystal}} = c \left(|E_{\text{xr}_c}|^2 + |E_{\text{xr}'}|^2 - 2 |E_{\text{xr}_c}| |E_{\text{xr}'}| \cos \varphi \right) \quad (8.28)$$

It may be seen from equation (8.28) that the voltage output from the crystal detector is a sinusoid if the quantities $|E_{\text{xr}_c}|$ and $|E_{\text{xr}'}|$ remain constant. The quantity $|E_{\text{xr}_c}|$ remains essentially constant during burning rate measurement, but $|E_{\text{xr}'}|$, the reflection from the burning surface, increases in magnitude as the propellant burns. From equation (8.28), the contribution of $|E_{\text{xr}'}|$ to V_{crystal} is included in the term $|E_{\text{xr}'}|^2$ and in the amplitude of the $\cos \varphi$ term. If $|E_{\text{xr}'}|$ increases at a sufficiently slow rate with respect to the effective circular frequency of $\cos \varphi$, the quantity $|E_{\text{xr}'}|^2$ may be filtered from the signal along with $|E_{\text{xr}_c}|^2$ by employing a high pass filter. Such a filter was used in the subject investigation. The variation of $|E_{\text{xr}'}|$ still appears in the signal, however, as the variable amplitude of the $\cos \varphi$ term, which is transmitted through the high pass filter with little effect. The received signal is therefore, according to equation (8.28), a sinusoid of varying amplitude according to $|E_{\text{xr}'}|$.

The signal waveform deduced above is the output of a single crystal detector mounted in the difference arm of a single hybrid tee. Equation (8.28) has been used to show that the signal is basically a sinusoid, distorted and changed in amplitude by the changing level $|E_{\text{xr}'}|$. While the distortion is reduced by filtering the output signal,

the varying amplitude of the sinusoidal component makes automatic, continuous data reduction a difficult problem. It is possible to obtain a signal which is more easily handled, however. The use of two hybrid tees in a microwave bridge arrangement as described in Reference 27 permits the display of $\tan \phi$ directly on an oscilloscope. This method appears to have considerable merit, but requires more equipment than was available for the subject investigation.

Microwave Attenuation

It is inevitable that microwave power losses will occur in the measurement system. While power is not the measured quantity, the direct result of power loss is reduction of signal voltage level at the detector, and difficulty in performing the required measurements. An analysis of the loss mechanisms and an estimate of their magnitudes is desirable.

The propagation of microwave energy in a waveguide is not loss free. The magnitude of loss incurred depends upon the frequency and propagational mode of the microwaves in the particular guide employed. Attenuation in ordinary waveguide propagating the TE mode, as employed in the present investigation, is well documented. For standard RG - 96/U waveguide and a microwave frequency of 30 GHz, attenuation of approximately 1.3 db/meter is observed²⁸, representing a loss of 16 per cent in measurable signal voltage per meter of waveguide run. Thus, it is seen that these losses cannot be neglected, especially when

microwave power is limited and for the case of long waveguide runs as are necessary for safety when measuring rocket motor burning rates. The signal path in the subject investigation was approximately four meters long.

Solid propellants are, electromagnetically speaking, lossy dielectric materials. Microwave energy is absorbed in such materials by molecular scale processes whose description is outside the scope of the phenomenological approach taken here. What is desired is a method which will allow the calculation of the complex permittivity of the propellant from the test data. Solid propellants are assumed to be non-magnetic dielectrics, with real magnetic permeability μ equal to that of free space.

The vector wave equation for propagation of plane waves in lossy media is

$$E_x = E_0 \exp(-jkz) = E_0 \exp(-k''z) \exp(-jk'z) . \quad (8.29)$$

It may be noted that the equation is identical in form to the usual equation for loss-free media. However, the wave number k is assumed complex, and is written as

$$k = k' - jk'' . \quad (8.30)$$

where k' is the "intrinsic phase constant".

k'' is the "intrinsic attenuation constant" .

The definitions of phase velocity and wavelength for uniform plane

linearly polarized waves are altered from the usual representation replacing k with k' ,

$$v_p = \frac{\omega}{k'} \quad \text{and} \quad \lambda_p = \frac{2\pi}{k'} = \frac{v_p}{f} \quad (8.31)$$

The components of the complex permittivity $\epsilon = \epsilon' - j\epsilon''$ are expressible in terms of the complex wave number. Thus, for "good" dielectrics ($\epsilon' \gg \epsilon''$),

$$\epsilon' = \frac{k'^2}{\omega^2 \mu} \quad \text{and} \quad \epsilon'' = \frac{2k''}{\omega} \sqrt{\frac{\epsilon'}{\mu}} \quad (8.32)$$

where

ϵ' is the a - c capacitivity of the material.

ϵ'' is the dielectric loss factor.

μ is the a - c inductivity, assumed equal to that for free space with little error.

Combining equations (8.31) and (8.32) for λ_p and ϵ' and solving for ϵ' ,

$$\epsilon' = \frac{1}{\mu} \left(\frac{2\pi}{\omega \lambda_p} \right)^2 = \frac{1}{\mu} \left(\frac{1}{f \lambda_p} \right)^2 \quad (8.33)$$

Equations (8.29) through (8.33) permit the calculation of the complex permittivity of solid propellants.

The wavelength λ_p of the radiation in the solid propellant may be determined, since the propellant charge is a known length and it is known that two cycles of the received signal occur for every wavelength displacement of the burning surface. Thus,

$$\lambda_p = \frac{2L_p}{N} \quad (8.34)$$

where L_p is the length of the propellant charge.

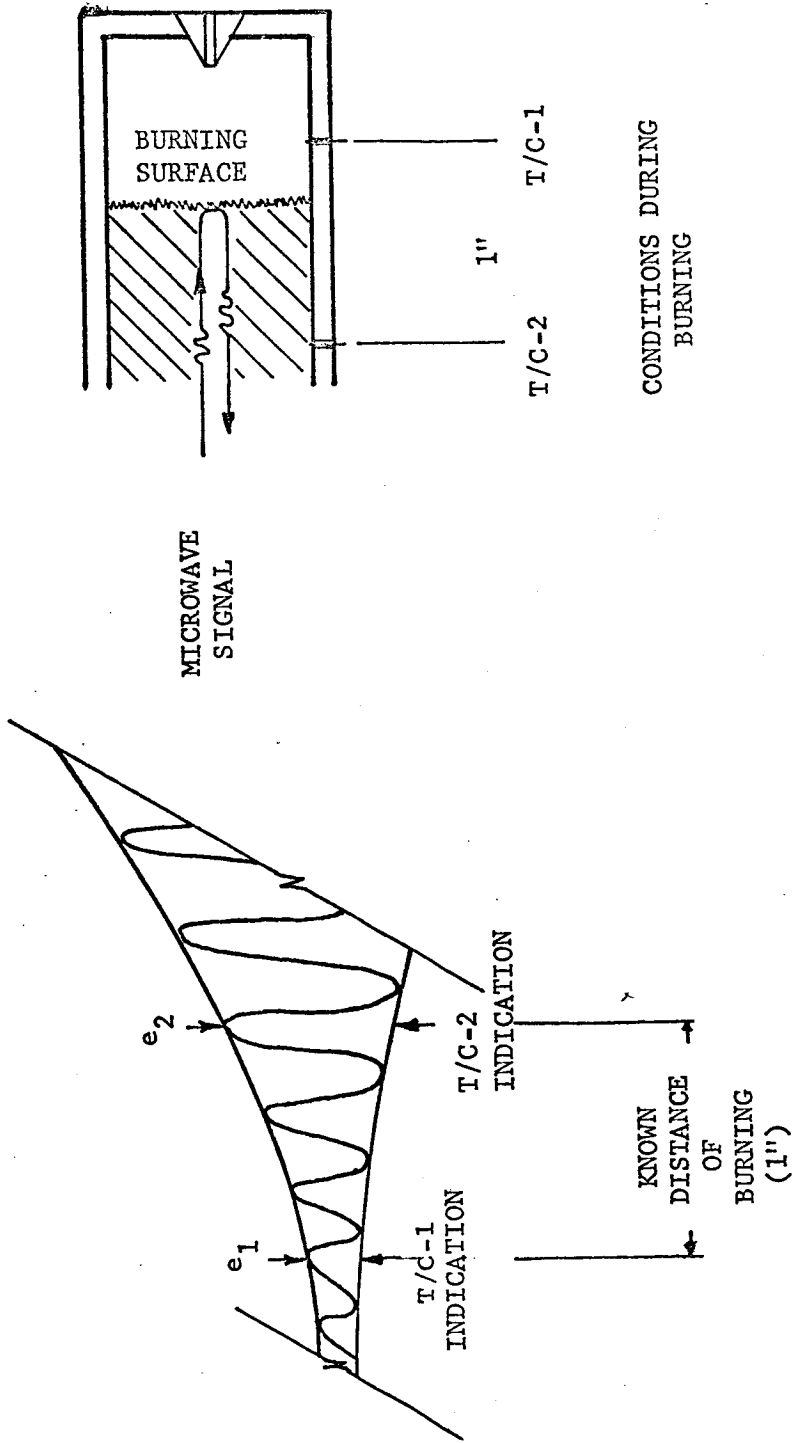
N is the number of complete cycles of the recorded signal.

Employing equation (8.33), ϵ' may be determined for the particular frequency used, under the assumption $\mu = \mu_0$.

The attenuation of the measured signal results in a relatively low level signal at the start of burning, and a steady increase in signal level as burning progresses. This effect is due solely to the decrease in signal path length resulting from combustion of the propellant, since all other signal loss mechanisms remain constant. The relative increase in signal level that is observed may be used to determine k'' of the propellant. Equation (8.32) may then be employed, with the value of ϵ' as determined above, to calculate ϵ'' .

Referring to Figure 8, the experimental arrangement was such that the received signal levels could be correlated with a measured burning surface movement. Indication of burning surface passage was provided by thermocouples in the test rocket motor wall, spaced one inch apart. In Figure 8, two such thermocouples are shown, designated T/C-1 and T/C-2. The increase in signal level e_1 to e_2 corresponds to a decrease of two inches in the distance that the microwave signal must travel.

It is necessary to correlate the change of signal amplitude as produced by the detector with the change of rms amplitude of the



OBSERVED SIGNAL AS
BURNING OCCURS

Figure 8. - Models for attenuation analysis.

reflected signal from the burning surface. From the waveform analysis, the equation for the detected signal is

$$V_{\text{crystal}} = c \left(|E_{\text{xr}_c}|^2 + |E_{\text{xr}'}|^2 - 2 |E_{\text{xr}_c}| |E_{\text{xr}'}| \cos \varphi \right) \quad (8.35)$$

assuming square-law response of the detecting crystal. A capacitor is incorporated in the signal path to the recorder to eliminate the non-periodic components $|E_{\text{xr}_c}|^2$ and $|E_{\text{xr}'}|^2$ from the record. Thus, the recorded signal is actually

$$V_{\text{recorded}} = \left(- 2 |E_{\text{xr}_c}| |E_{\text{xr}'}| \cos \varphi \right) G \quad (8.36)$$

where G is the lumped gain of all amplifiers in the signal path (note that this is constant only for the case of no variable gain elements in the signal path). It is seen that the amplitude of the recorded signal, shown as e in Figure 8, varies directly with $|E_{\text{xr}'}|$ and thus is a measure of $|E_{\text{xr}'}|$, the rms amplitude of the wave reflected from the burning surface. By measuring e_1 and e_2 , and noting that the signal path has changed a total of two inches, a direct measure of the attenuating properties of the propellant is obtained.

Referring to equation (8.29) the amplitude of the wave E_x is

$$|E_x| = E_0 \exp(-k'' z)$$

Assuming that $|E_x|$ represents the wave reflected from the burning surface $|E_{\text{xr}'}|$, then, for a traveling wave,

$$e_1 \propto \left| E_{xr} \right|_1 = E_o \exp (-k'' z_1) \quad (8.37)$$

$$e_2 \propto \left| E_{xr} \right|_2 = E_o \exp (-k'' z_2) \quad (8.38)$$

Dividing equations (8.37) and (8.38)

$$\frac{e_1}{e_2} = \frac{E_o \exp (-k'' z_1)}{E_o \exp (-k'' z_2)} \quad (8.39)$$

Equation (8.39) may be solved for k'' . Thus

$$k'' = - \frac{\log_e e_1/e_2}{(z_1 - z_2)} \quad (8.40)$$

where it is noted that $(z_1 - z_2)$ is the change in path distance for the microwave signal, equal to two inches in Figure 8. Returning to equation (8.32), ϵ'' may now be calculated.

If the value of the complex permittivity is available for a particular propellant, a reverse procedure may be employed to compute the loss of signal in the propellant. This information, and knowledge of the sensitivity of the crystal detector used permits an estimate of the microwave power required for a given thickness of propellant.

Summary

The analyses presented in this section summarize the underlying principles of the microwave burning rate measurement technique. In addition, results of the analyses provide the basis for the data reduction techniques employed. The conclusion of the waveform analysis

section is that the detected signal approximates a sinusoid of varying amplitude. Thus, reduction of the data contained in the detected signal can be made with reference to a sinusoid. Information necessary to calculate the complex permittivity of the propellant is also contained in the detected signal. Two firings of the test rocket motor were made especially for the purpose of computing the complex permittivity. Results will be found in the appropriate section.

Reference to the preceding analyses will show that those regarding microwave reflections and attenuation are made assuming plane wave propagation in unbounded media, while signal waveforms are analyzed with reference to TE waveguide propagation. Obviously, microwave signal additions and mixing take place in the waveguide system and the waveform analysis is appropriate. The reflection and attenuation of the microwaves which are of interest to this investigation occur in the solid propellant. A lens-corrected horn was employed in the experimental apparatus to collimate the microwaves. The end burning rocket motor that was used is of sufficient diameter with respect to the horn-waveguide system that microwave propagation conditions were assumed to be those in unbounded media.

Experimental Apparatus

The apparatus employed in the subject investigation may be conveniently grouped as (1) instrumentation, (2) simulator, and

(3) test rocket motor and equipment. The following section describes the experimental arrangement in detail.

Instrumentation.

The microwave and associated equipment that was employed may be described as a 30 GHz recording microwave interferometer. Figure 9 shows a block diagram of the system, and Figure 10 shows a photograph of the actual experimental setup. Microwave power at 15 GHz was generated by a Hewlett-Packard SHF signal generator Model 626A. The microwave power was square wave amplitude modulated by the generator at a frequency of 1000 Hz. Output power level was approximately +7 dbm*. The 15 GHz microwave energy was directed to a frequency doubler, Hewlett Packard model 938A. The output of the doubler was a 30 GHz, 1000 Hz amplitude modulated microwave signal, at a power level of approximately -6 dbm. This signal was the source signal for the microwave measurements.

An absorption type frequency meter was inserted in the microwave system at the output of the frequency doubler. Absorption frequency meters absorb a large amount of microwave power when tuned to resonance, and transmit nearly all of the supplied power when tuned far from resonance. Measurement of the output frequency of the doubler was thus possible on a sampling basis but not continuously or during a data run.

* 1 dbm = 1 milliwatt.

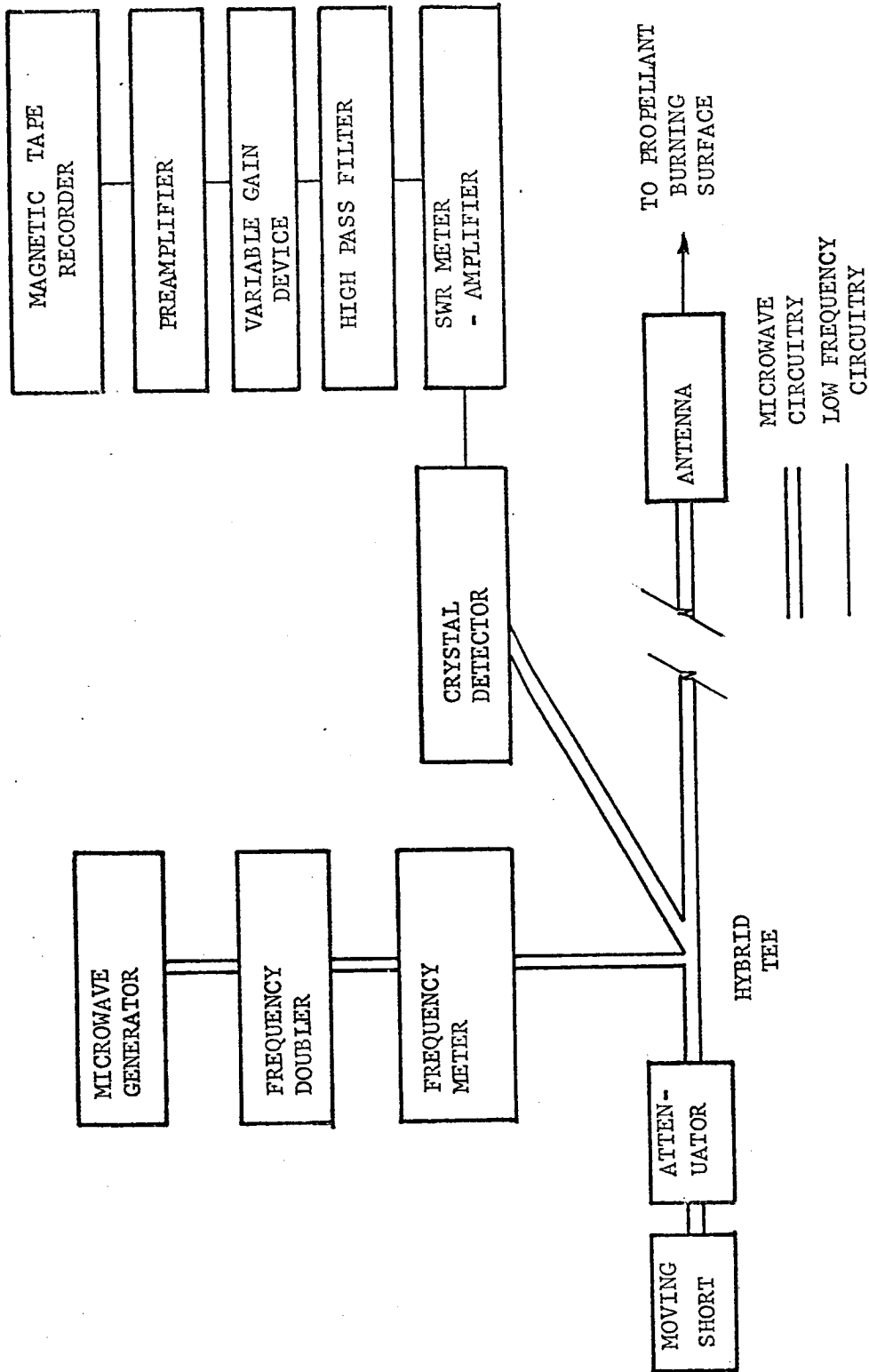


Figure 9. - Block diagram of microwave burning rate measurement system.

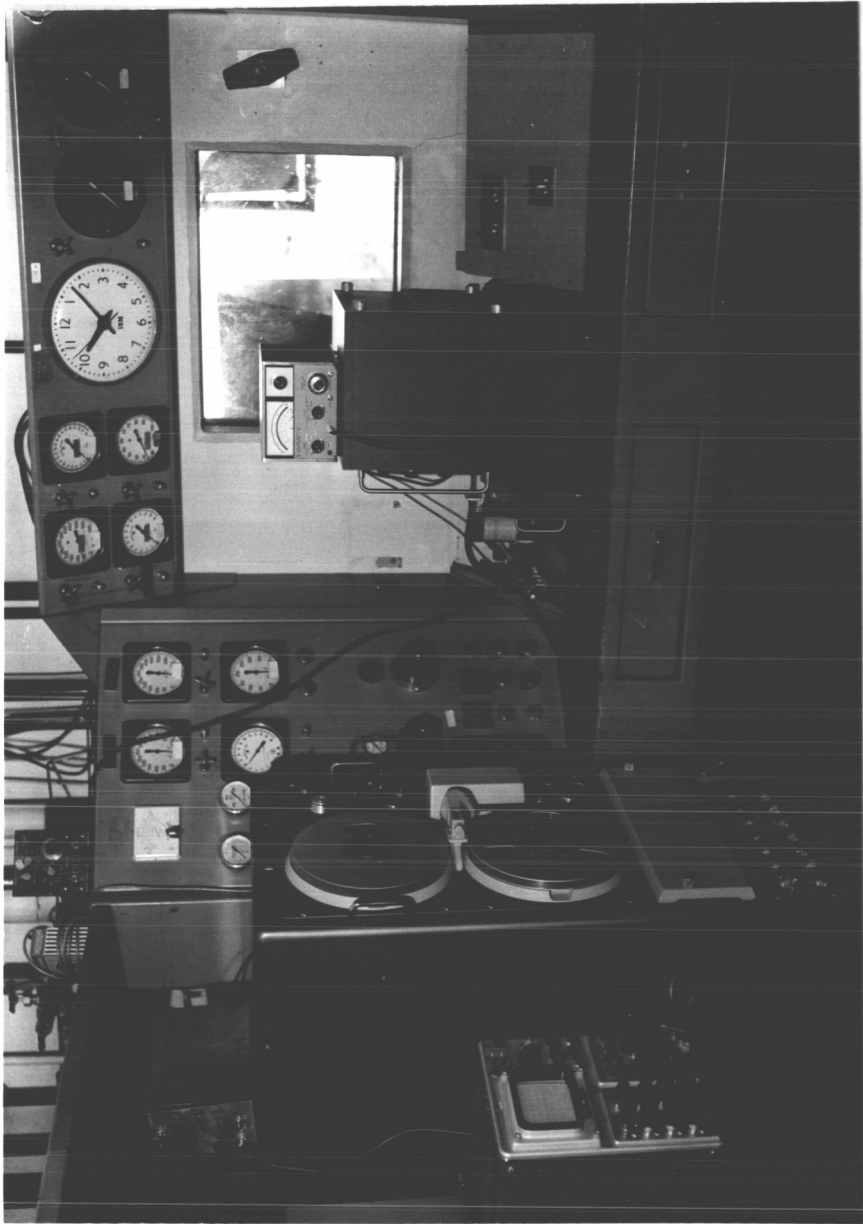


Figure 10. - Photograph of microwave burning rate system equipment arrangement.

A waveguide hybrid tee was used to divide the microwave power between the measuring and the reference leg. That portion of the microwave power which traveled to the reference leg passed through a 0-20 db attenuator and was reflected from a movable short. The attenuator provided control of the level of the reference signal and the movable short provided control of the phase. A reference signal of controllable amplitude and phase could thus be provided at the crystal detector. The portion of the microwave power that was fed to the measuring leg of the system traveled through approximately eight feet of rigid waveguide and a short section of flexible waveguide to reach the antenna, a microwave lens-corrected horn designed to produce a collimated beam.

Figure 11 shows the design of the microwave lens-corrected horn and the window-seal piston assembled in the test rocket motor. The microwave horn and lens were specially designed for this application as described in Appendix B. The horn was a lead-antimony casting, and the lens was machined from methyl methacrylate stock. The window-seal piston was designed for sealing pressures up to 1000 psi, while allowing passage of the microwaves. It was machined from methyl-methacrylate stock.

The crystal detector employed was a Hewlett-Packard Model K422A, having a nominal sensitivity of 0.1 mv/microwatt. The output of the crystal detector was amplified by a Hewlett Packard Model 415E SWR meter. This meter served as an indicator of the output level of the

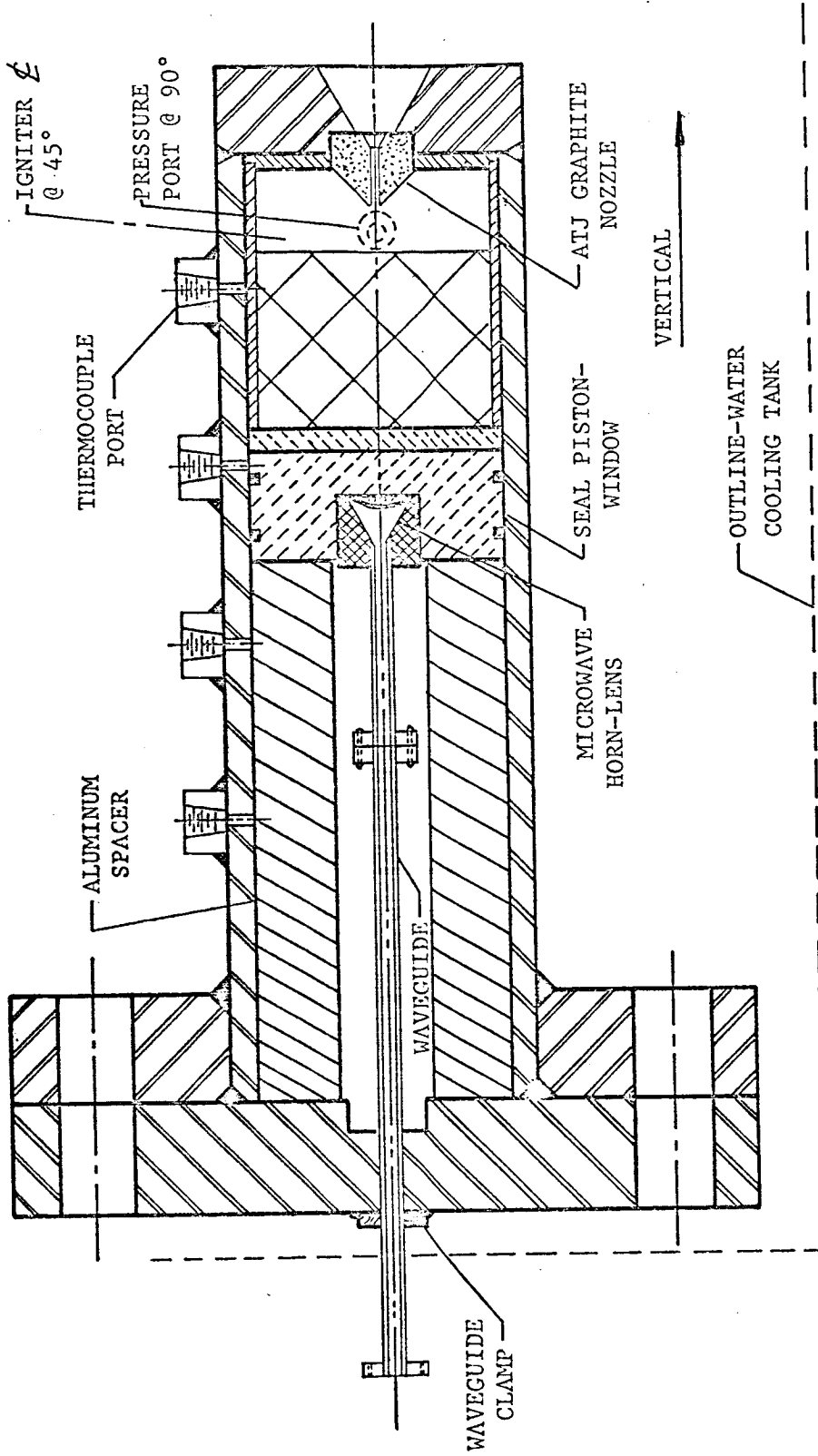


Figure 11. - Test rocket motor assembly.

crystal and was used for initial set up of the measuring system. The SWR meter was also provided with a recorder output connection, which allowed the measured signal to be fed to the remaining system components. The SWR meter was actually a narrow band high gain amplifier, tunable to modulating frequencies near 1000 Hz. The requirement of the meter/amplifier for 1000 Hz modulation was met by the modulation capability of the signal generator, already described. A detector was incorporated in the meter so that the recorder output was a d-c voltage level proportional to the amplitude of the 1000 Hz modulated input signal.

A high pass filter was incorporated in the circuitry leading to the variable gain device. The need for this filter was discussed in the waveform analysis section. As shown in Figure 12, the filter was a 6 μ f capacitor feeding a load of 10 K ohm. The response of this filter to sinusoidal input voltages was tested and found to be essentially flat to 5Hz, down 2 db at 3Hz, and down 9db at 1 Hz. The constant level or slowly varying portions of the signal were blocked by the filter. The sinusoid carrying the burning rate information was at a frequency of approximately 3.5 Hz, and so was passed relatively unattenuated.

The variable gain device shown in Figure 12 was found to be necessary to accommodate the widely varying signal amplitudes which were obtained during a test run. Because of the burning of the propellant and the resultant shortening of the microwave signal path,

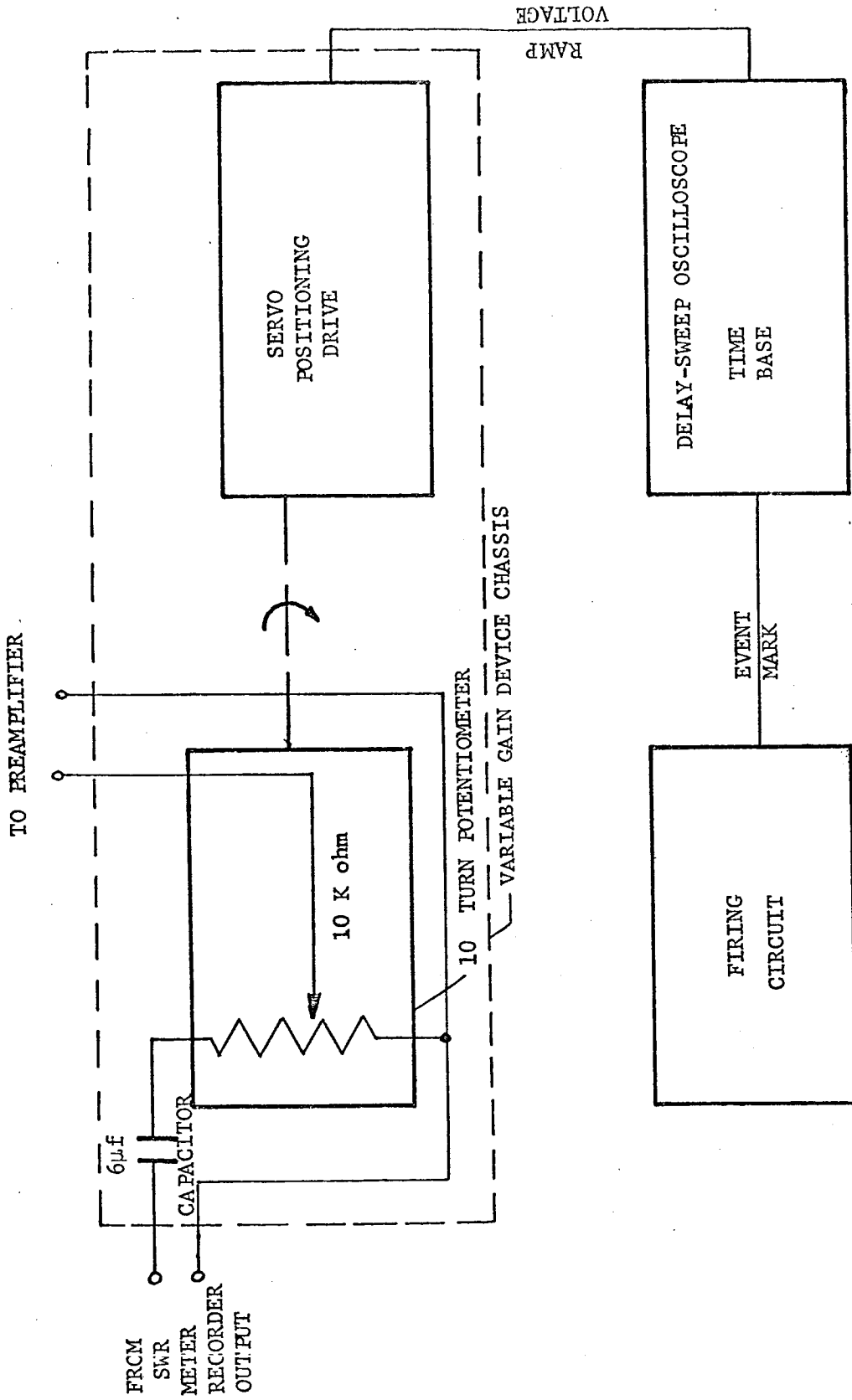


Figure 12. - High pass filter and variable gain device.

the amplitude of the detected signal was observed to vary from an initial low to approximately 20 times the initial value at burnout of the propellant. Since the recording equipment would not accommodate such a wide dynamic range, the variable gain device was constructed. It was basically a null-seeking servo positioning drive, attached to a gain reducing 10-turn potentiometer. The servo was driven from a delay-sweep oscilloscope timebase. It was thus possible to control the variable gain device automatically during a test firing. The oscilloscope time base was adjusted to a predetermined delay and sweep rate and triggered by the firing pulse to the test motor. Typically, the arrangement provided a 3.5 second delay so that gain was not reduced while the signal was small. An approximate four second period of gain turn-down then resulted in a gain reduction of 9 to 9.5 times. The total amplitude change of the recorded signal during a test run was thus greatly reduced.

The signal output of the variable gain device was channeled to a preamplifier, actually a part of the magnetic tape data recording system. Data from the test runs were recorded for later playback and data reduction. The magnetic tape recorder was a Sanborn Model 2000, operated in the FM mode at a tape speed of 60 inches per second.

The tape recorder was simultaneously used to record other data during the test runs. Figure 13 shows the general data acquisition system arrangement. The pressure within the test rocket motor was measured by a four-active arm strain gage pressure transducer. The

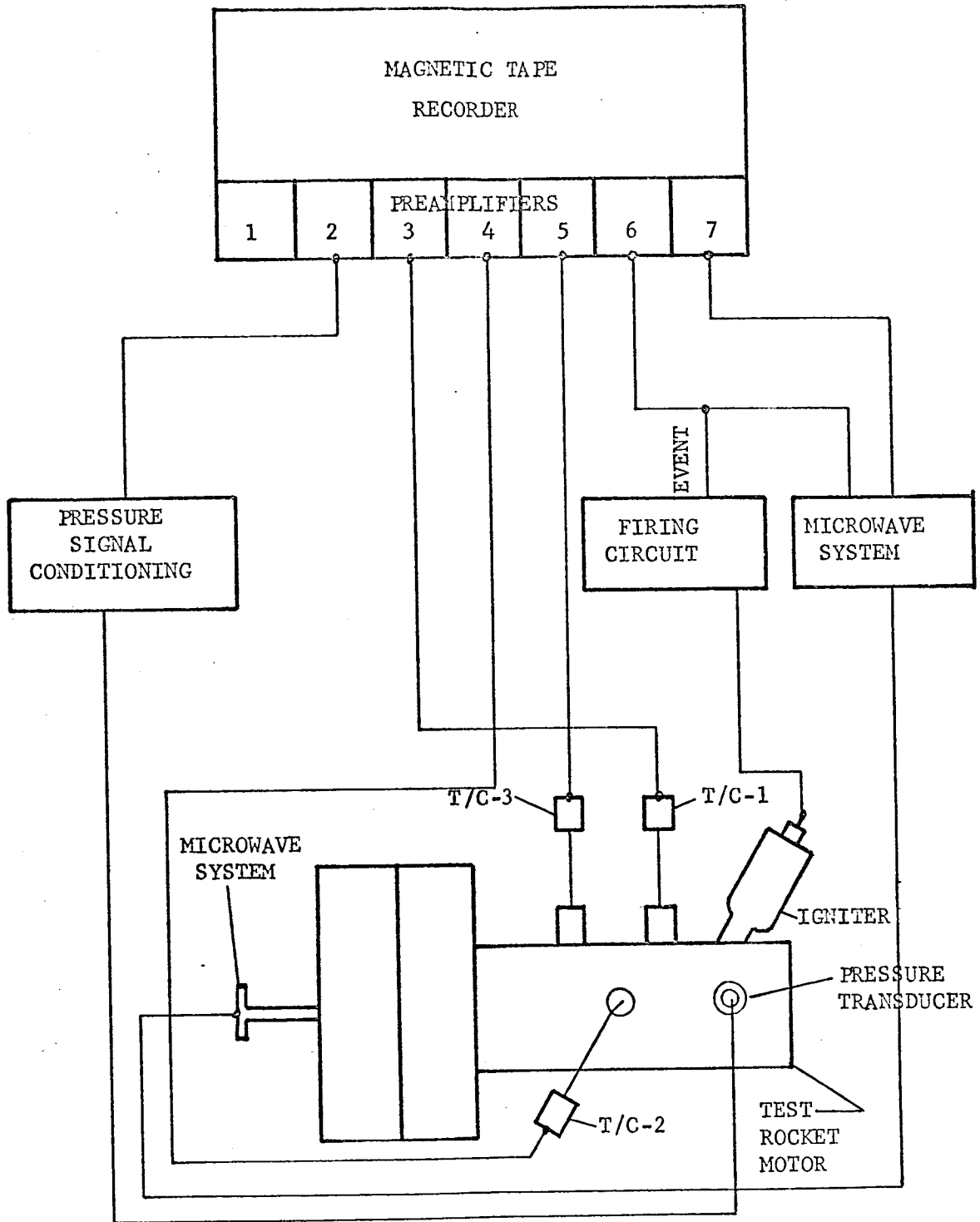


Figure 13. - Data acquisition system arrangement.

pressure signal conditioning system provided excitation, balancing and electrical calibration for the system. Electrical calibration was accomplished by placing a precision resistor across one arm of the transducer bridge. The equivalent pressure signal which was produced was compared with known pressures provided by a dead weight tester. It was thus possible to provide an electrical pressure calibration immediately prior to each test run.

Thermocouples were provided in the test motor to record the passage of the flame front as the propellant burned. The stainless steel sheathed thermocouples extended into the propellant through pressure glands in the test motor wall. Arrival of the flame front at each thermocouple position produced a sudden, sharp change in the thermocouple emf. This was recorded as shown in Figure 13. Since the exact position of the thermocouples was known, measurement of the elapsed time between two thermocouple signals provided a check on the average burning rate between the two thermocouples.

The firing circuit, in addition to providing firing current to the igniter, was arranged to provide an event marking pulse to the tape recorder. This event pulse also triggered the delay sweep on the oscilloscope. The microwave data were recorded on the tape recorder, through the instrumentation already described.

Simulator

Two types of simulated tests were conducted in the course of the experimental investigation. The first employed an oil-filled

cylinder in which a movable reflecting piston was driven. Figure 14 shows the arrangement. The microwave burning rate measurement system was tried in various configurations, leading finally to the system previously described. The basic simulator was designed with the best information then available to simulate the movement of the propellant burning surface inside the test rocket motor. The case of the simulator was two-inch O.D. methyl methacrylate with a wall thickness of 0.125 inches. One end was provided with an O-ring seal to allow movement of a shaft. This shaft was connected to a piston-like reflector which traveled inside the tube. The entire tube was covered with aluminum foil. The tube was closed at the other end with 1/8-inch methyl methacrylate sheet, which provided a microwave window into the simulator. A self-reversing variable speed lead screw drive was designed and constructed to drive the reflector in the simulator. It was thus possible to conduct experiments with the microwave instrumentation while the simulator piston moved forward and backward at a fixed speed. The simulator provided much valuable information for the design of the microwave system that was used in the actual rocket motor tests. Certain other simulated tests were conducted in the course of the investigation. As these were primarily procedural in nature, they are described in the later section, Test Procedure, Simulated Tests.

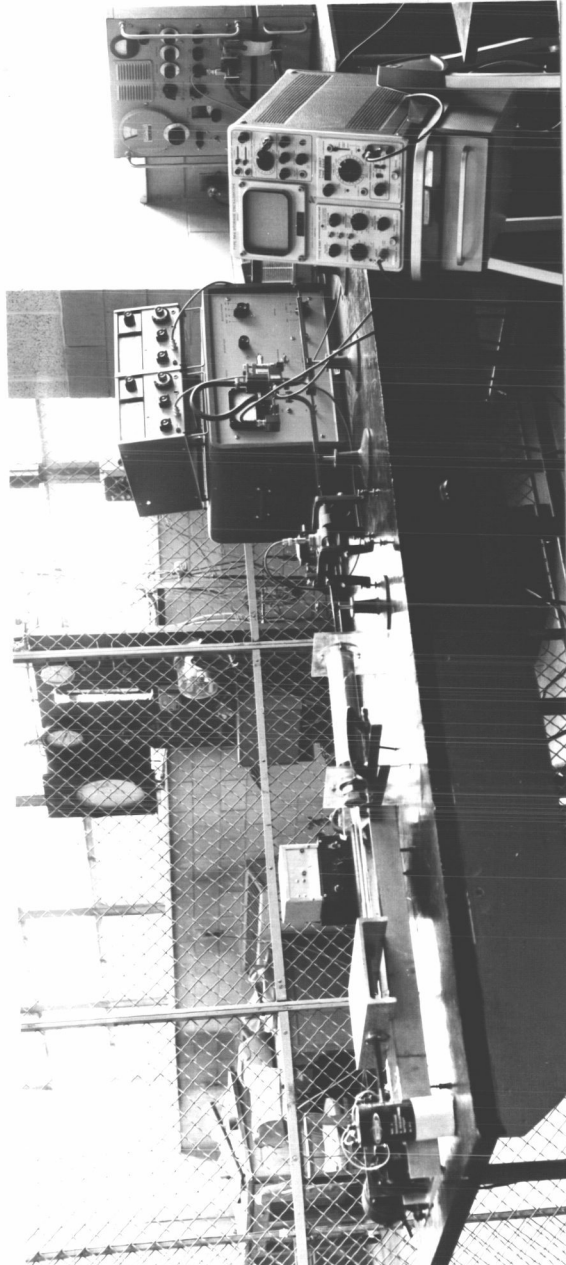


Figure 14. - Photograph of end burning rocket motor simulator used for simulated tests.

Test Rocket Motor

A special test rocket motor was designed and constructed to conduct burning rate measurements under actual rocket motor combustion conditions. Figure 11 shows an assembly drawing of the test rocket motor, and Figure 15 a photograph of the actual unit. Several design concepts were incorporated into the test rocket motor. The submerged nozzle was designed to eliminate the plugging effect on small nozzles caused by aluminized propellants. The nozzle was fabricated from Union Carbide Corporation ATJ graphite and set in silicone rubber to allow easy changing for each firing while providing a good seal. Two pressure taps were provided for pressure transducer connections, although only one was normally used. Conax catalog number MPGL thermocouple glands with lava seals were provided at one inch intervals. Conax 304 stainless steel sheathed iron constantan thermocouples (catalog number SS6J-G) having an outside diameter of 0.062 inches were used in the number required by the particular test. The sheathed thermocouples were inserted through drilled holes in the insulating liner and into the propellant to indicate flame front passage. The test motor was designed to accept up to seven thermocouples, for use with propellant charges up to eight inches long. The sliding seal piston design allowed the selection of any propellant charge length, with an appropriate spacer. Opening of the test motor was from the fore end, with a standard slip-on and blind pipe flange providing

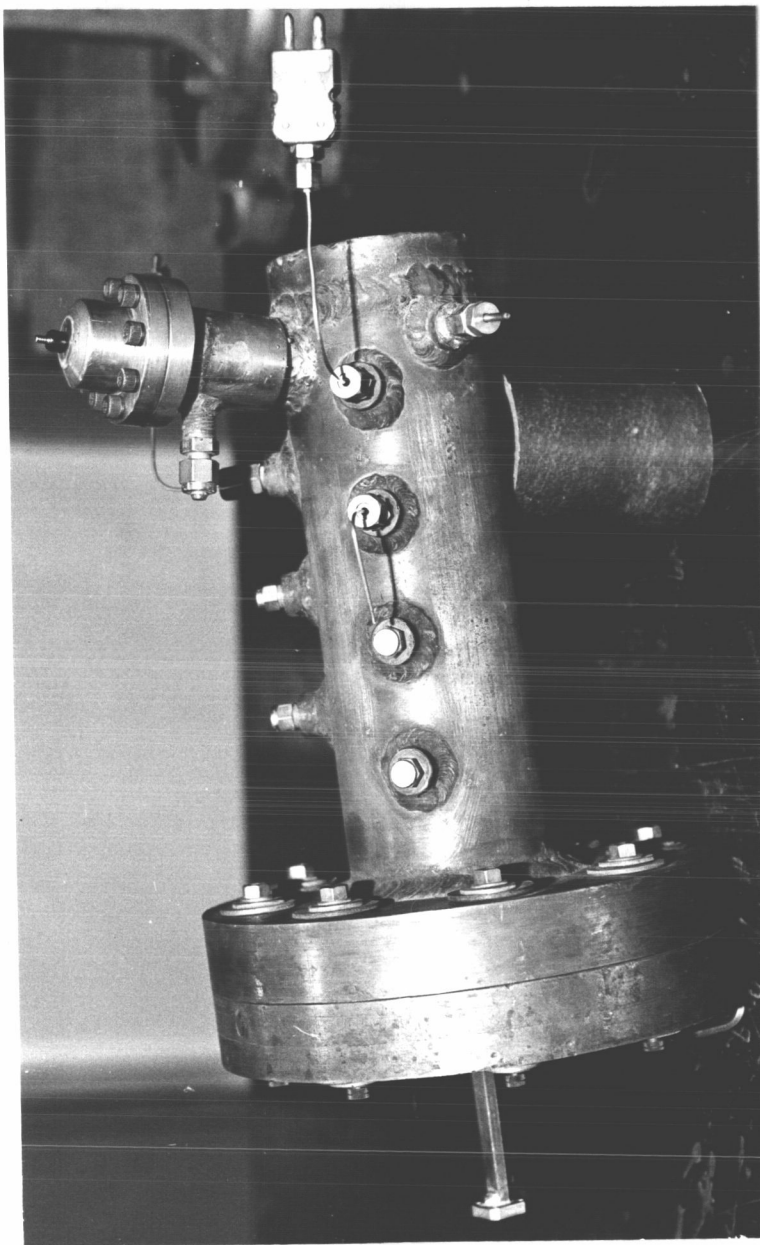


Figure 15. - Photograph of test rocket motor.

both access and overpressure protection. Eight fasteners through the flanges were designed so as to break at approximately 3500 psi, with expected operating pressures up to 1200 psi. The microwave waveguide entered the test motor through a slot in the blind flange.

The igniter system used on the test rocket motor was finalized after several tests. The arrangement used a model aircraft engine glo plug as the initiator, with a firing voltage of approximately 24 volts. Booster material was one gram of magnesium-teflon granules, contained within the igniter chamber. The propellant surface was coated with a nonconductive pyrotechnic film igniter supplied by Redel Corporation, Anaheim, California, their type NR. Hot particles from the magnesium teflon sprayed the propellant surface through the igniter nozzle, igniting the film igniter. The film igniter served both as a sustainer and to spread the ignition flame over the entire propellant surface, providing even ignition. The system proved to be quite reliable, producing smooth, reproducible ignition of the test rocket motor.

The entire test motor was mounted in a tank, the outline of which is shown in Figure 11. This tank served as a shield and provided for water cooling of the test motor. While calculations indicated that the insulating liner around the propellant charge was adequate for protection of the motor during operation, water cooling was provided to reduce heat soak after firings. The main concern was

for the methyl methacrylate seal piston, which would begin to soften at temperatures near 200 °F. Water cooling was used for all firings, and heating problems caused no difficulty. For firings, the test motor and tank were placed within a shield as shown in Figure 16.

The solid propellant charges were cast in a 3/16" thick, 2.880 inch outside diameter cylindrical asbestos phenolic liner which served both as an insulator and as a burning restrictor. The propellant was bonded to the asbestos phenolic tube with approximately 1/16-inch of a liner material, designated UR101-L. The propellant formulation was designated TPH-8009, and was manufactured by NASA Langley Research Center. Table 1 shows the approximate formulation of this propellant (the exact formulation is classified), as well as that for two other propellants used in the experimental work. Propellants AeReCo 1 and 2 were manufactured by Aerospace Research Corporation, Roanoke, Virginia. These propellants were used for preliminary evaluation of the penetrability of propellants by the microwaves and for burning tests at atmospheric pressure. It was originally planned to conduct tests using propellants AeReCo 1 and 2 in the test rocket motor. However, difficulties with the propellants were encountered and this was not done. The problems are discussed in Section IX, Discussion of Results.

Figure 17 shows the arrangement of the propellant charge and associated insulators as assembled into the rocket motor. The

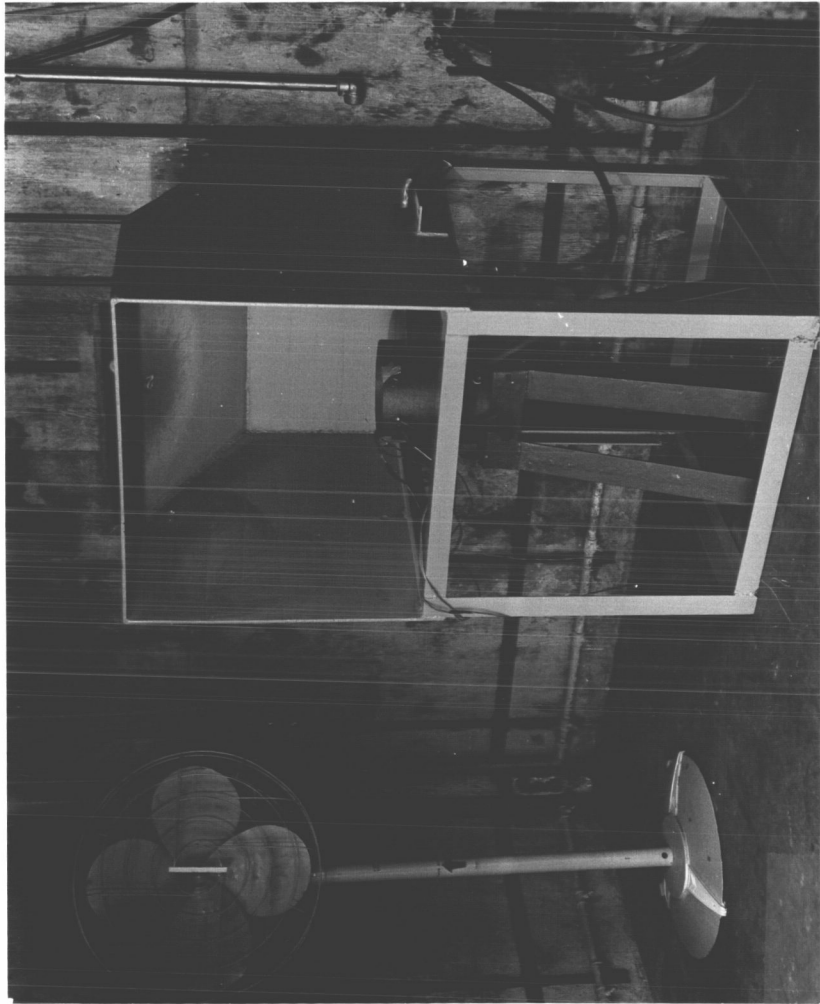


Figure 16. - Photograph of shield, cooling tank and rocket motor
in test cell.

TABLE 1

TEST PROPELLANT FORMULATIONS

Propellant Ingredients, Per Cent by Weight

	TPH-8009	AeReCo 1	AeReCo 2
Ammonium Perchlorate	70	70	60
Binder*	14	30	24
Aluminum	16	--	16

Formulations given are approximate.

* - Binder material for propellant TPH-8009 was PBAA (polybutadiene acrylic acid), for both AeReCo propellants a polyurethane.

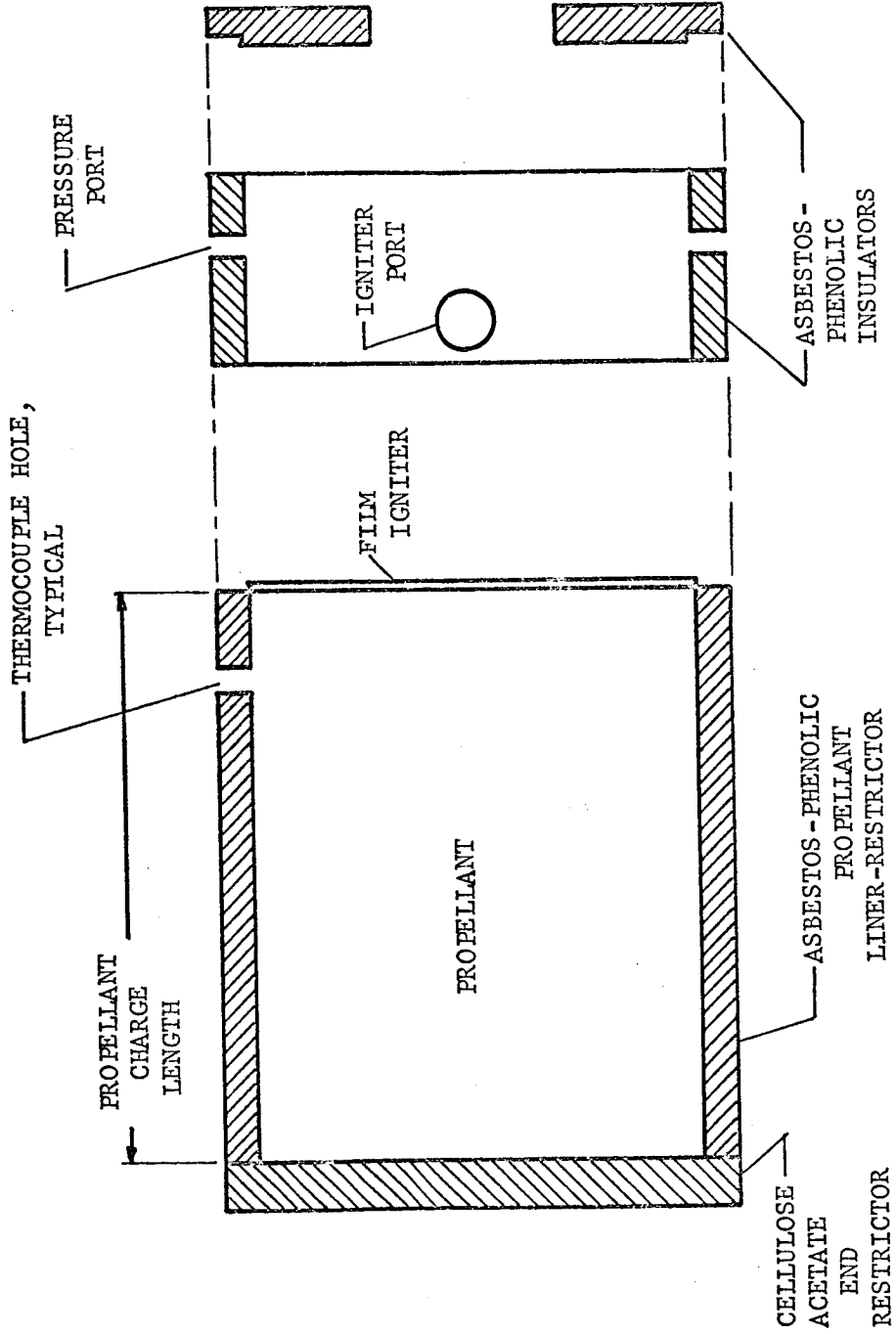


Figure 17. - Propellant charge and insulators.

propellant charge was cut to the desired length for each test. For the subject investigation, firings 1 through 20 utilized two-inch nominal length charges, while for firing number 21 a three-inch charge was used.

Following is a detailed list of the equipment used in the subject investigation.

List of Equipment.

1. Microwave signal generator. - Hewlett-Packard Co., Palo Alto, California, Model 626A, serial 609-00987, range 10 to 15.5 GHz, maximum power output 10 milliwatts. The microwave signal generator was used to generate and modulate the microwave energy.
2. Microwave frequency doubler. - Hewlett-Packard Co., Palo Alto, California, Model 940A, range 26.5 to 40 GHz, and power output approximately 0.3 milliwatts. The frequency doubler was used to convert the 15 GHz output signal of the signal generator to the 30 GHz signal used in the test work.
3. Microwave frequency meter. - Hewlett-Packard Co., Palo Alto, California, Model R532A, serial 552, range 26.5 to 40.0 GHz. The frequency meter was used to measure the frequency of the microwave signals.
4. Hybrid tee. - Demornay-Bonardi Co., Pasadena, California, Model DBD-650, waveguide type RG-96/U. The hybrid tee was used to split the microwave power between the measuring and reference legs, and to mount the crystal detector.
5. Variable attenuator. - Demornay-Bonardi Co., Pasadena, California, Model DBD-430, waveguide type RG-96/U, range 0-20db. The

variable attenuator was used to adjust the level of the reference signal

6. Adjustable waveguide short. - Hewlett-Packard Co., Palo Alto, California, Model R920A, waveguide type RG-96/U. The adjustable short was used to provide a variable phase reference reflection.
7. Crystal detector. - Hewlett Packard Co., Palo Alto, California, Model R422A, waveguide type RG-96/U, sensitivity 0.1 mv/ μ w. The crystal detector was used as the microwave detector in measurement system.
8. Microwave waveguide. - Various manufacturers, Type RG-96/U, frequency range 26.5 - 40.0 GHz, outside dimensions 0.360 x 0.220 inches. The microwave waveguide was used for the various microwave connections in the system, including the approximately eight foot run from the microwave generator to the test rocket motor.
9. Microwave lens - corrected horn. - Virginia Polytechnic Institute, Blacksburg, Va., Model 1, nominal 14db gain horn with collimating lens, outside diameter 1.250 inches. The lens-corrected horn was used to collimate and launch the microwaves into the test rocket motor.
10. Test Rocket Motor. - Virginia Polytechnic Institute, Blacksburg, Va., Model 1, designed to accept one to eight-inch solid propellant charges cast in 2.880 inch O.D. asbestos phenolic tubes, design pressure range to 1200 psig., water cooled. The test rocket motor was used to contain the propellant charges during burning rate tests.
11. Thermocouple - seal glands. - Conax Corporation, Buffalo, New York, Model SS6J-GPJFC-MICL-8", iron - constantan stainless steel sheathed thermocouple, 0.062 inch outside diameter. The

thermocouples were used in the test motor to sense the passage of the flame front.

12. Pressure transducer. - Advanced Technology Laboratories, Model 111-1-3000-35-10-61, serial 6310, range 0-3000 psig., nominal bridge resistance 350 ohms, four active arm type. The pressure transducer was used to measure the combustion pressure of the test rocket motor.
13. Pressure Signal Conditioner. - Aerospace Research Corporation, Roanoke, Virginia, Model 1, excitation voltage 10.0 volts, range dependent upon transducer used. The pressure signal conditioner was used to excite and balance the pressure transducer bridge and to electrically calibrate the pressure transducer.
14. Dead weight tester. - Manning, Maxwell and Moore, Inc., Stratford, Conn., Type Ashcroft 1305B-50, range 0 to 5000 psig. The dead weight tester was used for absolute calibration of the pressure transducer and the electrical calibration resistor.
15. SWR meter. - Hewlett Packard Co., Palo Alto, California, Model 415E, serial 545-01289, frequency 1000 Hz. The SWR meter was used to amplify the signals from the microwave detector and to adjust the reference level in the microwave system.
16. Variable gain device. - Virginia Polytechnic Institute, Blacksburg, Va., Model 1, gain turndown range to 1/20. The variable gain device was used to limit the amplitude increase of the burning rate signal as the propellant burned.
17. Magnetic tape recorder - Sanborn Division, Hewlett-Packard Co., Waltham, Massachusetts, Model 2000, serial 257, speed 60 ips, 54kc FM electronics, with preamplifiers for up to 1 mv/v sensitivity, seven channels. The magnetic tape recorder was used to record all data generated during the test rocket motor firings.

18. Data recorder - Sanborn Company, Waltham, Massachusetts, series 150, serial 2945, model 154-100B, four channels, paper speeds to 100mm/sec. with AC-DC preamplifiers for up to 1 mv/mm sensitivity. The data recorder was used to read out data from the magnetic tape recorder.
19. Oscilloscope. - Tektronix Co., Portland, Oregon, Type 564, serial 003698, with four trace vertical amplifier, type 3A74, delay sweep timebase type 3B1. The oscilloscope was used to monitor signals throughout the data acquisition system and to drive the variable gain device.
20. Microwave power meter. - Hewlett-Packard Co., Palo Alto, California, Model 431C, serial 651-02377, range 0.01 to 10 milliwatts full scale, with Thermistor Mount Model R486A. The microwave power meter was used to measure microwave power at the point of entrance to the test rocket motor.

Test Procedure

The tests conducted during the subject investigation may be conveniently classified as those performed under simulated conditions, with combustion at atmospheric pressure, and with combustion at conventional rocket motor pressures in the test rocket motor. All simulated tests which did not involve propellant combustion were conducted in the laboratories of the Mechanical Engineering Department, Virginia Polytechnic Institute, Blacksburg, Virginia. Atmospheric pressure tests and those with the test rocket motor were conducted at Aerospace Research Corporation, Roanoke, Virginia, where hazardous test facilities were available.

Simulated Tests. - A variety of equipment development tests were performed with the simulator previously described. A majority of these tests were concerned with the choice and development of the microwave collimating device. Several different types of collimators could conceivably have been used. The test procedure involved setting the simulator at a constant speed, placing the collimating device under test at the end of the simulator, and observing the waveform of the signal produced by the rate sensing system. Microwave collimating devices which were tested included open waveguide placed against the simulator, cylindrical and rectangular polyrod antennas, open waveguide illuminated lenses, microwave horns and lens-corrected horns. Performance improved in the order named. The performance of the collimating system was judged with regard to the sinusoidal character and the relative amplitude of the waveform produced. It was noted early in the test work with the simulator that the waveform produced by open waveguide against the simulator was distorted and erratic. While this might be expected in view of the theoretical pattern for radiation from open waveguide, it was shown experimentally. Apparently the effect resulted from reflections within the simulator, as well as multimode propagation. Cylindrical and rectangular polyrod antennas were tested in various diameters and lengths. Construction materials included polyethelene, polystyrene and polymethyl methracrylate. Both straight and tapered rod antennas were sized in accordance with

the copious reference material available in the literature. While waveforms of the detected signal were improved, the quality of the signal using polyrod antennas never approached that produced by simple plano convex lenses illuminated by open waveguide at the focal point. This experience plus the fact that, at least in theory, it was possible to design a horn-lens combination to produce collimated radiation (i.e., plane phase fronts) led to the use of the lens-corrected horn. After the design and construction of the horn-lens, tests with the simulator produced the best waveform obtained. It should be noted, however, that waveforms obtained with the simulator were never of the sinusoidal quality which were obtained from actual combustion tests.

Additional tests were also conducted under simulated conditions. Blocks of live solid propellant, both TPH-8009 and AeReCo 1 and 2, were placed against the microwave collimator to determine penetrability of the propellants. The test method was to move a metal plate as a microwave reflector on one side of a propellant block, while beaming microwave energy from the other side. Indication of the movement of the metal reflector by the microwave system was taken as proof that the propellant block under test was being penetrated, and that the burning of the far propellant surface could possibly be sensed.

The pattern of the radiation produced by the horn-lens collimator was studied. The most satisfactory method involved the use of several

metal reflectors with circular holes cut on center. A cylindrical block of AeReCo 2 propellant 3-3/4 inches in diameter by 3 inches long was placed in front of the horn-lens collimator. A solid metal reflector was placed against the other end of the propellant and moved away from the propellant to a distance of 5mm. Since the wavelength of 30 GHz radiation in free space is 10mm, the 5mm movement produced a full cycle of the signal from the microwave measurement system. The maximum voltage value during this cycle was recorded. Subsequently, metal reflectors having circular holes of 1/2-inch to 2-1/2-inch diameter in 1/4" steps were placed in front of the propellant and moved as above and the voltage recorded. The per cent of influence of a reflector beyond a specified dimension with reference to a solid reflector could thus be measured and plotted. The data are presented in the Data and Results Section.

Atmospheric Tests.

While the simulated tests provided much valuable input to the design of the microwave burning rate measurement system, it was recognized that setup procedures, signal voltage levels, etc. could only be determined under conditions produced by actual burning of solid propellant. In order to avoid the relatively complex and expensive tests with the test rocket motor for microwave system shakedown, atmospheric pressure combustion tests were conducted.

For these tests, propellants AeReCo 1 and 2 were cast into the asbestos phenolic cylinders used for the liner in the test rocket motor. Charges were cut to lengths of 2, 4 and 6 inches and assembled into a wrapping of 0.010 inch thick aluminum foil, with the actual cellulose acetate restrictor, seal piston and microwave horn-lens in place (see Figure 11). The only mechanical difference from the actual test rocket motor firings was the lack of the steel pressure vessel. A steel plate frame was constructed to hold the assembly during tests. Figure 18 shows the frame and a test in progress. The propellant was ignited by flame from a propane torch. Thermocouple data were taken in addition to microwave data as a part of the operational check of the system. Operation of the measurement equipment and procedures during each atmospheric test were the same as those described for the test rocket motor firings below.

Test Rocket Motor Firings - Twenty-one firings of the test rocket motor were conducted using propellant TPH-8009. All firings produced usable microwave data except Number 1, which was intended as a shake-down test for the rocket motor.

Before each firing, the propellant charge to be tested was selected by use of X-ray data provided by NASA Langley Research Center and cut to length. The cellulose acetate end restrictor was glued to one end of the propellant using Testor's household cement. One thin coat of the film igniter was applied with a small paint

brush to the other end. The propellant-restrictor-igniter assembly was allowed to dry for a minimum period of 12 hours. The propellant assembly was then removed from the propellant process area to the test loading area.

Initial assembly of the test rocket motor involved the insertion of the end liner, spacer and propellant charge into the test motor. The ATJ graphite nozzle had previously been drilled to the desired size and set in the silicone rubber seal. The transducer pressure port, igniter, and thermocouple holes were marked through the ports in the test rocket motor. The propellant charge and spacer were then removed for drilling. Pressure port, igniter and thermocouple holes were drilled as shown in Figure 17. The spacer and propellant charge were then reassembled in the test motor and the drilled holes aligned with their respective ports. Thermocouples were inserted through the seal glands and into the propellant. The seal piston, microwave horn, waveguide and aluminum spacer were then assembled into the test motor and the rear flange was bolted in place. The igniter was loaded with one gram of magnesium-teflon granules, and the glo plug initiator was screwed into place. The assembled test motor was then mounted in the cooling tank and shield, and pressure transducer and thermocouple connections were made. The cooling tank was filled with water. Igniter connections were made as a last step immediately before each firing.

Instrumentation was located in a control room attached to the concrete test cell which housed the test motor and shield. Before each firing, voice identification information was recorded on the tape recorder. The microwave system was adjusted so that a 200 mv signal appeared at the amplifier output of the SWR meter. This level adjustment was accomplished with the sliding short and attenuator in the reference leg of the microwave system. The 200 mv level was found to be satisfactory from the atmospheric pressure combustion tests.

In final preparation for each firing, the test rocket motor was armed and the 24 volt firing power supply was energized in a standby mode. The tape recorder was then started and the electrical calibration for the pressure channel was applied. This was the only calibration required, since all other measurements were with reference to the time base automatically supplied by the tape recorder. Immediately following, the 24 volt igniter switch was thrown manually. The oscilloscope time base and the event channel also received the ignition pulse. The firing pulse was recorded on the event channel of the tape recorder. The oscilloscope time base was previously adjusted for a predetermined delay and sweep time, and operated the variable gain device accordingly. For example, for nominal seven second firings, the oscilloscope time base - variable gain device permitted full system gain for a period of 3.5 seconds, then began linear gain turndown to approximately 0.1 of original gain in four

seconds. At the conclusion of each firing, all data were retained on the magnetic tape for subsequent data reduction.

To prepare the test rocket motor for the next firing, the motor was disassembled, cleaned and a new ATJ graphite nozzle was set in silicone rubber. The test rocket motor performed well throughout the 21 firings, requiring only replacement of combustibles and the nozzle for each firing. The same seal piston-window was used for all tests, with no apparent leakage or damage.

Data Reduction Techniques

The simulated and atmospheric tests produced data on the performance of the microwave system which required no special reduction techniques. The data gathered from the test rocket motor firings, however, required reduction techniques that must be outlined. All test rocket motor data were recorded on magnetic tape during the test runs. At the completion of testing, tapes were replayed and data recorded on the Sanborn Series 150 recorder. This recorder was a four channel model, allowing graphical presentation of the pressure, microwave and two thermocouple records simultaneously. The voice signal, recorded on a separate magnetic tape channel, was monitored for run identification. Figure 19 shows the data recorded during a typical test run.

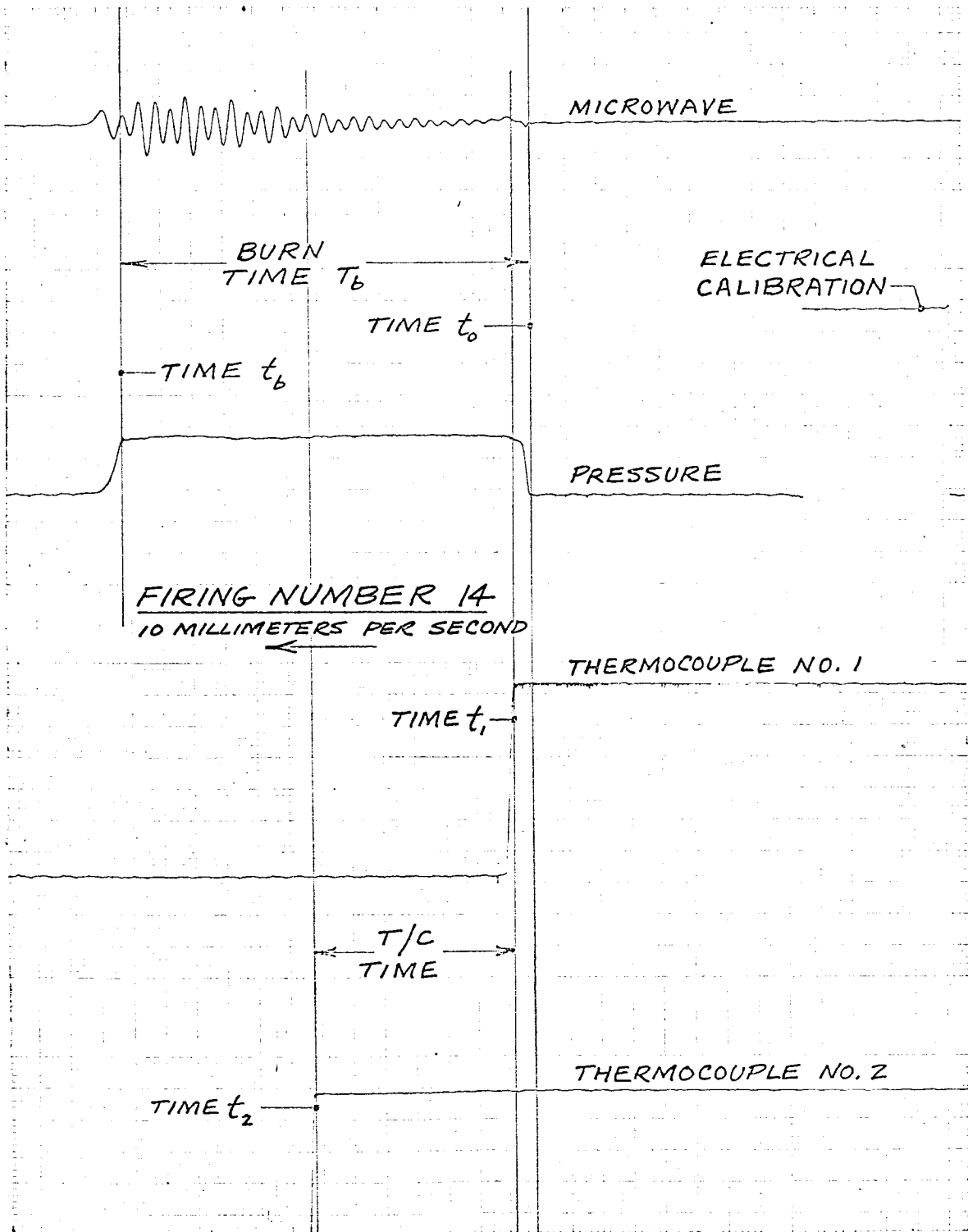


Figure 19. - Typical data from test rocket motor firing.

Pressure Data

To compare the average burning rate of the propellant with standard values, it was necessary to determine the average combustion pressure during each test run. Average pressure was determined by first measuring the area under each curve with a polar planimeter, thus obtaining the pressure-time integral. The pressure time integral was then related to average pressure by equation 8.41.

$$P_{avg} = \frac{\int_{t_o}^{t_b} p dt}{T_b} \quad (8.41)$$

where t_o is the time of first sensible pressure rise

t_b is the time at burnout of the propellant

T_b is the burn time interval

Time t_b was clearly evident on most pressure traces as a sharp drop in the pressure trace. Where no such sharp drop was apparent, the conventional tangent bisector method was employed to determine t_b . The pressure calibration was determined from the electrical calibration immediately preceding each run. Time reference was supplied by the data recorder speed, which was 25 mm per second as the pressure data were reproduced by the tape recorder.

Thermocouple Data

As shown in Figure 19, the thermocouples produced a sharp, clearly identifiable voltage rise when reached by the flame front.

The time of the sharp voltage rise was designated t_1 and t_2 for thermocouples number 1 and 2 respectively, with reference to time t_0 . T/C time was then determined as $(t_2 - t_1)$. The relative position of thermocouples 1 and 2 was measured with a micrometer caliper to 0.001 inch accuracy. The average burning rate during the time t_1 to t_2 was thus

$$r_{\text{avg}} = \frac{d}{t_2 - t_1} \quad (8.42)$$

where d was the distance between the thermocouples.

For best accuracy, the thermocouple data were recorded at 100 mm/sec chart speed, along with the microwave data signal.

Microwave Data

The microwave data were recorded in the form of a variable amplitude sinusoid, as discussed in the previous section, Waveform of the detected signal. For good resolution, readout from the magnetic tape recorder on to the data recorder chart was at 100 mm/sec. It was decided to reduce the data by measuring the distance between one-half wavelengths of the recorded signal, corresponding to one-quarter wavelength of movement of the propellant burning surface. The reasons for this choice are discussed in Section IV, Discussion of Results.

From previously discussed analyses, the microwave signal was seen to complete one full cycle for each one-half wavelength (in the

propellant) of movement of the propellant burning surface. Graphical measurement of the time required for completion of one-half cycle by the microwave signal gave the time required for burning one-quarter wavelength of propellant. Since the wavelength of the 30 GHz radiation in the propellant was assumed constant, the one-half cycle time measurements represented the average burning rate during that half cycle. The complete burning of a two inch nominal length propellant charge resulted in approximately 27 full cycles and a potential 54 measurements of burning rate.

The measurement of the one-half cycle times from the 100 mm/sec record was not as straightforward as would appear. Before the data were reduced, a 3.5 Hz test signal from a low frequency oscillator was recorded at 100 mm/sec, and one-half cycle times were measured. (The microwave burning rate data signal was at approximately 3.5 Hz). The oscillator-recorder arrangement provided the capability of recording 3.5 Hz signals at constant amplitude, variable amplitude and variable DC level. Under constant or variable amplitude conditions, it was found that measurement of the one-half cycle times from the apparent maximum and minimum points of the recorded signal produced the correct one-half cycle times for the 3.5 Hz signal. However, when the DC level of the signal was varied, severe distortion of the times was noted. Study of the microwave burning rate data (see Figure 19) showed that significant amplitude changes of the signal occurred in periods of less than one-half cycle. This was in

addition to the slow amplitude increase of the signal as burning progressed. Equation (8.28) for the waveform of the detected signal was used to analyze the effects of such rapid amplitude variation, and is repeated here for convenience.

$$V_{\text{crystal}} = c \left(\left| E_{\text{xr}_C} \right|^2 + \left| E_{\text{xr}'} \right|^2 - 2 \left| E_{\text{xr}_C} \right| \left| E_{\text{xr}'} \right| \cos \varphi \right)$$

It was noted in the waveform analysis section that a high pass filter was employed to eliminate the nearly constant quantities $\left| E_{\text{xr}_C} \right|^2$ and $\left| E_{\text{xr}'} \right|^2$. However, rapid variation of the amplitude of the $\cos \varphi$ term indicated that $\left| E_{\text{xr}_C} \right|$ and/or $\left| E_{\text{xr}'} \right|$ were varying rapidly. Since these terms appear squared in the detector output, rapid variations of their value would be passed by the high pass filter and result in a variable DC level imposed upon the $\cos \varphi$ sinusoid.

Whatever the cause, it was necessary to devise a method to eliminate the distortion of the maximum and minimum points of the data signal. The fact that distortion did occur may be reinforced by forming the time derivative of equation (8.28) and setting it equal to zero, thus obtaining the conditions for an apparent maximum or minimum of the value of V_{crystal} . In time function notation, equation (8.28) may be expressed as

$$F(t) = c(f_1(t)^2 + f_2(t)^2 - 2 f_1(t) f_2(t) \cos \omega t), \quad (8.43)$$

letting $\varphi = \omega t$. Forming the time derivative of the right side of equation (8.43) and setting it equal to zero,

$$2f_1(t) f_1'(t) + 2f_2(t) f_2'(t) - 2f_1(t) f_2'(t) \cos \omega t - 2f_1'(t) f_2(t) \cos \omega t + 2\omega f_2(t) f_1(t) \sin \omega t = 0 \quad (8.44)$$

The last term of equation (8.44) predicts that maximums and minimums of $F(t)$ will occur at $t = \frac{n\pi}{\omega}$, excluding the other terms. This would be expected if $F(t)$ were a pure cosine wave of constant amplitude. However, for $f_1'(t)$ and/or $f_2'(t)$ non-zero, i.e., for a varying $f_1(t)$ and/or $f_2(t)$, the observed maximum and minimum points of the signal will not be the maximum and minimum points of the $\cos \omega t$ term of equation (8.43). In other words, the apparent maximum and minimum points of the recorded signal were a distorted facsimile of the desired signal.

An improved method was devised by experiment which apparently eliminated most of the distortion caused by rapidly varying amplitudes. Figure 20 shows an actual recording at 100 mm/sec of an approximately 3.5 Hz sinusoid with variable amplitude and variable DC level superimposed. Above the record are one-half cycle times determined from apparent maximum and minimum points, while values below the record were determined by the improved method. The method involved striking tangents to the apparent maximum and minimum points of the signal, then determining the peak of the signal opposite each tangent with reference to the tangent. The values determined by the improved method were quite uniform, and agree well with those determined from constant amplitude signals at the same frequency. Some of the spread in the values was due to variations of the oscillator, as similar variations were noted in the constant amplitude case. The improved method was used to reduce all microwave data gathered in the subject investigation.

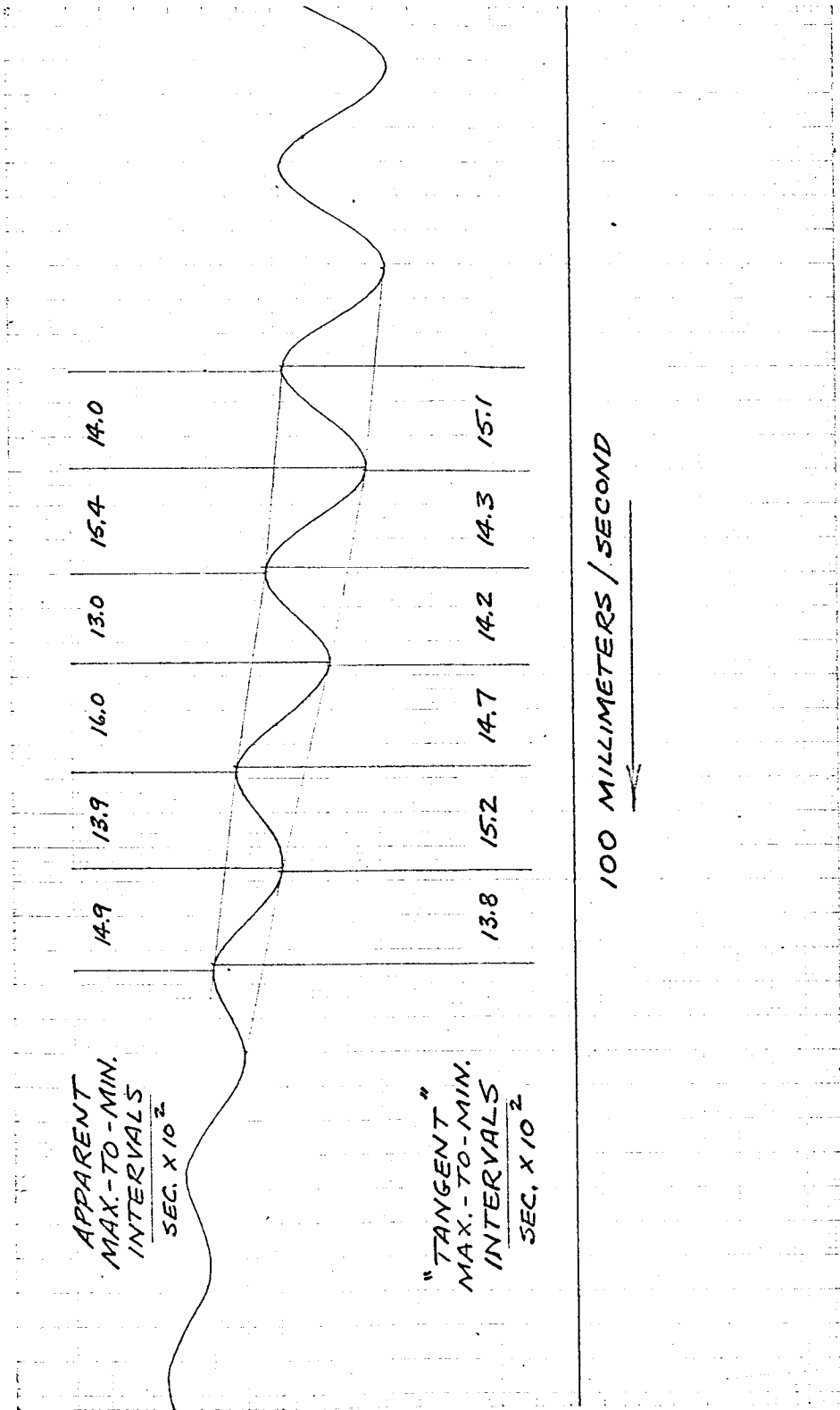


Figure 20. - Reduction method for microwave data.

The wavelength of the 30 GHz electromagnetic radiation in the propellant was determined by counting the number of full cycles of the microwave signal during the burning of each known length of propellant. Equation (8.15) was then employed to calculate λ_p . k'' of the propellant was calculated employing equation (8.46). ϵ'' and ϵ' were also calculated employing equations (8.32) and (8.33) respectively.

Data and Results

Following the previous organization, the data and results are classified as those gathered in simulated tests, atmospheric tests, and test rocket motor firings.

Simulated Tests

The penetrability of propellants TPH-8009 and AeReCo 1 and 2 by the 30 GHz microwaves was investigated. Using the horn-lens collimator, it was found that the microwave system could sense the movement of a metal reflector through six inches of the aluminized propellant AeReCo 2. The same movement could be sensed through eight inches of the unaluminized AeReCo 1. While the largest specimen of propellant TPH-8009 that was available at the time was two inches thick, no difficulty was encountered in sensing metal reflector movement through this sample.

The radiation pattern of the horn-lens collimator was studied as described in the test procedure. Results were summarized in Table 2.

TABLE 2

EFFECT OF DIFFERENT METAL REFLECTORS ON RETURN SIGNAL
TRANSMITTED THROUGH THREE INCHES OF
AeReCo PROPELLANT 2

Reading No.	Center hole diameter in metal reflector, inches	Influence of reflector with center hole as a fraction of that from a solid reflector
1	0.00 (solid reflector)	1.000
2	0.50	0.875
3	0.75	0.690
4	1.00	0.500
5	1.25	0.430
6	1.50	0.250
7	1.75	0.125
8	2.00	0.125
9	2.25	0.000

Atmospheric Tests

The atmospheric combustion tests allowed the first shakedown tests of the microwave system, and provided additional information on the penetrability of propellants AeReCo 1 and 2 by the microwaves. Results will be found in Table 3. Microwave power was measured by breaking the waveguide system at the input flange to the horn-lens collimator. The measurement was made employing a thermistor and microwave power meter. With the microwave system adjusted for operation as described in the test procedure, a power level of 0.03 milliwatts was measured. While additional power losses occurred in the collimator, the measured power was indicative of the power radiated into the propellant. This power level was essentially unchanged for atmospheric tests and those in the test rocket motor.

Test Rocket Motor Firings

Data and results produced by the test rocket motor firings are shown in Tables 4 through 8. Tables 4 through 6 summarize what may be described as average data and results for all of the 21 test firings. All firings were conducted without propellant temperature conditioning, with the propellant charge at the ambient temperature of the day. Ambient temperature readings are recorded in Table 4. In Table 6, average burning rate-change length is the propellant charge length divided by the burn time T_b . The average burning rate-microwave is to be compared with this value. The average burning rate-thermocouples is the distance between T/C-1 and T/C-2

TABLE 3

RESULTS OF ATMOSPHERIC COMBUSTION PRESSURE TESTS -
PENETRABILITY OF PROPELLANT CHARGES
BY MICROWAVES

Run Number	Propellant type	Propellant charge length inches	Results
ATM-1	AeReCo 2	2	Strong, sinusoidal signal throughout test run.
ATM-2	AeReCo 1	2	Same as above, signal amplitude higher.
ATM-3	AeReCo 1	4	Good signal throughout run, large amplitude increase.
ATM-4	AeReCo 2	4	Very weak but intelligible signal from start of burning, large amplitude increase
ATM-5	AeReCo 1	6	Good signal throughout run, large amplitude increase.
ATM-6	AeReCo 2	6	Signal unintelligible at beginning of run, good signal for last 3-1/4 inches of burning

TABLE 4
TEST CONDITIONS AND DATA
ROCKET MOTOR FIRINGS

Firing Number	Date	Ambient Temperature, of	TPH-8009 Propellant Charge Length, inches	T/C-1 to T/C-2 Distance, inches	Nozzle Throat Diameter, inches
1	6- 2-67	77	2.020*	---	0.185
2	6- 7-67	80	2.022	---	0.185
3	6- 8-67	79	2.025	---	0.185
4	6-14-67	86	2.008	1.040*	0.201
5	6-15-67	89	2.015	1.040*	0.199
6	6-22-67	80	2.030	1.040*	0.199
7	6-26-67	74	2.045	1.080	0.199
8	6-26-67	78	2.031	---	0.173
9	6-27-67	77	2.035	---	0.173
10	6-27-67	78	2.032	1.040	0.173
11	6-28-67	80	2.045	1.009	0.173
12	6-28-67	82	2.020	1.007	0.154
13	6-29-67	76	2.021	0.992	0.154
14	6-29-67	78	2.045	1.017	0.166
15	6-30-67	78	2.042	1.000	0.161
16	6-30-67	82	2.030	1.020	0.149
17	7- 5-67	78	2.025	1.029	0.161
18	7- 5-67	82	2.025	0.917	0.149
19	7- 6-67	69	2.039	1.128	0.185
20	7- 6-67	72	2.020	1.020	0.185
21	7- 7-67	73	2.994	0.982	0.185

*Estimated

TABLE 5
TEST DATA
ROCKET MOTOR FIRINGS

Firing Number	Burn Time T _b , seconds	Average Microwave 1/2 Cycle Time, seconds	T/C-1 to T/C-2 Time, seconds	Average Microwave/Thermocouples 1/2 Cycle Time, seconds
1	6.80	---	---	---
2	7.06	0.1370		
3	6.97	0.1326		
4	7.28	0.1366		0.1330
5	7.40	0.1381		0.1344
6	7.15	0.1354		0.1329
7	7.43	0.1381		0.1371
8	6.88	0.1286		
9	6.89	0.1290		
10	6.99	0.1305		
11	6.96	0.1318		
12	6.43	0.1211		
13	5.96	0.1141		
14	6.52	0.1233		
15	6.43	0.1211		
16	5.93	0.1128		
17	6.26	0.1198		
18	5.88	0.1127		
19	7.03	0.1326		
20	7.38	0.1406		
21	10.16	0.1288		
			No thermocouple data	
			3.726	0.1330
			3.733	0.1344
			3.830	0.1329
			3.880	0.1371
			No thermocouple data	
			3.524	0.1262
			3.434	0.1247
			3.109	0.1159
			2.947	0.1122
			3.236	0.1214
			3.239	0.1200
			2.984	0.1099
			3.555	0.1181
			2.910	0.1094
			3.719	0.1316
			3.972	0.1373
			3.460	0.1291

TABLE 6
 AVERAGE TEST RESULTS
 ROCKET MOTOR FIRINGS

Firing Number	Average Pressure, psig	Average Burning Rate- Charge Length, inches/second	Average Burning Rate- Microwave, inches/second	Average Burning Rate- Thermocouples, inches/second	Average Burning Rate-Microwave/ Thermocouples, inches/second
1	482	0.297	Microwave system not in use		
2	473	0.286	0.278	No thermocouple data	
3	475	0.290	0.286		
4	389	0.276	0.279	0.279	0.286
5	376	0.272	0.274	0.279	0.283
6	405	0.284	0.281	0.272	0.286
7	396	0.275	0.274	0.278	0.278
8	552	0.295	0.296	No thermocouple data	
9	553	0.295	0.294	No thermocouple data	
10	528	0.291	0.291	0.295	0.301
11	515	0.294	0.288	0.294	0.305
12	720	0.314	0.314	0.324	0.328
13	927	0.339	0.334	0.337	0.339
14	685	0.314	0.308	0.314	0.313
15	740	0.317	0.314	0.309	0.317
16	944	0.342	0.337	0.342	0.346
17	774	0.323	0.317	0.289	0.322
18	936	0.344	0.338	0.315	0.347
19	498	0.290	0.287	0.303	0.289
20	403	0.273	0.270	0.257	0.277
21	514	0.295	0.296	0.284	0.294

TABLE 7
INDIVIDUAL MICROWAVE
ONE-HALF CYCLE TIMES

Firing Number 14

Data Starting Time after
 $t_0 - 0.351$ seconds

Reading Number	Time Interval seconds	Reading Number	Time Interval seconds
1	0.123	27	0.119
2	0.121	28	0.118
3	0.109	29	0.119
4	0.114	30	0.123
5	0.126	31	0.129
6	0.131	32	0.127
7	0.128	33	0.112
8	0.126	34	0.116
9	0.113	35	0.122
10	0.111	36	0.126
11	0.118	37	0.130
12	0.130	38	0.117
13	0.125	39	0.113
14	0.125	40	0.121
15	0.119	41	0.125
16	0.114	42	0.124
17	0.127	43	0.119
18	0.121	44	0.121
19	0.124	45	0.120
20	0.123	46	0.119
21	0.118	47	0.139
22	0.126	48	0.128
23	0.106	49	0.136
24	0.129	50	0.125
25	0.127	51	0.139
26	0.122	52	0.168

TABLE 8

TEST RESULTS

INDIVIDUAL ONE-HALF CYCLE
MICROWAVE BURNING RATES
AND CUMULATIVE VALUES

Firing Number 14		Burning Rate, inches/sec	Cumulative Burning Distance, inches	Cumulative Burning Time, seconds	Reading Number	Burning Rate, inches/sec	Cumulative Burning Distance, inches	Cumulative Burning Time, seconds
1	0.309	0.038	0.474	16	0.333	0.608	2.284	
2	0.314	0.076	0.595	17	0.299	0.646	2.411	
3	0.349	0.114	0.704	18	0.314	0.684	2.532	
4	0.333	0.152	0.818	19	0.306	0.722	2.656	
5	0.302	0.190	0.944	20	0.309	0.760	2.779	
6	0.290	0.228	1.075	21	0.322	0.798	2.897	
7	0.297	0.266	1.203	22	0.302	0.836	3.023	
8	0.302	0.304	1.329	23	0.358	0.874	3.129	
9	0.336	0.342	1.442	24	0.295	0.912	3.258	
10	0.342	0.380	1.553	25	0.299	0.950	3.385	
11	0.322	0.418	1.671	26	0.311	0.988	3.507	
12	0.292	0.456	1.801	27	0.319	1.026	3.626	
13	0.304	0.494	1.926	28	0.322	1.064	3.744	
14	0.304	0.532	2.051	29	0.319	1.102	3.863	
15	0.319	0.570	2.170	30	0.309	1.140	3.986	

(CONTINUED ON NEXT PAGE)

TABLE 8 (CONTINUED)

Firing Number 14

Reading Number	Burning Rate, inches/sec	Cumulative Burning Distance, inches	Cumulative Burning Time, seconds	Reading Number	Burning Rate, inches/sec	Cumulative Burning Distance, inches	Cumulative Burning Time, seconds
31	0.295	1.178	4.115	42	0.306	1.596	5.448
32	0.299	1.126	4.242	43	0.319	1.634	5.567
33	0.339	1.254	4.354	44	0.314	1.672	5.688
34	0.328	1.292	4.470	45	0.317	1.710	5.808
35	0.311	1.330	4.592	46	0.319	1.748	5.927
36	0.302	1.368	4.718	47	0.273	1.786	6.066
37	0.292	1.406	4.848	48	0.297	1.824	6.194
38	0.325	1.444	4.965	49	0.279	1.862	6.330
39	0.336	1.482	5.078	50	0.304	1.900	6.455
40	0.314	1.520	5.199	51	0.273	1.938	6.594
41	0.304	1.558	5.324	52	0.226	1.976	6.762

divided by the measured time between flame front indications. To be compared with this is the average burning rate-microwave/thermocouples, calculated as the average microwave measured burning rate between T/C-1 and T/C-2 indications. Table 7 gives the entire microwave data generated by firing number 14. Table 8 is this same microwave data converted to burning rate of the propellant by the methods previously described. The conversion equation was

$$r_b = \frac{1/2 \text{ cycle time}}{1/2 \text{ cycle distance}} = \frac{1/2 \text{ cycle time}}{0.038 \text{ inches}} \quad (8.45)$$

The value of 0.038 inches for the 1/2 cycle distance was the average value for all firings of propellant TPH-8009 to the nearest 0.001 inch. The value is actually 1/4 of the wavelength of the 30 GHz electromagnetic radiation in the propellant, computed by methods previously described.

Cumulative time figures shown in Table 8 represent the time interval following the first sensible pressure rise for the firing (t_0 in Figure 19). Cumulative distance figures represent simple addition of the known distance between each data point (0.038 inches). Since no distance datum was available, the cumulative distance figures are distance intervals only, starting at zero with the first data point.

Each of the firings 2 through 21 generated an amount of data similar to that recorded in Tables 7 and 8. In the interest of brevity,

this data is not presented, but is retained in the records of the investigator.

Electromagnetic property data are given in Table 9. Values of k' , k'' , ϵ' and ϵ'' were calculated following procedures already described. The quantities ϵ_r' and ϵ_r'' are defined by the equations (8.46),

$$\epsilon_r' = \frac{\epsilon'}{\epsilon_0} \quad \epsilon_r'' = \frac{\epsilon''}{\epsilon_0} \quad (8.46)$$

where ϵ_0 is the permittivity of free space, 8.854×10^{-12} farad per meter. The values of ϵ_r' and ϵ_r'' for propellant TPH-8009 are presented for convenience in comparing the observed values with those for other materials. Tables of electromagnetic property data in the literature normally present ϵ_r' and ϵ_r'' .

TABLE 9

ELECTROMAGNETIC PROPERTY
DATA AND RESULTS

PROPELLANT TPH-8009

Firing Number	T/C-1 to T/C-2 distance, inches	Amplitude e ₁ , millimeters	Amplitude e ₂ , millimeters	k'	k"	10 ¹² e'	10 ¹² e"	ε _r '	10 ⁴ ε _r "
						-- mks units --			
19	1.128	3.5	4.5	1628	28.6	59.34	2.084	6.70	2354
20	1.020	18	29.5	1628	36.3	59.34	2.645	6.70	2987
Averages				1628	32.5	59.34	2.365	6.70	2671

Microwave frequency - 30 GHz

Average microwave power loss - 2.8 db/centimeter of propellant

Microwave wavelength in propellant - 0.386 centimeters

IX. DISCUSSION OF RESULTS

Simulated Tests

While the simulated tests previously described did not produce the primary results of the subject investigation, valuable results were obtained.

Reasons for the choice of the lens-corrected horn collimator were discussed in the Data and Results section. Figure 21 shows the data of Table 2 in graphical form. Interpretation of the results of this test was a difficult problem. Actually, the curve shown in Figure 21 cannot be said to represent anything other than the results of the specified test, i.e., the influence on the return signal of metal reflectors having various centered circular holes. Extrapolation of the data to the propellant burning case would indicate, however, that at a three inch distance, burning of propellant outside a one inch diameter cross sectional area centered on the horn-lens collimator axis had little effect on the data signal observed. While such extrapolation might seem hazardous, it was felt that the data figures were in order of magnitude representative of the performance of the collimator under propellant combustion conditions. More conventional methods for the study of antenna patterns were not employed because it was assumed that such data might lead to erroneous conclusions. In the subject measurement system, only the strength of

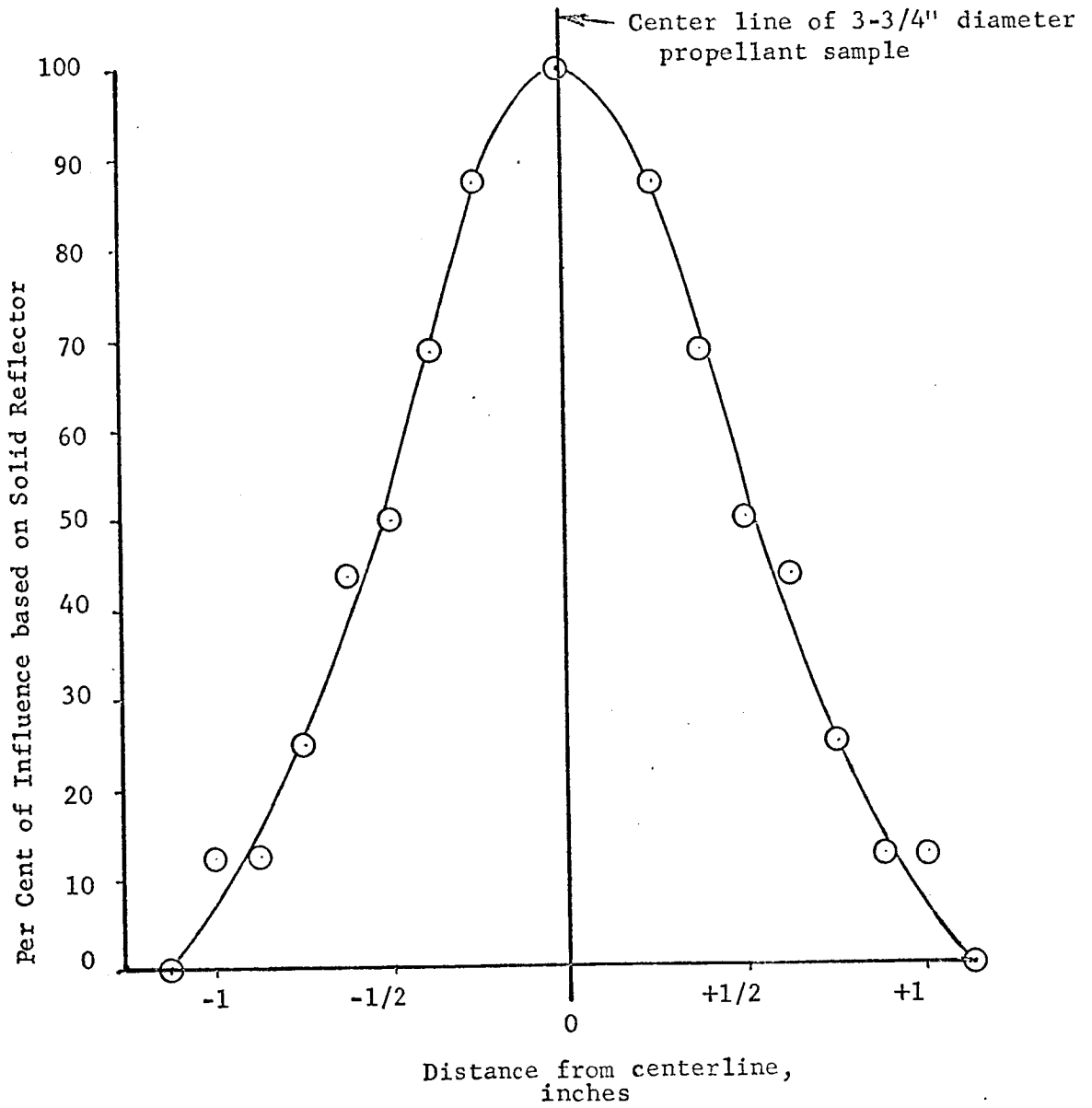


Figure 21. - Area of burning surface influencing return signal through 3" of AeReCo 2 aluminized propellant (using horn/lens collimator),

the return signal as a function of reflector position was of interest. Antenna pattern measurements would have yielded information on the "illuminated" area of the propellant burning surface, but not on reflection conditions.

It was noted that the waveform of the signal produced by tests with the test rocket motor simulator was never of the quality of that produced under actual combustion conditions. This effect was assumed to have been caused by multiple reflections within the simulator which were attenuated by the propellant in the actual combustion tests. The simulator was filled with oil which, while more lossy than air, did not approach a simulation of the microwave losses in the propellant.

It was possible to penetrate considerably more propellant with the microwaves to detect the movement of a metal reflector than to detect the burning surface movement, as shown in the Data and Results section. This was unexpected, in view of the fact that equation (8.12) predicts approximately the same magnitude of signal return in both cases; that is, the partially transparent propellant/combustion zone interface would be expected to return a rate signal approximately equivalent to that returned by a metal reflector moved in front of the propellant interface. Although the metal reflector may be assumed to reflect all microwave energy incident upon it, the energy suffers two reflections at the propellant/air interface in

proceeding from the microwave system to and from the metal reflector. The approximate equality of reflection signal would thus be expected. A possible explanation for the weaker than expected combustion interface reflection is that the combustion process effectively "matched" the solid propellant to the gas-filled area above it, reducing the reflection from the interface. Further study to clarify the nature of the microwave reflection from the combustion interface would be desirable.

Atmospheric Tests

Reference to Table 3 shows that it was possible to observe burning surface movement through approximately six inches of propellant AeReCo 1, and 4 inches of the aluminized AeReCo 2 propellant. In the test rocket motor firings, it was found that burning could be sensed through a maximum of two inches of propellant TPH-8009. Clearly, microwave losses were not as severe in the polyurethane binder AeReCo propellants as in the TPH-8009 propellant, which had a PBAA binder. Also, the presence of 16 per cent aluminum in the AeReCo 2 propellant caused greater microwave losses. Variable microwave losses dependent on propellant composition and an increase in losses in aluminized propellants was reported in References 16 and 19. It was originally planned to use propellants AeReCo 1 and 2 for firings in the test rocket motor. Apparently these propellants were

not as "lossy" in the microwave sense as propellant TPH-8009, and would have allowed burning rate measurement through longer charges. Repeated attempts to obtain ignition and stable burning in the test rocket motor using the AeReCo propellants were not successful, however. Whenever enough ignition energy to prevent a hangfire condition was supplied, overpressure occurred and the test rocket motor ruptured at the mating flanges. Whether the difficulty was due to ignition problems or the failure of the propellant bond to the asbestos-phenolic burning restrictor was not determined. The AeReCo 1 and 2 propellants were replaced with propellant TPH-8009 after several unsuccessful firing attempts. No further difficulty of this type was encountered.

Test Rocket Motor Firings

Good agreement was obtained between the various measurements of burning rate which were made during each run. Referring to Table 6, the average burning rate based on charge length closely matched the average burning rate as determined by microwaves. Typical errors of a few thousandths of an inch per second were noted. The largest error occurred in firing number 2, where error was 2.8 per cent, based on the burning rate-charge length value. Average error for all firings was 1.1 per cent. Firing number 14, presented as a typical firing, produced an error of 1.9 per cent. Again

referring to Table 6, the average burning rate - thermocouples was to be compared with the average burning rate - microwave/thermocouple. For these measurements, firing number 17 produced the largest error of 11.4 per cent based on the thermocouple measured burning rate as a standard. Average error for all 16 firings which produced data was 3.6 per cent. Microwave measurements for firing number 14 were in error 0.3 per cent, based on the thermocouple measurements.

It is difficult to offer an explanation for the errors of measurement which were noted. For the average burning rates determined over the entire charge length, the average error of 1.1 per cent is certainly near the basic accuracy capability of the system components. It is felt that accuracy of this order is highly satisfactory for measurements of this type involving a complex instrumentation setup. In the case of the thermocouple burning rate measurements, considerably larger errors were noted. As a possible explanation, it may be recalled that the sheathed thermocouples were 0.062 inches in diameter. The location and orientation of the measuring junction within the thermocouple could have varied several thousandths of an inch, causing variable response. The data reduction technique which was employed to determine when the flame front reached the thermocouple was also a potential error source. In some cases, the thermocouple signal did not rise sharply enough to prevent some uncertainty in choosing the point.

Comparison of average burning rates as measured by the microwave system with other data for propellant TPH-8009 also yielded good results. Figure 22 shows the data obtained in the subject investigation and that obtained by ultrasonic measurements described in Reference 7. As can be noted from the figure, some measurements are so close as to obscure the individual values on the graph. Agreement was good throughout the combustion pressure range. Figure 23 shows the same data collected in the subject investigation compared with strand burning rate values. The strand burning rates were measured in a closed bomb, using propellant from the same mix from which propellant for the subject investigation was taken. Data were supplied by NASA Langley Research Center. While agreement was adequate, it was not of the same quality as shown in Figure 22. The most probable explanation for the variance is that propellant combustion under actual rocket motor combustion conditions is not adequately simulated by closed bomb tests. The ultrasonically measured burning rates from Reference 7, shown in Figure 22, were measured in a small end burning rocket motor.

Figure 24 shows propellant surface position as a function of time for firing number 14. The curve is a plot of the data shown in Table 8. Time at zero distance (0.351 seconds) is the time at which the microwave burning rate signal became intelligible after t_0 , the start of burning. Distance shown is the cumulative propellant burned after 0.351 seconds. Study of the regression curve shows

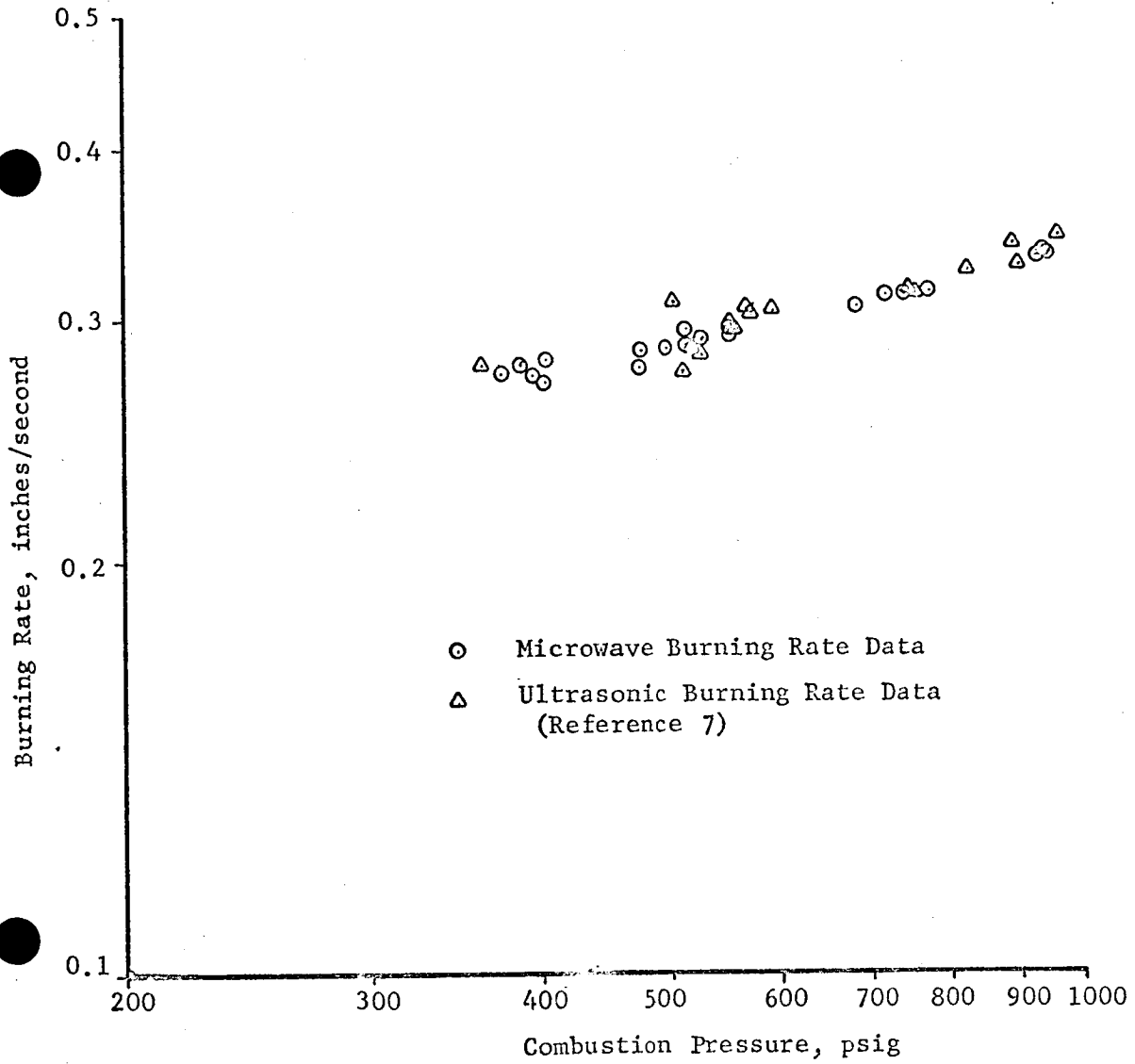


Figure 22. - Comparison of microwave measured burning rates with ultrasonic measured burning rates (Reference 7) for propellant TPH-8009.

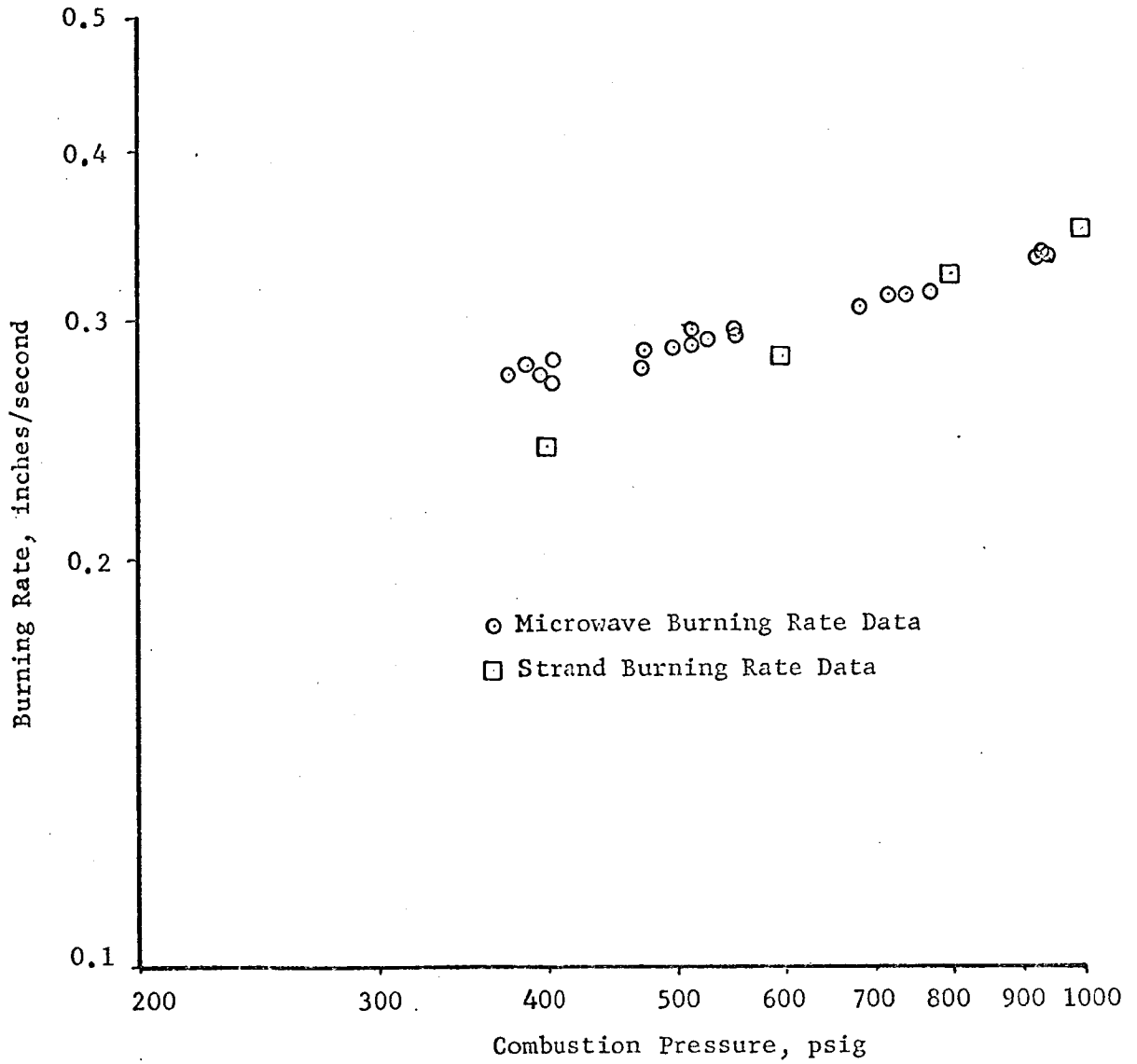


Figure 23. - Comparison of microwave measured burning rates with strand burning rates for propellant TPH-8009.

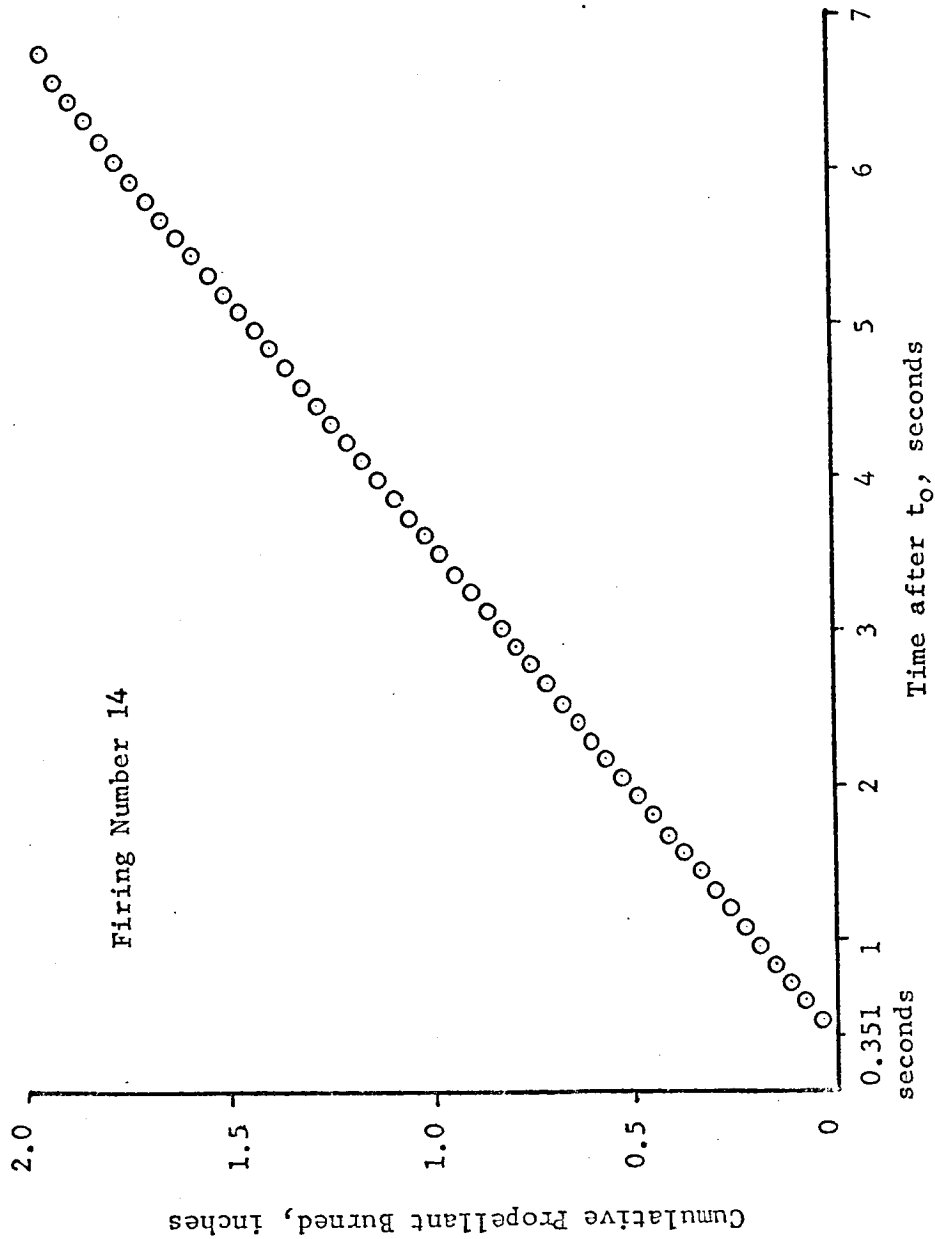


Figure 24. Typical propellant burning surface regression history measured by microwave method.

that the burning of the propellant was nearly linear with time, as would be expected for the nearly neutral pressure history produced by firing number 14. However, apparent small variations in the rate of burning can be noted. The variations in burning rate were not so small as would appear, however. Figure 25 shows the burning rate between each of the points of Figure 24, as measured by the microwave system. Since the data points represent burning through a distance of 0.038 inches, each rate value shown in Figure 25 is an average burning rate for 0.038 inches. The average burning rate for the entire firing was 0.308 inches/second and is shown as a line through the points. Considerable scatter of the individual burning rates about the average value is apparent. Some of this scatter was caused by the data reduction method, since an error in reading one time interval would have an opposite effect on the next; that is, a high reading would produce a subsequent low reading. However, it is difficult to explain the several instances of points which show a relatively slow burning rate change as anything but actual burning rate variation. As an example, the series of points between 3.25 and 4.25 seconds in Figure 25 can be noted. It should also be noted that the 0.038 inch measurement interval may be approaching the burning surface roughness of the propellant. Variations in the roughness of the surface as burning proceeded could have affected the results. However, since the horn-lens collimator illuminated an area over the burning surface, the rate results should indicate an

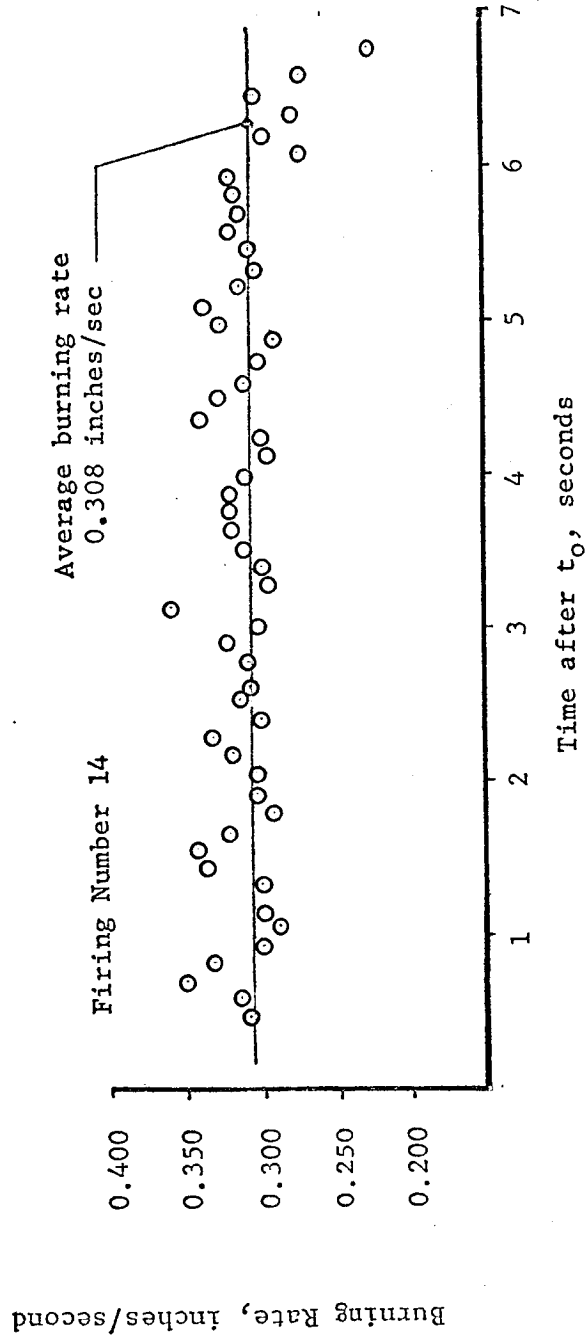


Figure 25. - Typical propellant burning rates at intervals of 0.038 inches measured by microwave method.

average burning rate for this area, which was desired. It is felt that this question deserves further study, especially with higher frequency, shorter wavelength microwave radiation.

The manual data reduction technique employed to reduce the microwave data was not completely satisfactory. The technique was laborious and considerable care was required to avoid substantial errors. It was originally planned to devise an electrical means for data reduction, but this was not accomplished. Of those investigated, the most promising techniques included an automatic, self balancing Wien bridge and an oscillographic technique using a Lissajous figure. Experimental models of the two devices were constructed and it was possible to measure the frequency of an approximately 3.5 Hz sinusoid generated by an oscillator. In the case of the Wien bridge, indication of a frequency shift of 0.1 Hz was sensed essentially instantaneously, while the Lissajous figure technique produced a frequency indicating pulse at approximately 0.025 second intervals. The difficulty with both techniques was that it was not possible to make the devices amplitude insensitive, and the microwave data signal exhibited variable amplitude. Based on the experience gained in working with the two devices, it would seem more desirable to eliminate the variable amplitude characteristics of the signal rather than to attempt to accommodate them. A microwave bridge method to accomplish this was described in Reference 27. Another method made feasible by recent microwave equipment developments performs

phase measurements directly between the 30 GHz data and reference signals.

The amplitude variation which caused the most difficulty was not the slow increase in amplitude as the propellant burned, but that which occurred quickly, often within one-half cycle (see Figure 19). The source of these amplitude variations was not explained by conventional attenuation analysis. A possible cause was a resonance effect dependent upon the length of unburned propellant. In Reference 19, similar amplitude variations were observed and were attributed to standing wave effects.

Electromagnetic property data were computed from results of firing numbers 19 and 20. These firings were purposely conducted without the variable gain device in operation, so that measurement of microwave attenuation could be made. The results showed that the propellant had a relatively high ϵ' (a-c capacitivity) and produced large microwave power losses. Comparison of the computed values with those for other selected materials may be noted in Table 10. While the property values for the materials other than propellant TPH-8009 were measured at a microwave frequency of 3 GHz, an order of magnitude comparison is provided. Microwave power losses were computed as 2.8 db/centimeter of propellant. This value compares quite favorably with a value of 2.3 db/centimeter calculated from results of tests described in Reference 19. These tests were conducted at a microwave frequency of 24 GHz, and average power losses were found to be

TABLE 10

COMPARISON OF ELECTROMAGNETIC
PROPERTY DATA

Quantity	Material				
	Propellant TPH-8009	Polystyrene*	Neoprene* Compound	Pyranol* 1478	Water*
ϵ_r	6.70	2.55	4.00	3.80	76.7
$10^4 \epsilon_r''$	2671	8.5	1350	8800	120000

* Electromagnetic property data at 25 °C, for 3GHz, taken from Reference 26.

0.144 db/cm/per cent of aluminum in the propellant. Assuming that the results can be applied to the 16 per cent aluminum TPH-8009 propellant, the value of 2.3 db/centimeter results.

X. SUMMARY AND CONCLUSIONS

The Doppler microwave technique for the sensing of propellant burning rates has been shown by previous investigators to be feasible. The method appeared especially attractive for measurement of localized burning rates, since microwave radiation could be focused. The potential for truly continuous burning rate measurement was also inherent in the microwave method. With the exception of the initial feasibility study, no investigation of the microwave burning rate measurement technique per se has previously been conducted. The subject investigation treated the general problem of burning rate measurement employing a Doppler microwave technique.

Analyses supporting the experimental portion of the subject investigation were presented. Included were considerations of microwave reflections, the waveform of the signal output of the system, and electromagnetic properties of solid propellants. An experimental program was conducted, including preliminary tests under simulated conditions, combustion tests at atmospheric pressure, and solid propellant burning rate measurement under actual rocket motor combustion conditions. For the latter tests, a special test rocket motor was designed. The test rocket motor incorporated a pressure sealing microwave window, a lens-corrected horn microwave collimator, and thermocouple flame front sensors to provide a check on measured

burning rates. Microwave burning rate data were recorded from a series of 20 test firings. Two of these firings were designed to provide information for the calculation of the electromagnetic properties of the test propellant.

Burning rate values measured by the microwave system during the 20 test firings were computed and compared with the burning rate of each charge based on its length, with the thermocouple flame front sensors, and with the data of other investigators. Agreement was good in all cases. Electromagnetic property data were computed and compared with other selected substances. Microwave power loss in the test propellant was calculated from the experimental results and compared with results of another investigation.

The following conclusions may be drawn from the results of the subject investigation:

- (1) The burning rate of solid rocket propellants may be measured employing Doppler microwave techniques under actual rocket motor combustion conditions.
- (2) Employing the methods of the subject investigation, the position of the burning surface of propellant TPH-8009 may be sensed at intervals of 0.038 inches using Doppler microwave techniques. The average burning rate of the propellant in the 400 to 1000 psig combustion pressure range was measured with an average accuracy of 1.1 per cent, based on the average burning rate of the entire charge as a standard. For the same pressure

range, the average burning rate was measured with an average accuracy of 3.6 per cent based on flame front sensing thermocouples placed at known distances along the periphery of the propellant as a standard.

(3) Continuous burning rate information is contained in the microwave signal. Amplitude and level variations in the received signal mask this information, and cause serious data reduction problems.

(4) Collimation of microwaves in solid rocket propellants for the sensing of local burning rates is feasible. In a small end burning rocket motor, severe distortion of the burning rate data signal occurs in the absence of a properly designed collimator.

(5) The solid rocket propellants tested are lossy dielectric materials, highly absorbing to 30 GHz microwaves. Propellant TPH-8009 produced an average loss of 2.8 db per centimeter of propellant in the path of the microwaves.

XI. RECOMMENDATIONS

The results and experience gained during the subject investigation suggest several areas for additional investigation. The following are considered to be especially pertinent:

- (1) The techniques of the subject investigation should be extended, employing microwave equipment capable of generating radiation of higher power and/or shorter wavelength. Methods of improving the sensitivity of the receiver-detector should be investigated. An improved system should result, capable of better resolution in measuring burning rates through greater propellant thicknesses.
- (2) Further study of the collimating device should be conducted, directed toward optimizing the gain and directional pattern. A method for defining the area of the propellant burning surface affecting the return signal should be devised.
- (3) The microwave method should be employed to measure the burning rate of propellants of current interest other than those used in the subject investigation.
- (4) Improvement of the data reduction technique used in the subject investigation should be undertaken. The use of a microwave bridge to produce direct phase angle measurements

appears desirable. Recent developments in microwave instruments have provided the capability of measuring phase angles directly at frequencies up to 40 GHz. The use of such instruments should be considered.

(5) The application of the microwave system to the measurement of the burning rate in solid propellant grains of complex geometry should be investigated. Initially, the use of internal burning grains having a cylindrical perforation is suggested.

(6) The character of the solid propellant combustion zone as a microwave reflector should be studied. Information is needed regarding the magnitude of the reflection, as well as the effective position of the reflection in the combustion zone.

XII. ACKNOWLEDGEMENTS

Sincere appreciation is expressed to the National Aeronautics and Space Administration, Langley Research Center, whose support made this investigation possible. Special appreciation is extended to the personnel of the Propulsion Branch, Langley Research Center, for their advice and assistance throughout the course of the investigation.

XIII. BIBLIOGRAPHY

1. Crawford, B. L., Jr., Huggett, C., Daniels, F., and Wilfong, R. E.: "Direct Determination of Burning Rates of Propellant Powders"; Analytical Chemistry, Vol. 19, No. 9, September 1947, pp. 630-633.
2. Stewart, D. H. and Moon, E. L.: "An Improved Method for the Measurement of Solid-Propellant Strand Burning Rates in Closed Bombs"; NAVWEPS Report 8070, NOTS TP 3076, May 1963.
3. Barrere, M., Jaumotte, A., De Veubeke, B. F., and Vandekerckhove, J.: Rocket Propulsion. Elsevier Publishing Co., Amsterdam, 1960.
4. Osborn, J. R., Burick, R. J., and Ho, P. Y.: "Techniques for the Continuous Measurement of Solid Propellant Burning Rates", Final Report on Grant AF-AFOSR 207-64, Jet Propulsion Center, Purdue University, Lafayette, Indiana, February 1966.
5. Ho, P. Y.: "Feasibility Study of the Microwave and the Ultrasonic Techniques on the Continuous Measurement of Solid Propellant Burning Rates", M. S. Thesis, Purdue University, Lafayette, Indiana, August 1965.
6. Osborn, J. R., and Burick, R. J.: "Continuous Measurement of the Burning Rates of Solid Rocket Propellants," Interim Report, Grant AF-AFOSR 207-63, Jet Propulsion Center, Purdue University, Lafayette, Indiana, April 1964.

7. Hale, H. J.: "The Demonstration of an Ultrasonic Technique to Measure Solid Propellant Burning Rates Under Actual Combustion Conditions," M. S. Thesis, Virginia Polytechnic Institute, Blacksburg, Virginia, June 1967.
8. Hermance, C. E.: "Continuous Measurement of the Burning Rate of a Composite Solid Propellant," AIAA Paper Number 67-69, presented at the 5th Aerospace Sciences Meeting, New York, January 1967.
9. Seamons, R. D.: "Cineradiography of Five-Inch Solid Propellant Motors," Symposium on Nondestructive Testing of Solid Propellant Rocket Motors, CPIA Publication No. 29, August 1963.
10. Seamons, R. D.: "Cineradiography for Solid Rocket Motor Testing," Space/Aeronautics, June 1965, pp. 73-76.
11. Dickenson, L. A., Jackson, F., and Odgers, A. L.: "Erosive Burning of Polyurethane Propellants in Rocket Engines," Eighth International Symposium on Combustion, 1960.
12. Osborn, J. R., and Bethel, H. E.: "Techniques for Measuring Burning Rates of Solid Propellants," Review of Scientific Instruments, Vol. 35, No. 9, September 1964.
13. Feasibility Demonstration of a Rocket Engine Ablation Gauge, Task I Summary Report, Tech. Rept. AFRPL-TR-66-313, TRW Systems, Inc., November 1966.
14. Johnson, D. L.: "Microwave Measurements of Solid Propellant Burning Rates," Technical Note, Giannini Controls Corporation, Duarte, California, July 1962.

15. Cauley, L. S.: "A Feasibility Study of the Use of Microwaves to Measure Radial and Differential Burning Rates in Solid Propellant Rockets," M. S. Thesis, Virginia Polytechnic Institute, Blacksburg, Virginia, June 1967.
16. Cole, R. B.: "High Pressure Solid Propellant Combustion Studies Using a Closed Bomb," Report No. S-68 on Contract DA-01-021 ORD-11, 909(Z), Rohm and Haas Company, Huntsville, Alabama, October 1965.
17. Jenks, J. C. and Devault, J. B.: "Microwave Measurements of Solid Propellant Burning Rates and Burning Profiles," Bulletin of the First Meeting, ICRPG Working Group on Static Testing, CPIA Publication No. 24, September 1963. (CONFIDENTIAL)
18. R. Zimmer-Galler and T. D. Austin: "The Effect of Burning Rate Modifiers on the Thermal Decomposition of Polyester - RDX Propellants," Third Combustion Conference, ICRPG, CPIA Publication No. 138, Vol. II, October 1966. (CONFIDENTIAL)
19. Brandon, W. W., Jr.: "Applications of Microwaves in the Non-Destructive Testing of Solid Propellants," Report No. S-53 on Contract DA-01-021 ORD-12341(Z), Rohm and Haas Company, Huntsville, Alabama, November 1964.
20. Harvey, A. F.: Microwave Engineering, Academic Press, London, 1963. pp. 6-8.
21. Hey, J. S., Pinson, J. T., and Smith, P. G.: "A Method of Determining the Velocity of a Shock Wave," Nature, Vol. 179, No. 4571, June 8, 1957.

22. Cawsey, G. F., Farrands, J. L., and Thomas, S.: "Observations of Detonation in Solid Explosives by Microwave Interferometry," Proc. Roy. Society of London, Vol. 248A, 1958.
23. Johnson, E. G.: "A Microwave Technique for Studying Detonation Phenomena," Report No. S-87, Contract DA-01-021 ORD-11, 909(Z), Rohm and Haas Company, Huntsville, Alabama, September 1965.
24. Dunn, M. G., and Blum, R. J.: "Continuous Measurement of Shock Velocity Using a Microwave Technique," NASA CR No. 490, May 1966.
25. Aro, T. O. and Walsh, D.: "Microwave Interference Method of Measuring Shock Velocity in a Shock Tube," Journal of Scientific Instruments, Vol. 43, No. 8, August 1966.
26. Harrington, R. F.: Time-Harmonic Electromagnetic Fields, McGraw-Hill Book Company, New York, 1961.
27. TRG, Incorporated, Boston, Massachusetts: "Plasma Diagnostics with Millimeter Waves," Bulletin B-4.
28. Demornay-Bonardi Corporation, Pasadena, California, Microwave Equipment Catalog, 1963/1964.
29. Fradin, A. Z., Microwave Antennas, Pergamon Press, New York, 1961, pp. 197-202.
30. Brown, J., Microwave Lenses, Methuen and Co., Ltd., London, 1953, pp. 4-10.

XIV. APPENDICES

Appendix A.

Electromagnetic Nomenclature and Symbolism

The mathematical description of electromagnetic fields is based upon the well-known Maxwell equations. While the development of field expressions from the Maxwell equations is standard, considerable variation of notation occurs in the literature. The following material provides background for the notation used in the subject investigation. The notation follows that of reference 26.

The Maxwell equations are given in vector notation as

$$\begin{aligned}\overline{\nabla} \times \overline{E} &= - \frac{\partial \overline{B}}{\partial t} \\ \overline{\nabla} \times \overline{H} &= \frac{\partial \overline{D}}{\partial t} + \overline{I} \\ \overline{\nabla} \cdot \overline{B} &= 0 \\ \overline{\nabla} \cdot \overline{D} &= q_v\end{aligned}\tag{A-I-1}$$

The quantities which arise in the discussions in the subject investigation are \overline{E} , the electric intensity, and \overline{H} , the magnetic intensity.

The constitutive relationships

$$\begin{aligned}\overline{D} &= \epsilon \overline{E} \\ \overline{B} &= \mu \overline{H}\end{aligned}\tag{A-I-2}$$

define the permittivity of a medium, ϵ , and the permeability of a medium, μ . In general, ϵ and μ are complex quantities but in a vacuum or "free space",

$$\epsilon_0 = 8.854 \times 10^{-12} \text{ farad per meter}$$

(A-I-3)

$$\mu_0 = 4\pi \times 10^{-7} \text{ henry per meter.}$$

for the mks system of units. The ratio of ϵ to ϵ_0 for a particular medium is called the dielectric constant of the medium. For the dielectric materials of interest to the subject investigation,

$$\mu \approx \mu_0.$$

Power flux is expressed by the Poynting vector,

$$\overline{S} = \overline{E} \times \overline{H} \quad . \quad (A-I-4)$$

When the electromagnetic fields to be studied are harmonic, as in the subject investigation, complex quantities can simplify the analysis. A complex \overline{E} is defined as related to an instantaneous \overline{E} according to

$$\overline{E} = \sqrt{2} \operatorname{Re} (E e^{j\omega t}) \quad . \quad (A-I-5)$$

\overline{E} is called the complex electric intensity. Similarly a complex magnetic intensity \overline{H} can be related to the instantaneous field quantity, \overline{H} . By substituting complex relationships such as equation (A-I-5) in the Maxwell equations (A-I-1), the Maxwell equations in complex

form are obtained. A satisfactory solution for the complex Maxwell equations is obtained by assuming that E in a perfect dielectric has only an x component independent of x and y in three-dimensional space. The result is

$$E_x = E_o e^{-jkz}$$

and

$$E_x = \sqrt{\frac{\mu}{\epsilon}} H_y \quad (A-I-6)$$

In equation (A-I-6), the quantity $\sqrt{\frac{\mu}{\epsilon}}$ is called the wave impedance of the medium, η . The quantity k is called the wave number of the medium. The corresponding instantaneous fields are formed by substituting equations (A-I-6) into (A-I-5). Thus,

$$\overline{E_x} = \sqrt{2} \operatorname{Re} [E_o e^{-jkz} e^{j\omega t}] \quad (A-I-7)$$

$$\overline{H_y} = \frac{\sqrt{2}}{\eta} \operatorname{Re} [E_o e^{-jkz} e^{j\omega t}]$$

The wave described by equation (A-I-7) is called a plane wave.

Examination of equations (A-I-7) shows that the spatial variation of the electric and magnetic intensities may be studied by use of the complex quantities E_x and H_y . This procedure was followed in the subject investigation. All propagation was assumed to be in the form of plane waves.

The term plane wave means plane phase fronts. The velocity at which an equiphase plane travels in a medium is called the phase

velocity, v_p , in the medium. In a dielectric medium, the phase velocity is

$$v_p = \frac{1}{\sqrt{\epsilon\mu}} \quad (\text{A-I-8})$$

The wavelength λ in a medium is defined as the distance in which the phase increases by 2π at any instant. Thus,

$$\lambda = \frac{2\pi}{k} = \frac{2\pi v_p}{\omega} = \frac{v_p}{f} \quad (\text{A-I-9})$$

where f is the frequency in cycles per second.

Appendix B.

Design of 30 GHz Microwave Lens-Corrected Horn Collimator

The microwave horn used in the subject investigation was designed from data presented in Reference 29. Results of analyses outlined in Reference 29 showed that a pyramidal horn of optimum dimensions existed as a function of the antenna gain of the horn. Design values for horn dimensions, with electromagnetic radiation wavelength as a parameter, were presented graphically. The horn used in the subject investigation was designed for 14 db gain, and for a wavelength of one centimeter.

The lens, located in the aperture of the horn, was intended to "correct" the ray paths emanating from the horn so that plane phase fronts were radiated. Design of the plano-convex lens was based on ray-path techniques, identical to those employed in optics. The equation for the radial distance of the surface of a plano-convex lens from the focal point is³⁰

$$r = f \left(\frac{n - 1}{n \cos \theta - 1} \right) \quad (\text{A-II-1})$$

where r is the radial distance to the lens surface from the focal point.

f is the focal length of the lens.

n is the refractive index of the dielectric material used for construction of the lens ($n > 1$).

The lens was designed to fit the dimensions of the horn. The design procedure for such a lens is to adjust the focal length so that the focal point of the lens is at the apex of the pyramid forming the interior of the horn. However, the lens must also seat in the aperture of the horn, so that a second design constraint exists. It was necessary to choose a focal length for the lens, then to calculate the dimensions of that lens to check for a fit in the horn aperture. A trial and error procedure was thus required. A digital computer program was written and employed to calculate lens profiles for various focal lengths. The resulting lens which fitted the horn had a focal length of 0.500 inches for an index of refraction of 1.61. Construction material was polymethyl methacrylate round bar stock.

The lens was turned on a lathe, using a form-cutting tool shaped to the proper profile. The tool was hand fitted to a 10 to 1 enlargement of the computer generated lens profile, employing optical magnification. Cut-off of the lens from the base material was accomplished on a milling machine. The final step was to mount the lens in the horn aperture, using liquid cement.

The horn and lens were shown in assembly in Figure 11, in the main body of this thesis.

Supplemental Progress Report

On

NASA Research Grant

NGR 47-004-024

A STUDY OF THE APPLICATION OF MICROWAVE TECHNIQUES TO THE
MEASUREMENT OF SOLID PROPELLANT BURNING RATES

Submitted To
The
National Aeronautics and Space Administration

By



Henry L. Wood
Professor of Mechanical Engineering

Period Covered: September 1, 1967 - April 30, 1968

Virginia Polytechnic Institute
Blacksburg, Virginia
April, 1968

TABLE OF CONTENTS

	Page
I. INTRODUCTION	5
II. TEST PROGRAM	5
III. DATA AND RESULTS	6
IV. DISCUSSION	6
Comparison of Results with Strand Burning Data	6
Microwave Characteristics of BF-117 Propellant	19
V. CONCLUSIONS	21
VI. RECOMMENDATIONS	21
VII. ACKNOWLEDGEMENTS	22

LIST OF FIGURES

	Page
Figure 1. Comparison of Average Burning Rate from Charge Length with Strand Burning Rate	12
Figure 2. Comparison of Microwave Burning Rate with Strand Burning Rate	13
Figure 3. Comparison of Thermocouple Burning Rate with Strand Burning Rate	14
Figure 4. Pressure and Microwave Records of Run BF-24	17
Figure 5. Comparison of Instantaneous Burning Rates with Strand Burning Rate	18

LIST OF TABLES

	Page
Table 1. Test Data	7
Table 2. Average Test Results	10

I. INTRODUCTION

Following experimentation with the high aluminum content propellant, TPH-8009, attention was directed to a low aluminum content propellant, BF-117, also supplied by NASA Langley Research Center. The supplemental progress report describes the results of a series of test rocket motor firings using BF-117 propellant.

II. TEST PROGRAM

The test procedures and equipment, including the rocket motor, were identical with those employed with TPH-8009 propellant. A series of 28 test firings were conducted with BF-117 propellant.

The propellant charges were cut from 12-inch lengths which had been cast by NASA Langley Research Center in phenolic asbestos tubing. Each 12-inch length had been x-rayed to determine the presence of voids or inclusions. Charge lengths were nominally 2, 3, or 4 inches. The maximum charge length that could be cut, free of voids, was 4 inches.

During early tests considerable difficulty was experienced with severe nozzle erosion. Fabrication of nozzles from ZTA graphite reduced erosion to a negligible amount.

As noted in the tabulated results, the klystron (microwave generator) became inoperative during the course of a number of tests.

The malfunction was finally traced to a thermal relay in the generator circuits. Operation of the generator from an isolated power source and at increased voltage precluded further malfunction.

III. DATA AND RESULTS

The data and results of the test rocket firings are presented in Tables 1 and 2. The average microwave burning rates were evaluated over the time interval of passage of the combustion front between the first two (if more than two were employed) thermocouple sensors. Results from measurements between other thermocouple sensors in the three and four inch charges are not presented but are retained in the files of the investigator.

IV. DISCUSSION

Comparison of Results with Strand Burning Data

In the progress report covering the TPH-8009 propellant, microwave measurements were compared with those made at NASA Langley Research Center by ultrasonic methods. Ultrasonic data is not available on the BF-117 propellant and comparison can be made only with strand burning data supplied by Langley Research Center.

Figures 1, 2, and 3 present a graphical comparison of the three burning rates measured with strand burning rates. Figure 1 is a comparison of the burning rate determined from total charge length

TABLE 1
 Test Data - BF-117 Propellant

Firing Number	Date	Charge Length, Inches	T/C-1 to T/C-2 Distance Inches	Nozzle Throat Diameter, Inches PRE	Nozzle Throat Diameter, Inches POST	Remarks
1	10-5-67	2.100	0.996	0.201	0.204	
2	10-5-67	2.008	1.088	0.201	0.228	Severe nozzle erosion
3	10-10-67	2.001	1.018	0.201	0.206	Klystron stopped
4	10-10-67	2.020	1.009	0.201	0.204	
5	10-12-67	2.005	0.969	0.221	0.224	
6	10-12-67	2.004	1.003	0.221	0.223	
7	10-17-67	2.003	0.975	0.209	0.210	Klystron erratic
8	10-17-67	2.003	1.006	0.209	0.210	Klystron stopped
9	10-24-67	3.055	1.045	0.209	0.270	Severe nozzle erosion
10	10-31-67	2.918	0.963	0.209	0.221	Severe nozzle erosion, Klystron stopped
11	11-2-67	1.951	1.006	0.221	0.221	Klystron stopped
12	11-2-67	1.890	0.980	0.201	0.201	Klystron stopped

TABLE 1 (Continued)

Firing Number	Date	Charge Length, Inches	T/C-1 to T/C-2 Distance Inches	Nozzle Throat Diameter, Inches PRE	Nozzle Throat Diameter, Inches POST	Remarks
13	11-9-67	4.030	0.989	0.221	0.231	Klystron stopped
14	11-9-67	1.944	1.003	0.221	0.222	
15	11-14-67	4.070	1.017	0.221	0.228	
16	11-30-67	2.070	1.013	0.221	0.222	Long pressure tail-off
17	11-30-67	2.008	0.979	0.221	0.223	
18	12-5-67	1.992	1.013	0.221	0.222	Klystron erratic
19	12-5-67	2.024	0.982	0.201	0.206	Klystron erratic, ZTJ Graphite
20	12-7-67	2.022	0.971	0.196	0.200	ZTJ Graphite
21	12-7-67	2.988	0.996	0.182	0.189	ZTJ Graphite
22	12-13-67	3.042	1.000	0.182	0.189	ZTJ Graphite
23	12-14-67	2.017	0.984	0.209	0.213	ZTJ Graphite
24	1-22-68	2.024	0.964	0.201	0.228	TC-2 inoperative, severe erosion
25	1-22-68	2.002	0.990	0.201	0.201	Klystron erratic, ZTJ Graphite

TABLE 1 (Continued)

Firing Number	Date	Charge, Length, Inches	T/C-1 to T/C-2 Distance Inches	Nozzle Throat Diameter, Inches PRE	Nozzle Throat Diameter, Inches POST	Remarks
26	1-24-68	3.002	0.989	0.201	0.203	ZTJ Graphite
27	1-24-68	3.036	1.000	0.193	0.201	
28	1-29-68	3.988	0.950	0.213	0.215	Noise on microwave signal, ZTJ Graphite

TABLE 2

Average Test Results - BF117 Propellant

Firing Number	Average Pressure, PSIG	Burn Time Seconds	Average Burning Rate- Charge Length, inches/second	Average Burning Rate- Microwave TC/1 to TC/2 inches/second	Average Burning Rate, Thermocouple, TC/1 to TC/2 inches/second	Average Microwave 1/2 Cycle Distance, inches
1	769	4.16	0.505	0.495	0.483	0.0462
2	644	4.42	0.445	-	0.530	-
3	749	4.05	0.494	0.506	0.496	0.0440
4	625	4.30	0.470	0.487	0.471	0.0430
5	468	4.83	0.416	0.429	0.416	0.0427
6	473	4.85	0.413	0.435	0.497	0.0431
7	560	4.43	0.453	-	0.459	-
8	576	4.38	0.458	-	0.411	-
9	382	7.83	0.384	0.454	0.453	0.0439
10	523	6.62	0.441	-	0.447	-
11	425	4.69	0.416	-	0.412	-
12	714	3.84	0.488	-	0.488	-

TABLE 2 (continued)

Firing Number	Average Pressure, PSIG	Burn Time Seconds	Average Burning Rate- Charge Length inches/second	Average Burning Rate- Microwave TC/1 to TC/2 inches/second	Average Burning Rate, Thermocouple, TC/1 to TC/2 inches/second	Average Microwave 1/2 Cycle Distance, inches
13	454	10.09	0.402	-	0.388	-
14	496	4.69	0.415	0.425	0.413	0.0427
15	457	9.87	0.413	0.419	0.416	0.0436
16	600	4.13	0.488	0.427	0.434	0.0625
17	506	4.83	0.414	0.433	0.431	0.0429
18	480	4.95	0.404	-	0.401	-
19	685	4.28	0.469	0.493	0.488	0.0427
20	970	4.01	0.500	-	0.508	-
21	1100	5.55	0.539	0.563	0.542	0.0426
22	1130	5.53	0.544	0.570	0.559	0.0432
23	578	4.45	0.451	0.470	0.461	0.0429
24	566	4.55	0.443	-	-	0.0431
25	702	4.17	0.480	-	0.492	-
26	702	6.41	0.468	0.482	0.493	0.0439
27	890	5.98	0.504	0.530	0.508	0.0440
28	527	9.125	0.436	-	0.445	-

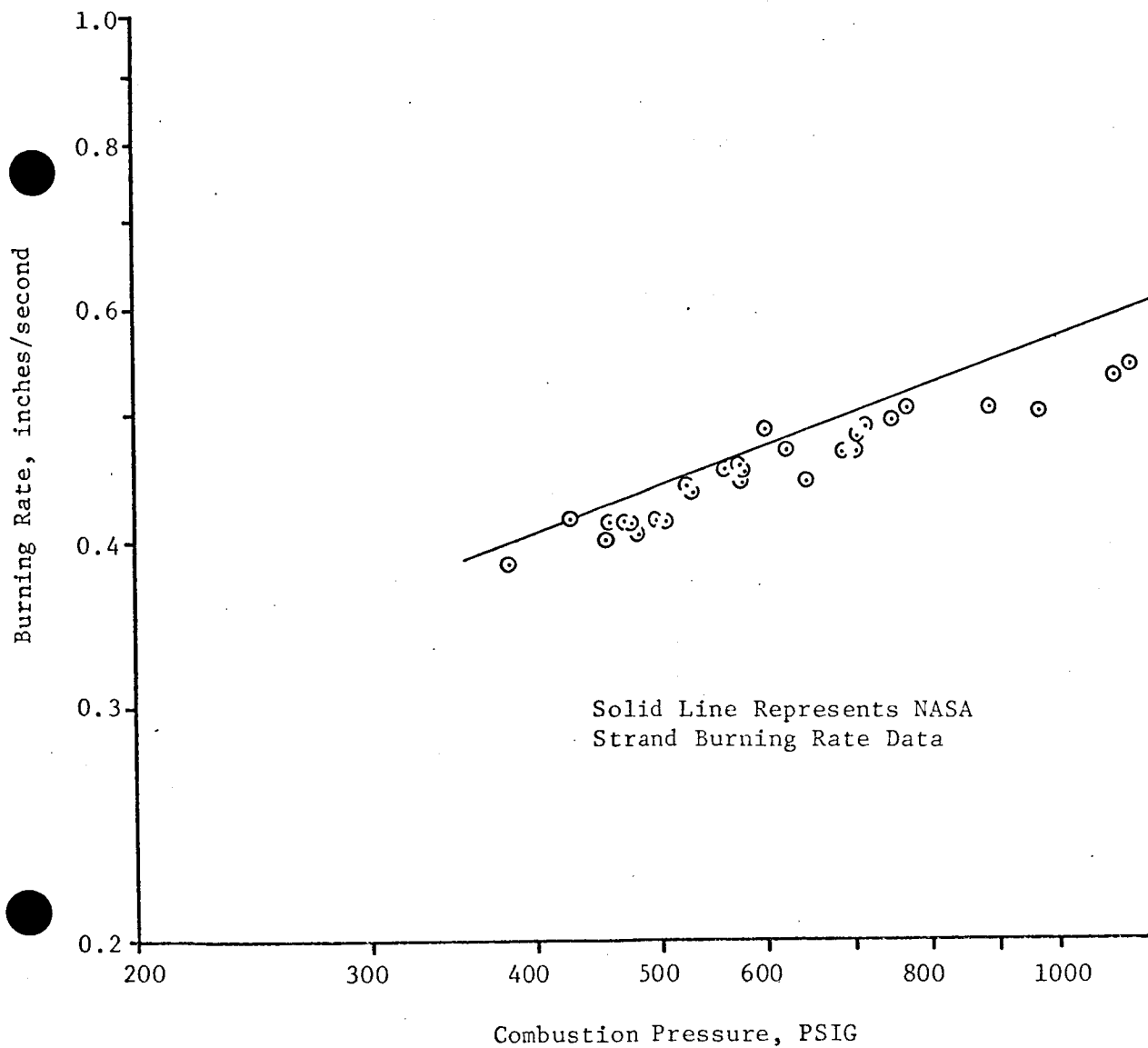


Figure 1. Comparison of Average Burning Rate from Charge Length with Strand Burning Rate (BF117 Propellant)

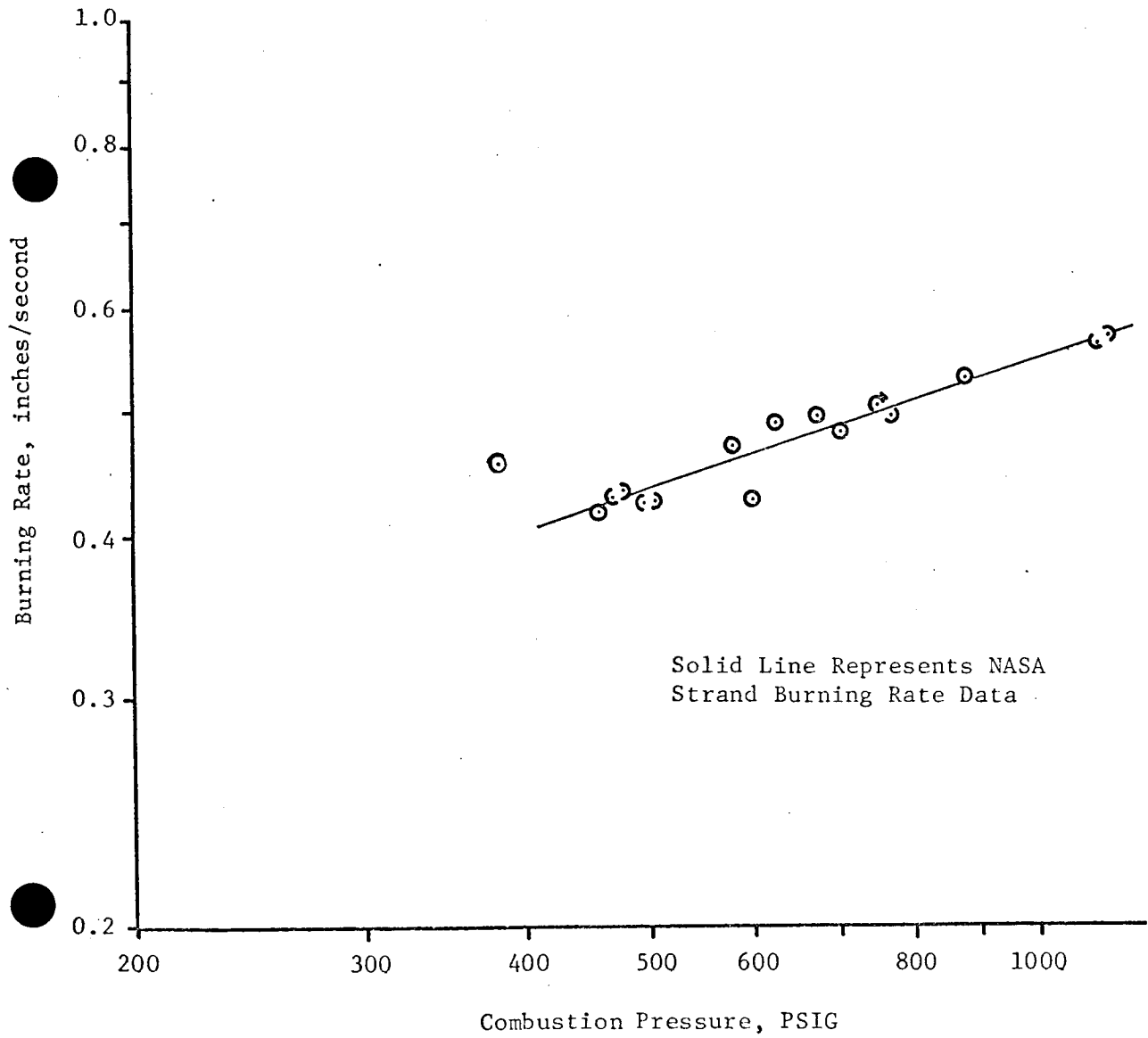


Figure 2. Comparison of Microwave Burning Rate with Strand Burning Rate (BF117 Propellant)

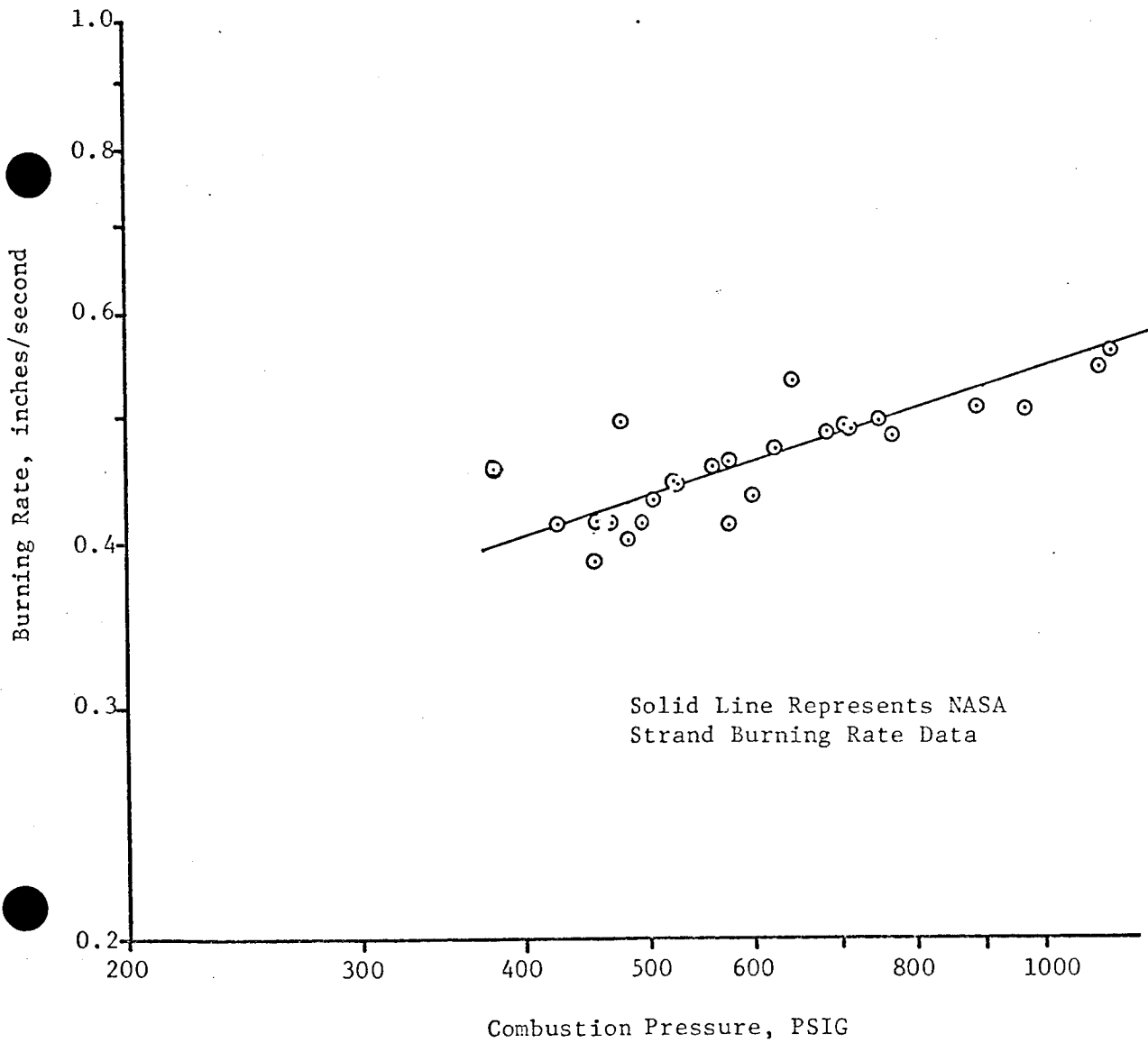


Figure 3. Comparison of Thermocouple Burning Rate with Strand Burning Rate

and total burning time as measured conventionally from the pressure records of the tests. Generally good agreement, except at higher pressures, is seen to exist between the two sets of data.

Figure 2 presents a comparison between average microwave burning rates and strand burning data. The microwave burning rate was computed from the half-cycle distance and the number of cycles in the time interval of passage of the combustion zone between the first two thermocouples. The microwave burning rate is, therefore, evaluated during the first few seconds of combustion. If nozzle erosion existed, with a resultant decrease in chamber pressure as combustion progressed, it would be expected that the microwave burning rates would be somewhat higher than those obtained from total charge length. Comparison of Figures 1 and 2 shows this general tendency, particularly at higher combustion pressures where erosion was more severe.

In addition, the usage of average combustion pressure (evaluated from the pressure-time integral) as a correlation parameter for burning rates other than average rates over the entire charge length is not desirable. For example, reference is made to the data point in Figure 2 at 382 psig and 0.454 inches/second as determined from firing BF-9. The data appears to be considerably in error. However, in firing BF-9, severe nozzle erosion occurred, with combustion pressure decreasing rapidly after approximately 2.5 seconds. The microwave rate was calculated at a pressure much higher than the

average combustion pressure. The average pressure during the time interval in question was 605 psig. If 605 psig were used instead of 382 psig, the data point would be almost exactly on the line representing strand burning rate data.

The same general comments can be made regarding thermocouple data as presented in Figure 3. The data point from Firing BF-9 would again fall well within normal scatter if the average pressure for the appropriate time interval were used.

If thermocouple and microwave burning rate over the same time interval are compared, the results are more favorable. No graphical comparison is presented but, if the test results of Table 2 are reviewed, it will be seen that the microwave and thermocouple burning rates for the same time interval (and, in general, for a reasonably constant combustion pressure) are within $\pm 4\%$ of each other. The errors involved here may well have been caused by the distortion present in the microwave signal which precluded precise data reduction. Distortion will be considered in a later portion of this report.

Additional insight into the capability of the microwave measurement technique was obtained from analysis of data from firings in which combustion pressure decays were caused by nozzle erosion. Typical of such is Firing BF-24. Figure 4 is a reproduction of the pressure and microwave recordings for Firing BF-24. As may be seen, a maximum pressure of 785 psig was attained, but decayed

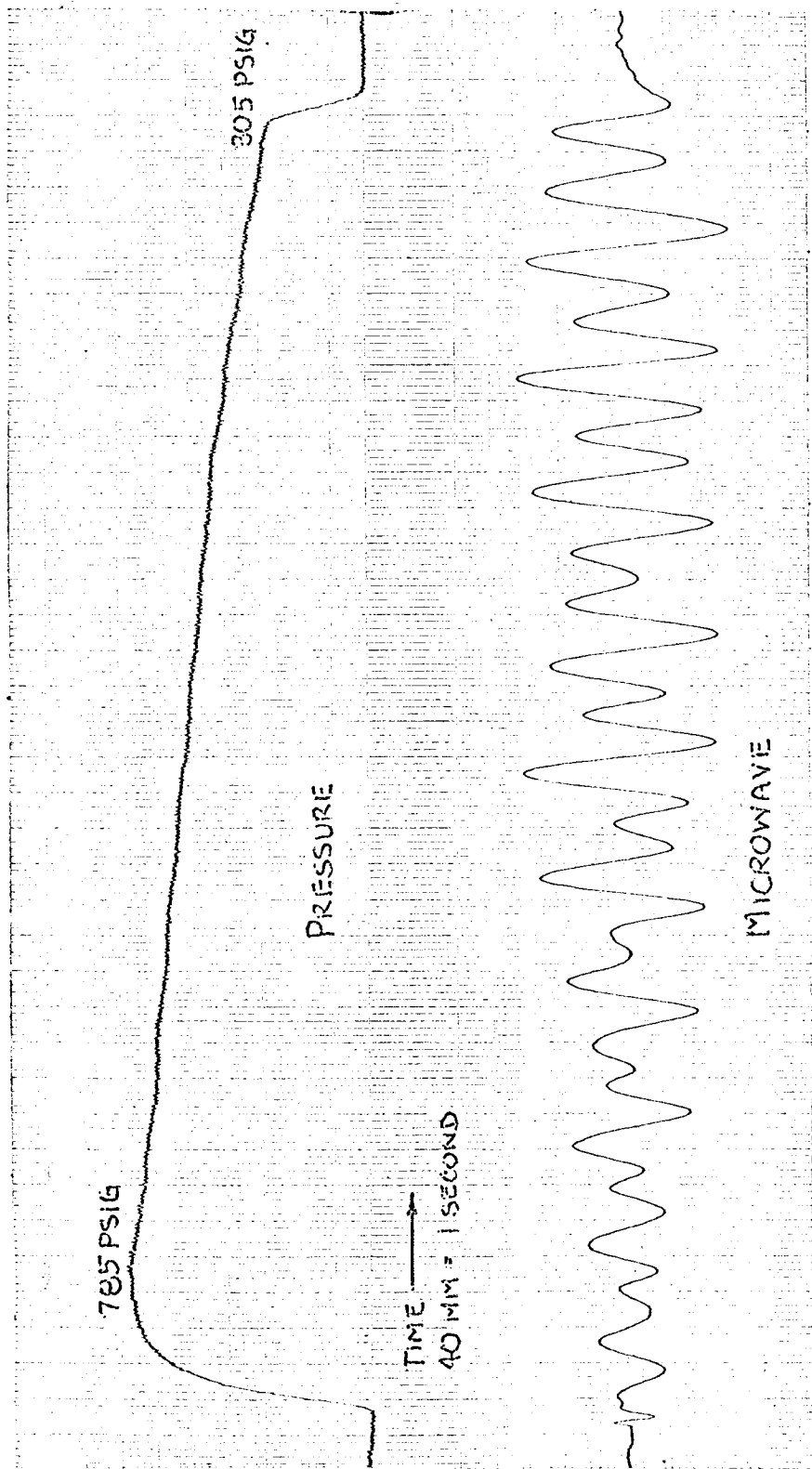


Figure 4. Pressure and Microwave Records of Run BF-24.

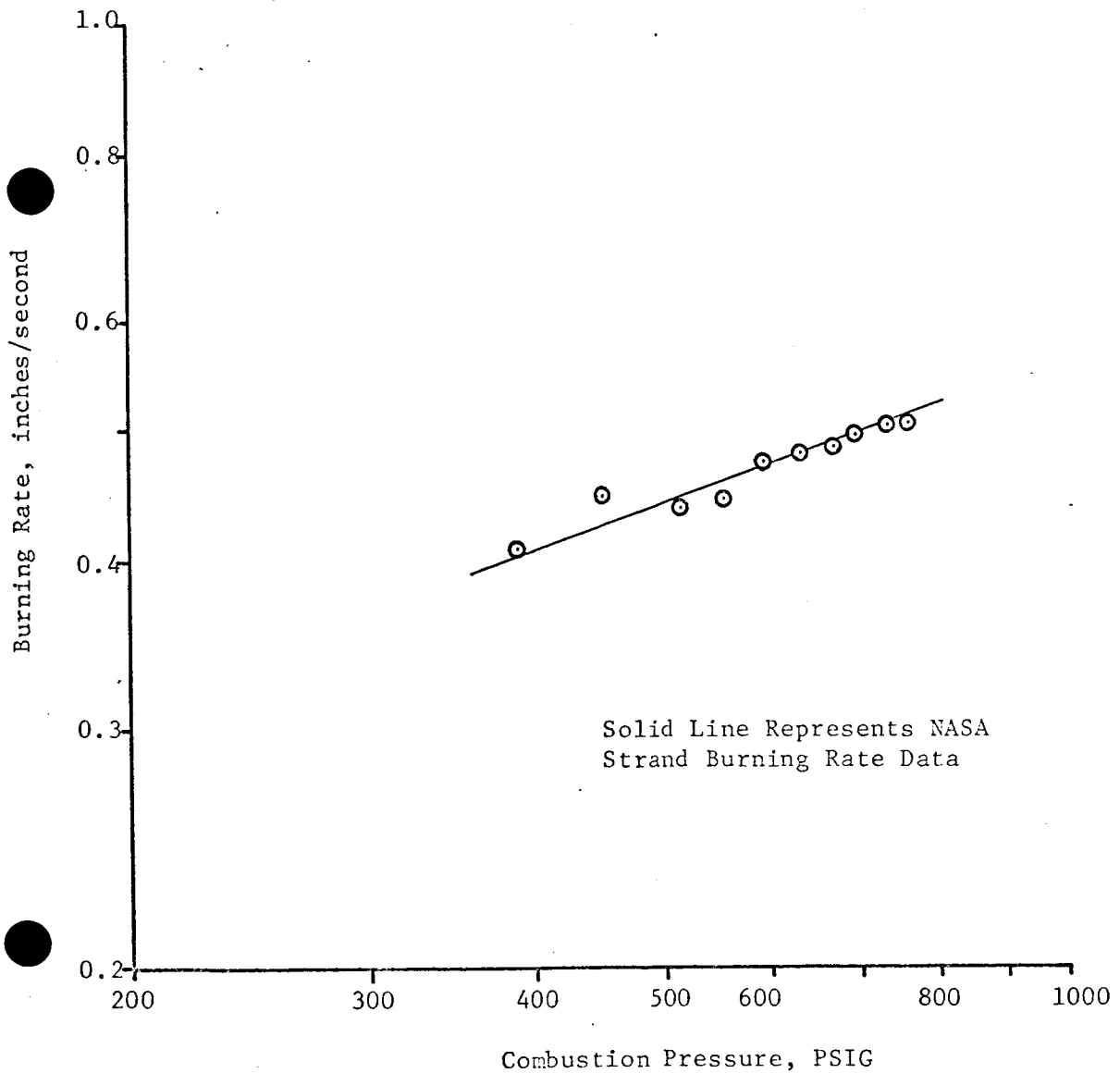


Figure 5. Comparison of Instantaneous Microwave Burning Rates with Strand Burning Rate (Run BF-24)

approximately linearly with time to 305 psig at tail-off. Taking two-cycle intervals for convenience (a propellant distance equal to 0.178 inches), "instantaneous" burning rates were calculated for the interval. Average combustion pressures were obtained from the pressure record for the same time interval. The results are presented graphically in Figure 5. Superimposed is the NASA strand burning data.

The correlation of the foregoing "instantaneous" burning rate is considered quite good in view of the amplitude distortion present in the microwave signal. The results obtained from such analyses point out the capability of the microwave technique for determination of burning rate under transient conditions. It should be observed that the transients involved here are not rapid ones, and that further substantiation of transient capability is necessary. Clearly shown, however, is the fact that the microwave technique is applicable to the relatively slowly occurring transients that occur from the combustion of propellant grains designed to give varying thrust programs.

Microwave Characteristics of BF-117 Propellant

In the experimentation with TPH-8009 propellant it was possible to obtain values for the electromagnetic constants by measurements from tests in which no automatic gain change was employed. Such was not possible in experimentation with BF-117

propellant due to amplitude and frequency distortion of the microwave signal.

BF-117 propellant was found to be much less "lossy" than TPH-8009, undoubtedly because of its low aluminum content. As a result, reflections from the burning surface were many times stronger. Several microwave engineers that were consulted are of the opinion that adequate isolation of the microwave generator from return, or reflected, signals does not exist in the present equipment. It is felt that this lack of isolation allows the strong reflected signals to pull the generator off frequency producing distortion. In addition, the half-bridge arrangement does not eliminate amplitude variation in either incident or reflected waves. The combined effect of the foregoing apparently produced the distortion which precluded both measurement of electromagnetic constants and precise interpretation of microwave data. The nature of the distortion is shown in Figure 4.

The microwave power required to penetrate a given length BF-117 propellant was considerably less than that required in TPH-8009. In an effort to improve isolation of the generator, up to 15 db of attenuation was inserted at the output of the microwave generator. Isolation was not improved appreciably. However, a grain two inches in length was easily penetrated and a useful microwave signal received. The total power involved was approximately 1/70 of the power employed with TPH-8009. Maximum penetrable grain length was not determined inasmuch as grains

longer than four inches were not available. Four inch grains were readily employed. It thus appears that no power limitations exist in application of the microwave technique to low aluminum content propellants of the BF-117 class.

V. CONCLUSIONS

The following conclusions can be drawn from the results of experimentation with BF-117 propellant:

- (1) The microwave burning rate measurement technique can readily be employed with low-aluminum content propellants.
- (2) The power required for measurement is much less than that for highly aluminized propellants.
- (3) Transient measurements of burning rate are possible with the microwave technique.

VI. RECOMMENDATIONS

In addition to the recommendations contained in the progress report covering the period September 1, 1966 to August 31, 1967 the following is offered:

Precise data reduction depends upon distortion free phase angle measurement. The most important recommendation is that the microwave system be modified such that proper isolation be provided for the microwave generator and that the phase angle measurement be made

amplitude insensitive. Use of a full interferometric bridge with ferrite isolators is deemed necessary.

VII. ACKNOWLEDGEMENTS

Sincere appreciation is expressed to the National Aeronautics and Space Administration, Langley Research Center, whose support made this investigation possible. Special appreciation is extended to the personnel of the Propulsion Branch, Langley Research Center, for their advice and assistance throughout the course of the investigation.